Axisymmetric Buckling Analysis for the AP600 Standard Plant Containment Vessel

Prepared by
L. Greimann, F. Fanous, R. Challa, D. Bluhm

Ames Laboratory
Iowa State University

Prepared for
U.S. Nuclear Regulatory Commission

Enclosure 2

ABSTRACT

A review of the structural design of the Westinghouse AP600 containment vessel was completed. In this report, the stress analysis and the evaluation of the structure for buckling were performed with an axisymmetric model using BOSOR4 and BOSOR5 finite difference software, respectively. The loads and load combinations were based on the guideline of the Safety Review Plan (SRP) Section 3.8.2 and the American Society of Mechanical Engineers (ASME) Code. The Westinghouse AP600 containment vessel was modeled as an axisymmetric shell consisting of different segments and mesh points with the additional mass of the penetrations and other appurtenance smeared around the circumference. The stresses due to the individual loads (dead loads inclusive of crane loads, internal and external pressures, wind loading inclusive of normal and tornado conditions, temperature loading inclusive of uniform and striping conditions, and seismic loads) were computed using the stress analysis option in the BOSOR4 program. The stresses from individual loads were combined according to the ASME Code into stress intensities. All stress intensities were within allowable limits specified in Section NE3221 of the ASME Code. Sensitivity studies were conducted to investigate the effects of the axisymmetric imperfection parameters, i.e., the imperfection amplitude and wave length on the buckling load for each of the load combinations in SRP 3.8.2. The minimum factors of safety against buckling were 3.03 (Design Conditions and Service Level A) and 2.02 (Service Levels C and D). A buckling evaluation for loading beyond the safe shutdown earthquake (SSE) was also performed considering the containment dead load and increasing the SSE loading by a factor of 4.60 until buckling occurred. In a separate report, a three-dimensional analysis was performed which emphasized the region around the major penetrations, discontinuities and concentrated masses.

TABLE OF CONTENTS

Page

LIST OF TABLES

LIST OF FIGURES

Page

ACKNOWLEDGMENT

The authors would like to express their appreciation for the members of the U.S. Nuclear Regulatory Commission, Dr. Thomas Cheng (Project Officer), Dr. Seung Lee (Structural Engineer), Mr. David Terao (Section Chief), Mr. Goutam Bagchi (Chief, Civil Engineering and Geosciences Branch), and Mr. Bernard L. Greiner, (Program Manager, Division of Engineering) for their help throughout the course of this work. The authors would also like to acknowledge the project secretaries, Ms. Jeanine Crosman and Ms. Denise Wood, for word processor operations and secretarial services associated with this project. Additionally, they would like to thank Ms. Connie Bates, Administrative Specialist, for her assistance on financial planning and tracking.

EXECUTIVE SUMMARY

The objective of the present work is to perform an independent analysis of the Westinghouse AP600 containment vessel. In this report, the stress analysis and the evaluation for the structure for buckling were performed by using an axisymmetric model with BOSOR4 and BOSOR5 finite difference software, respectively. Analyses with a three-dimensional model are summarized in a companion report.

The Nuclear Regulatory Commission (NRC) Standard Review Plan (SRP) Section 3.8.2 stipulates that the design and analysis procedures be in compliance with the American Society of Mechanical Engineers (ASME) Boiler and Pressure Vessel Code. SRP Section 3.8.2 further prescribes the load combinations pertaining to Design Conditions and Service Limits classified by the ASME Code. Section NE3222.1 of the Code establishes the admissible factors of safety against buckling.

The AP600 Containment vessel is a cylindrical steel shell structure with an inner radius of 65 ft. and a wall thickness of 1.625 in. The top consists of an ellipsoidal head. The bottom is enclosed by another ellipsoidal head embedded into a concrete foundation at base. The cylindrical portion of the containment vessel is provided with two T-ring stiffeners and one box-girder stiffener. The latter services a crane girder supporting a crane bridge and a trolley. The major penetrations are two equipment hatches and two personnel locks located at different elevations. The major appurtenances are the containment air baffle, walkway, HVAC duct, cable trays, concrete on the external stiffener and the containment vessel recirculation unit platform. The containment vessel was modelled as an axisymmetric shell consisting of different segments and mesh points with the additional mass of the penetrations and appurtenances being smeared around the circumference.

The stresses due to the individual loads (dead loads, internal and external pressures and temperatures) were computed using the stress analysis option in the BOSOR4 program. The seismic loading to the structure was provided by the plant owner through NRC channels in the form of safe shutdown earthquake (SSE) response spectra. The modal stress quantities were combined by the Square Root of the Sum of Squares (SRSS) method. Seismic stresses for several meridians were compared to select the controlling meridian for the seismic case. The stresses from individual loads (dead load inclusive for crane loads, internal and external pressures, wind loading inclusive of normal and tornado conditions, temperature loading inclusive of uniform and striping conditions, and seismic loads) were combined according to ASME Code into stress intensities. All stress intensities were within allowable limits.

Stability was investigated using BOSOR5 with the axisymmetric model. The buckling assessment was performed using the worst meridian assumption, that is, the stresses on the most highly stressed meridian were assumed to exist uniformly around the circumference. Material nonlinearities and residual stresses were incorporated using stress strain constitutive relationships derived from the ASME Code Case N-284. A geometric axisymmetric imperfection was introduced into the model in the form of a sine wave. The amplitude of the sine wave satisfied ASME construction tolerances and the wave length was selected on the basis of sensitivity studies to minimize the buckling factor of safety. The calculated minimum factors of safety were 3.03 for Design Conditions and Service Level A and 2.02 for Service Levels C and D. The factor of safety for Service Level C does not satisfy ASME Section NE3222.1 but does satisfy ASME Code Case N-284 and Regulatory Guide 1.57.

A buckling analysis for seismic loading beyond SSE was also conducted using the axisymmetric model. Dead load was held constant and the SSE loading was increased by a factor of 4.60 at which point buckling occurred.

1. INTRODUCTION

1.1 Background

The AP600 steel containment vessel is a thin cylindrical shell structure with an approximately 1.78 to 1 smooth elliptical head as shown in Fig. 1.1. The cylindrical portion is provided with two T-ring stiffeners and an internal box stiffener which supports a crane. SA537 Class 2 steel plates are used to construct the main vessel. The bottom of the containment is enclosed by an ellipsoidal head which has the same geometrical shape as the top head and is embedded in concrete.

The AP600 nuclear reactor is designed to use a passive means for containment cooling, which includes natural draft and water film evaporation cooling by an airflow path in the annuli between the containment vessel and the air baffle and between the shield building and the air baffle. In this system water flows onto the top of the containment dome end down along the vertical walls of the containment. At the same time air flows into inlets near the top of the shield building, downwards past the air baffle wall in the space between the shield building and the containment vessel, around the bottom of the baffle, upwards between the baffle and the containment vessel and out of the chimney at the top of the shield building. A description of the relevant structures is provided in the AP600 Standard Safety Analysis Report [1.1 (Sec. 3.8.4.1)]. The operation of the passive containment cooling system is more fully described in [1.1 (Sec. 6.2.2.2.4)].

As the containment vessel is subjected to various loading conditions, regions of compressive membrane forces develop in the steel containment that may cause the shell to fail due to compression instability. In order that the containment performs its intended safety function and sustains these loads, a sufficient margin of safety against buckling and other types of failure should exist.

1.2 Objectives

The objectives of this work are to perform:

(1) an axisymmetric stress and buckling analysis to evaluate the containment design adequacy against the ASME Design Conditions and Service Levels A, C, and D, and

(2) an axisymmetric analysis to investigate the margin of containment beyond the design basis loads such as safe shutdown earthquake (SSE).

A three-dimensional analysis considering the effects of localized loads near penetrations such as the equipment hatch and personnel locks, which cannot be modeled in the axisymmetric model, is presented in Ref. [1.2].

1.3 Description of AP600 Containment

A cross-sectional elevation of the AP600 containment vessel is shown in Fig. 1.1. The containment consists of a cylindrical shell with an inner radius of 65 ft and a wall thickness of 1.625 in. The cylindrical shell is covered by smooth elliptical heads at both ends. The bottom is embedded into a concrete foundation below Elev. 100'. The cylindrical portion of the containment vessel is provided with two T-ring stiffeners and one box-girder stiffener. The later serves as a crane girder supporting a crane bridge and a trolley that weighs 634.6 kips [1.3].

Two equipment hatches and two personnel airlocks are located at different elevations within the cylindrical portion of the AP600 containment shell as shown in Figs. 1.1 and 1.2. The centerline of the larger equipment hatch barrel is located at Elev. 144' 6" and 67° Azimuth. The equipment hatch barrel is a circular cylinder with an inner diameter of 22 ft, a length of 5 ft 3 13/16 in. and a wall thickness of 4 3/4 in. The total weight of this penetration is estimated to be 105,000 lb [1.3]. Other details related to this hatch assembly is shown in Fig. 1.3. The other equipment hatch has a cylindrical barrel with a 16 ft inside diameter and is located at Elev. 112' 6" and 126° Azimuth. Figure 1.4 illustrates details related to this hatch. The weight of the 16 ft. equipment hatch was assumed to be 62,000 lb. [1.3]. Each personnel airlock has an inside diameter of 9 ft-10 in. and an assumed weight of 70,000 lb. The airlocks are located at 107° Azimuth at Elevs. 110' 6" and 137' 8", respectively.

Other attachments to the AP600 include the containment air baffle, walkway, HVAC duct, cable trays, concrete on the external stiffener, and the containment recirculation unit platform. The weight and the locations of these attachments are listed in Table 1.1 [1.3].

1.4 Analysis Methods

The widely recognized computer programs BOSOR4 [1.4] and BOSOR5 [1.5] were used herein to perform the axisymmetric analyses of the AP600 containment structure. These are finite difference programs for stress and buckling analyses of surface of revolutions. BOSOR4 has the capabilities to include geometric nonlinearities and to handle arbitrary loads, while BOSOR5 is capable of including the effects of both geometric and material nonlinearities but axisymmetric loads only.

The containment shell and stiffeners were modeled using BOSOR shell segments that are divided into small elements. The mass of the penetrations and attachments were included in the model.

The stress analysis of the geometrically perfect shell was conducted using the BOSOR4 program and elastic material. Different loads applied on the containment are dead load (including crane bridge and trolley), uniform internal and external pressure, wind and tornado loads (including uniform suction applied as a lateral load), temperature (including striping conditions due to the passive cooling mode), and seismic loads (in the form of response spectra). Calculation of the seismic stresses involved extraction of modal responses due to seismic input distribution by a response spectrum dynamic analysis. The modal responses were then combined using the SRSS method with the consideration of closely spaced mode effect. The non-symmetrical circumferential distribution of other loads such as the crane loads, wind loads, tornado loads, and temperature was modeled using the Fourier expansion option of BOSOR4. The stress analysis results were combined as per load combinations specified in U.S. NRC SRP 3.8.2 [1.6]. The stress intensities for each of the load combinations were checked with respect to the allowable values for different service limits as specified by the ASME Code [1.7].

The buckling analysis for each of the load combinations was performed using the BOSOR5 program using the worst meridian approach, which assumes that the compressive stresses on the most highly stressed meridian are distributed uniformly around the circumference. The stress resultants on the worst meridian were used to determine a set of equivalent axisymmetric static loads in form of pressures [1.8]. The equivalent static pressures were developed such that, when applied to the axisymmetric model, they generate a stress profile which closely resembles that on the worst meridian. The dead loads were input in the analysis in the form of ring loads. The external pressures and thermal loads were introduced into the analysis using the options provided in BOSOR5. The factor of safety against buckling was determined by proportionally increasing the applied loads until buckling occurs.

Since shell buckling is very sensitive to geometrical imperfections, geometric sinusoidal imperfections were assumed in the analysis. The imperfection amplitude was selected in accordance with the maximum tolerances specified in the ASME Code. Sensitivity studies with regard to the imperfection wavelength were performed to yield a minimum buckling factor of safety for each of the loading combinations defined in the U.S. NRC SRP. Material imperfections considering the effects of residual stresses were included in the analysis in the form of an idealized stress strain curves. The predicted buckling factors of safety were checked with the acceptance criteria listed in Section NE 3222.1 of the ASME, Regulatory Guide 1.57 and ASME Code Case N-284.

In addition to the buckling analysis for each of the load combinations listed in Sec. 3.8.2 of the U.S. NRC SRP, the seismic margin limit for the containment shell was determined. This was conducted to investigate the behavior of the AP600 containment during seismic loading beyond the safe shutdown earthquake. To accomplish this, the dead loads were held constant while increasing the seismic loads until buckling occurs.

1.5 Acceptance Criteria

The U.S. NRC SRP Section 3.8.2 [1.7] stipulates that the design and analysis procedure for the steel containment structures be in compliance with subsection NE of the ASME Code Section III [1.9] and with Regulatory Guide 1.57 [1.10].

1.5.1 Section NE 3222.1

Section NE 3222.1 of the ASME Code [1.8] specifies the basic allowable compressive stress for the stability of structures as:

"The maximum buckling stress values to be used for the evaluation of instability shall be either of the following:

(a) One-third the value of critical buckling stress determined by one of the methods given below.

(1) Rigorous analysis which considers the effects of gross and local buckling, geometric imperfections, nonlinearities, large deformations, and inertial forces (dynamic loads only).

(2) Classical (linear) analysis reduced by margins which reflect the difference between theoretical and actual load capacities.

(3) Tests of physical models under conditions of restraint and loading the same as those to which the configuration is expected to be subjected.

(b) The value determined by the applicable rules of NE 3133."

The stability limits for various loading conditions, such as the Design Conditions and Service Limits A, B, C, and D, have the factors of safety listed in Table 1.2. Method (a) (1) listed above will be used here.

1.5.2 ASME Code Case N-284

ASME Code Case N-284 [1.11] provides stability criteria for determining the structural adequacy against buckling of shells with more complex geometries and loading conditions than those covered by Section NE 3133. The rules are based on linear elastic bifurcation buckling theory which has been reduced by knockdown factors to account for the effect of imperfections, boundary conditions, material nonlinearities and residual stresses. The stability limits for the various loading conditions correspond to the factors of safety shown in Table 1.2. The factors of safety are lower than those specified by NE 3222.2 of the ASME Code, but are consistent with other ASME factors of safety for other failure criteria, e.g., yielding due to internal pressure [1.12].

1.5.3 Regulatory Guide 1.57

The Regulatory Guide 1.57 [1.10] delineates the acceptable design limits and appropriate loading combinations associated with normal operating conditions, design conditions and specified seismic events for the design of containment systems. The Regulatory Guide recognizes the design limits as specified in Section NE 3222 of the ASME Code. However, the Guide states that, "if a detailed analysis is performed, i.e., Method (a) (1), Note 7 to the regulatory position applies". Note 7 explicitly states that, "If a detailed rigorous analysis of shells that contain the maximum allowable deviation from true theoretical form is performed for instability (buckling) due to loadings that induce compressive stresses, such analyses, considering inelastic behavior, should demonstrate that a factor of at least two exists, between the critical buckling stress and the applied stress."

The factor of safety of two against buckling is not associated with a specific Service Limit. However, Regulatory Guide 1.57 states that, "the loading combinations should encompass that loading which produces the greatest potential for shell instability". Hence, this factor can be associated with Level C and D Service Limits, which usually produce the greatest compressive stress in the shell since they are associated with the SSE event.

1.6 References

1.1 "AP600 Standard Safety Analysis Report," Document prepared for U.S. NRC, San Francisco Operations Office, Westinghouse Electric Corporation, Document DE-ACO3-90 SF18495, June 26, 1992.

1.2 L. Greimann et. al., "Three-dimensional Buckling Analysis for the AP600 Standard Plant Containment Vessel," NUREG-CR/6461, final report to NRC, Washington, D.C., publication pending Oct. 1995.

1.3 "Seismic Model of Containment Vessel - AP600, Westinghouse," Calculation by Chicago Bridge and Iron (CBI) of Lumped Mass Stick Model, Sht 3A-14 through 3A-20, Sept. 1992.

1.4 Bushnell, D., "BOSOR4 Program for Stress, Buckling and Vibration of Complex Shells of Revolution," Structural Mechanics Laboratory, Lockheed Missiles and Space, Inc., Palo Alto, CA, 1975.

1.5 Bushnell, D., "BOSOR5 Program for Buckling of Elastic-Plastic Complex Shells of Revolution Including Large Deflection and Creep," Structural Mechanics Laboratory, Lockheed Missiles and Space, Inc., Palo Alto, CA, 1975.

1.6 "U.S. NRC Standard Review Plan (SRP)," Section 3.8.2, Ref. 1 - July 1981, pp. 3.8.2.4 and 3.8.3.11.

1.7 American Society of Mechanical Engineers, Boiler and Pressure Vessel Code, Section NE 3221 and Table NE-3221-1, 1989.

1.8 Greimann, L., et. al., "System 80+™ Containment - Structural Design Review," NUREG-CR/5957, NRC, Washington, D.C., April 1993.

1.9 American Society of Mechanical Engineers, Boiler and Pressure Vessel Code, Section NE 3220, 1989.

1.10 Regulatory Guide 1.57, "Design Limits and Loading Combinations for Metal Primary Reactor Containment Systems Components," NRC, Washington. D.C., June 1973.

1.11 American Society of Mechanical Engineers, Boiler and Pressure Vessel Code Case N-284, "Metal Containment Shell Buckling Design Methods," Supplement #2 to Nuclear Code Case Book, 1989.

1.12 American Society of Mechanical Engineers, Boiler and Pressure Vessel Code Appendix III, paragraphs 2100 and 3100.

2. AXISYMMETRIC STRESS ANALYSIS OF AP600 CONTAINMENT

2.1 Analysis Approach

The axisymmetric analysis of the AP600 containment vessel was performed by using the BOSOR4 program [2.1]. BOSOR4 can handle both axisymmetric and nonaxisymmetric loading but is limited to linear material properties. The program options include large-deflection axisymmetric stress analysis, small-deflection nonsymmetric stress analysis, modal vibration analysis, and buckling analysis with axisymmetric and nonsymmetric prestress.

This section summarizes the stress intensities induced in the AP600 containment vessel by the load combinations specified in the SRP Section 3.8.2 [2.2] and the ASME Code [2.3]. The different individual loads on the structure are the dead load, crane loads, accident and operating temperatures of 280°F and 120°F, internal pressures of 45 psig and 1 psig, external pressures of 2.5 psid and 3 psid, wind loads, tornado loads, temperature striping due to the cooling system used in this passive containment vessel, and seismic loads [2.4]. The structural analysis of the containment vessel was first performed for each individual load case utilizing the BOSOR4 program. The results were combined to calculate the stress intensities for the Design Conditions and Levels A, C, and D, which were compared to allowable stress intensities from the ASME Code [2.3].

2.2 Axisymmetric Modeling of the AP600 Steel Containment Vessel

The axisymmetric model of the AP600 containment vessel is shown in Fig. 2.1. Twenty-five shell segments were used in the BOSOR axisymmetric analysis model. Each segment was divided into a number of mesh points with a spacing less or equal to 0.5 $(rt)^{1/2}$ where, r and t are the containment vessel radius and wall thickness, respectively. In an axisymmetric model, all nonsymmetric attachments must be smeared around the circumference of the shell. Therefore, the beginning and ending locations of the segments where the equipment hatches and personnel airlocks are attached to the containment will be dictated by the location of these attachments. One segment was used to model the exposed portion of the bottom ellipsoidal head. Ten segments were used to model the cylindrical portion of the shell. The containment vessel ellipsoidal head was modeled using four segments. Other shell segments constitute the crane girder and hoop stiffeners. All the T-ring stiffeners and the crane girder were modeled using shell segments. This was selected instead of the discrete ring idealization option in BOSOR, since the latter is not recommended for buckling analysis [2.1]. The contribution of the radial stiffeners located inside the crane box girder and beneath the radial stiffener at Elev. 132' 3" was taken into account by adding axisymmetric diagonal shell segments that add only meridional stiffness to the containment vessel. In other words, the material of these diagonal segments was modeled as orthotopic with a non-zero elastic modulus in the meridional direction only, which was calculated so that these segments provides a stiffness equivalent to the shear stiffness of the radial stiffeners. The vertical stiffness of the radial stiffeners and the diagonal shell elements can be equated as (see Fig. 2.2),:

$$\frac{G\ t_{rs}\ h\ N}{b} = \frac{4\ \pi\ E_e\ r_{ave}\ t_e\ h^2}{L^3} \qquad (2.1)$$

where,

G	=	shear modulus
t_{rs}	=	thickness of the radial stiffener
h	=	height of the girder
L	=	length of the stiffener
b	=	width of the girder
N	=	number of plates used as stiffeners
E_e	=	equivalent Young's modulus for the shell segment
r_{ave}	=	average radius of the diagonal shell segment
t_e	=	equivalent thickness, taken to be the same as t_{rs}

A fixed support was assumed at Elev. 100' 0".

Table 2.1 lists the different shell segments and their corresponding mass densities. Weights of all attachments (Table 1.1) were distributed uniformly around the circumference of the containment vessel at the attachment locations. The total weight of the containment vessel as calculated by BOSOR program, including all attachments listed in the previous chapter, (excluding electrical and mechanical penetrations) the crane bridge and the trolley, is approximately 6,840 kips.

2.3 Individual Load Cases

The stress analysis for the dead load, crane load, uniform internal pressure, seismic wind and tornado loads and temperature are summarized in the following sections. Extreme fiber circumferential and meridional stresses as well as the circumferential and meridional stress resultants N_1 and N_2, respectively at different elevations are given. These stresses were used to check the design allowable stress limits. The stress resultants were utilized in performing the buckling analysis of the containment structure.

2.3.1 Dead Load

BOSOR4 program does not allow the user to directly specify the dead weight of a structure as an input for a stress or buckling analysis. Therefore, it is necessary that such a load be converted into pressures acting on the shell in the meridional and radial directions. Figure 2.3 indicates the meridional (N_1) and circumferential (N_2) stress resultants induced in the containment vessel under its dead weight. Figures 2.4 and 2.5 indicate the meridional ($Sigma_1$) and circumferential ($Sigma_2$) extreme fiber stresses induced in the containment vessel respectively. The maximum stresses induced in the meridional direction at the outer and inner fiber are -4950 psi and 3330 psi, respectively. The maximum stresses induced in the circumferential direction at the outer and inner fibers are -1490 psi and 1000 psi, respectively. All the maximum stresses occur at the base of the containment vessel, i.e., Elev. 100'. Notice the gradient in the meridional stresses near the containment base. This resulted from the meridional moment induced in the bottom ellipsoidal portion by the meridional stress resultant in the cylindrical portion of the shell.

2.3.2 Crane Load

As previously mentioned, the AP600 containment vessel is provided with a polar crane that is designed for lifting a load of 700 kips [2.5]. The crane bridge plus the trolley weigh 634.6 kips. The crane bridge is supported at each end on 8 wheels that transfer the reaction forces to the rail over a distance of approximately 47 ft. During plant operation, this crane is assumed to be parked at 10° Azimuth with the trolley located at one end of the crane bridge near the containment vessel as shown in Fig. 2.6. For the seismic analysis, the crane is conservatively assumed to be parked along N-S direction to add directly to the seismic stresses on the N-S meridian. The polar crane lift load is not included in the containment vessel analysis for plant operation loading conditions. In other words, the weight of the crane bridge and the trolley are the only crane loads to be considered in conjunction with the seismic loads in the vessel analysis for LOCA plus SSE.

The BOSOR4 program was utilized to calculate the stresses induced in the shell walls under the crane loads. Figure 2.7 shows a comparison between the crane vertical loads for plant operation and the Fourier expanded loads used in BOSOR program as a function of Azimuth. An 80 term Fourier expansion was used [2.6 (Sec. A.3.2)]. The stress solution was accomplished for each of the Fourier terms and the results were combined to calculate the stresses at any specified meridian caused by each load.

Figures 2.8 and 2.9 illustrate the meridional and circumferential stress resultants; respectively, on the meridians at 10°, 0°, and 90° Azimuth when the plant is in operation. As expected, stress concentrations in the shell are present in the vicinity of the crane girder (Fig. 2.8 and 2.9). The meridional stresses along the shell meridian below the crane are in compression (Fig. 2.8). However, near the crane box girder, tensile stresses are induced because the wheel loads are eccentric with respect to the shell. From Figs. 2.8 and 2.9, the meridian at 10° Azimuth is the most critical. This meridian was considered as the worst meridian for stress and buckling analysis. Figures 2.10 and 2.11 indicate the meridional and circumferential extreme fiber stresses induced in the containment vessel for the 10° Azimuth. The maximum stresses in the outer and inner fibers in the meridional direction are -2300 psi and 2410 psi, respectively. The maximum stresses in the outer and inner fibers in the circumferential direction are -1720 psi and -719 psi, respectively. The maximum stresses all occur at Elev. 208.4'.

2.3.3 Uniform Internal Pressure

The stresses induced in the AP600 steel containment vessel due to a design pressure of 45 psig were calculated using the BOSOR4 program. Figure 2.12 illustrates the meridional and circumferential stress resultant distribution along a containment vessel meridional. Remote from the stiffeners, the stress resultants in the cylindrical portion of the vessel due to the internal pressure p, were equal to those calculated using simple shell theory, i.e., pr and pr/2 in the circumferential and meridional directions, respectively. Figure 2.12 also shows that compressive stresses are induced in the knuckle region near the spring line suggesting that buckling may occur in this region under a higher pressure, e.g., an accident pressure. The analysis results due to this condition are discussed in Chapter 3. Figures 2.14 and 2.15 illustrate the extreme fiber stresses in meridional and circumferential directions. The maximum meridional stress in the outer fiber of 28,200 psi occurred at Elev. 100'. The maximum meridional stress in the inner fiber of 28,300 psi occurred at Elev. 208.4'. The maximum circumferential outer fiber stress of 24,300 psi occurred at Elev. 214.3'. The maximum circumferential inner fiber stress of 22,100 psi occurred at Elev. 111.6'.

The containment vessel stresses were also determined for an internal pressure of 1 psig and external pressures of 2.5 psid and 3.0 psid by simply scaling the stresses obtained above. This was possible since all the stresses above were in the elastic range.

2.3.4 Seismic Loading

Seismic loading results in nonaxisymmetric stresses. The mass due to the various penetrations, the attachments listed in Table 1.1, and the crane are smeared axisymetrically in the seismic model, since BOSOR4 can only accept axisymmetric mass. The mass density of each of the shell segments used in the BOSOR model is shown in Table 2.1.

A response spectrum analysis of the structure for a base excitation was performed by combining the modal responses to calculate the system maximum response. One approach to calculate the maximum response or stress quantity, R_{max}, for a particular response quantity is to combine the modal responses utilizing the SRSS method and to consider the effect of closely spaced frequencies on the overall response [2.7, 2.8, 2.9, 2.10 and 2.11]. Reference 2.11 suggests that modes should be considered to be closely spaced if their frequencies differ by less than 10 percent. The modified maximum SRSS response, R_{max}, caused by seismic excitations in the X, Y, Z directions can be calculated as:

$$R_{\max} = \left[\sum_{k=1}^{3} \left(\sum_{j=1}^{m} R_{kj}^{2} + 2 \sum_{l=1}^{p} \sum_{y=1}^{p} | R_{ky} \; R_{kl} | \right) \right]^{1/2} \tag{2.2}$$

where m is the number of modes considered in each direction (equal to 30 modes in this analysis), p is the number of closely spaced frequencies and k corresponds to the directions X, Y, and Z. Equations similar to Eq. 2.2 can be used to calculate maximum displacements, stresses, and stress resultants.

Figure 2.16 illustrates the SSE response spectra at El. 100'-0 [2.12] used herein to calculate seismic stresses. Two horizontal (North-South and East-West) and one vertical spectra are shown. The SSE response spectra were used to predict the seismic stress resultants at several different circumferential locations. The modal quantities were determined by performing a vibration analysis of the containment vessel using the BOSOR4 program. Figures 2.17 and 2.18 indicate the first four vertical modes and the first four horizontal modes, respectively. Tables 2.2 and 2.3 indicate the percentage of effective modal mass in the vertical modes and horizontal modes, respectively as represented by the number of modes considered in the seismic model.

The SRSS meridional and circumferential stress resultants, N_{1max} and N_{2max}, for the perfect shell are shown in Figs. 2.19 and 2.20, respectively. Note that these stress resultants are the same for all meridians since the North-South and East-West spectrum are identical (see Fig. 2.16). Figures 2.21, 2.22 and 2.23 illustrate the SRSS extreme fiber meridional, circumferential and shear stresses for the worst meridian. The maximum meridional stress in the outer fiber of 15,023 psi occurred at Elev. 100'. The maximum meridional stress in the inner fiber of 10,202 psi occurred at Elev. 100'. The maximum circumferential outer fiber stress of 4,507 psi occurred at Elev. 100'. The maximum circumferential inner fiber stress of 3,060 psi occurred at Elev. 100'. The maximum shear stress in the outer fiber of 1,573 psi occurred at Elev. 100.8'. The maximum shear stress in the inner fiber of 1571 psi occurred at Elev. 100'.

2.3.5 Wind and Tornado Loading

Even though a shield building surrounds the containment vessel, the containment vessel can experience wind effects through the air inlets used for passively cooling the containment vessel. To better understand the air flow and wind pressure distribution, Westinghouse sponsored several wind tunnel tests on a small scale model of the AP600 containment vessel and the surrounding buildings [2.13 and 2.14]. Pressure taps were mounted to measure the pressures around the containment vessel annulus, in the shield building annulus and the differential pressures on the air baffle between the containment vessel and the shield building at different levels as shown in Fig. 2.24. These results were expressed in the form of pressure coefficients. Reference [2.13] summarizes the results of the Phase II tests performed at the University of Western Ontario for a wide range of wind speeds and incident directions. The Phase IVa [2.14] report indicates the tests performed at the University of Western Ontario and National Research Council, Canada to ascertain the effects of Reynold's number and blockage of wind flow due to the cooling tower. Appendix C of [2.14] summarizes the test results and is used herein as the basis to determine the wind load cases. Over the time period of each test, maximum, minimum and mean pressure coefficients, C_p, were measured at each tap location. The pressure coefficients can be utilized to determine the wind pressure [2.14]:

$$p_r = C_p \, q_{roof} \tag{2.3}$$

$$q_{roof} = 0.5 \, I \, \rho \, v^2 \tag{2.4}$$

where,

p_r = wind pressure
C_p = wind pressure coefficient
q_{roof} = dynamic wind pressure at roof height
I = importance factor
ρ = density of air
v = mean hourly wind speed for the design wind velocity

The method of determining the dynamic wind pressure at roof height is discussed in Appendix D of [2.13] and is based on the ASCE Code methodology [2.15]. It is dependent upon an exposure coefficient for the terrain in which the building is situated, an importance factor based on the nature of occupancy and classification of the structure, and a gust response factor to convert the fastest wind speed to a mean hourly wind speed. The dynamic wind pressures for AP600 are 38.2 psf and 116 psf corresponding to the highest wind speed of 110 mph and to a tornado with wind speed of 300 mph, respectively.

Figure 2.24 is a sketch showing the location of the pressure taps. Table 2.4 indicates the pressure coefficients determined at Taps 141 to 148 (see Appendix C [2-14]), which are at Level 5 (the containment vessel roof) for a wind from 315° Azimuth. The pressure coefficient of -3.66 at Tap 145 is the maximum absolute value recorded in the report (the negative sign indicates suction). The pressure coefficients for other levels and wind Azimuths were lower. Table 2.4 also lists the wind pressures for the design wind and tornado conditions (Eq. 2.3). Figure 2.25 indicates, in plan, the distribution of wind pressures at Level 5 from Table 2.4 for the design wind. It should be noted that the recorded pressure coefficients are the peak values which occur during the time of the test and do not imply simultaneous occurrence. However, the following two load scenarios are developed based on Fig. 2.25. First, a net uniform suction on the containment vessel consisting of a uniform pressure of 1.0 psig (3.1 psig for tornado) around the containment vessel is conservative and bounds all the test results (Fig. 2.26). The second case is the net lateral load condition which produces the largest overturning moment, consisting of uniform pressure 1.0 psig (3.1 psig for tornado) on one half of the containment vessel acting only between the 145° Azimuth and 325° Azimuth (Fig. 2.27).

The net suction on the containment vessel is similar to a uniform internal pressures. For the uniform pressure of 1.0 psig case, Figure 2.28 illustrates the stress resultants induced in the containment vessel. Figures 2.29 and 2.30 illustrate the extreme fiber stresses in the meridional and circumferential directions. The maximum meridional stress in the outer fiber of 1,480 psi occurred at Elev. 100'. The maximum meridional stress in the inner fiber of -999 psi occurred at Elev. 100'. The maximum circumferential outer fiber stress of 539 psi occurred at Elev. 214.3'. Maximum circumferential inner fiber stress of 491 psi occurred at Elev. 150.5'. The analysis is repeated for application of internal pressure of 3.1 psig.

The nonaxisymmetric wind lateral load condition, shown in Fig. 2.27, was analyzed using the INDIC = 4 analysis option of BOSOR4. The load is input as a function of the circumferential angle and expanded as a sum of Fourier harmonics [2.6 (Sec. A.3.1)]. Eighty circumferential waves were used to achieve this expanded load function. The results of the analysis are illustrated on two meridians corresponding to the 235° Azimuth and 55° Azimuth i.e., along the vertical plane of symmetry where the maximum tensile and compressive meridional stresses occur. Figures 2.31, 2.32 and 2.33 illustrate the stress resultants and the extreme fiber stresses in meridional and circumferential directions on the 235° Azimuth, respectively. The maximum meridional stress in the outer fiber of -2,380 psi occurred at Elev. 100'. The maximum meridional stress in the inner fiber of 1,600 psi occurred at Elev. 100'. The maximum circumferential outer fiber stress of -713 psi occurred at Elev. 100'. Maximum circumferential inner fiber stress of 603 psi occurred at Elev. 256'. Figures 2.34, 2.35 and 2.36 illustrate the stress resultants and the extreme fiber stresses in meridional and circumferential directions on the 55° Azimuth, respectively. The maximum meridional stress in the outer fiber of 3860 psi occurred at Elev. 100'. The maximum meridional stress in the inner fiber of -2,600 psi occurred at Elev. 100'. The maximum circumferential outer fiber stress of 1160 psi occurred at Elev. 100'. Maximum circumferential inner fiber stress of -781 psi occurred at Elev. 100'.

2.3.6 Temperature

Two temperature conditions are analyzed for the AP600 containment vessel: (1) a design accident temperature of 280°F; and (2) an operating temperature of 120°F [2.16]. The containment vessel ambient temperature was assumed to be at 70°F.

The 120°F condition does not activate the emergency cooling system and, hence, the temperature is assumed to be uniform throughout the containment vessel.

Three cases are defined to analyze the design basis accident which produces the temperature condition of 280°F.

Case 1 assumes that the containment vessel is subjected to a uniform temperature of 280°F, i.e., malfunctioning of the passive containment cooling system. Figure 2.37 illustrates the stress resultants in the meridional and circumferential directions. Figures 2.38 and 2.39 illustrate the extreme fiber stresses in meridional and circumferential directions. The maximum meridional stress in the outer fiber of -62,100 psi occurred at Elev. 100'. The maximum meridional stress in the inner fiber of 62,600 psi occurred at Elev. 100'. The maximum circumferential outer fiber stress of -54,300 psi occurred at Elev. 100'. Maximum circumferential inner fiber stress of -24,300 psi occurred at Elev. 100.8'. Note that high compressive circumferential stress resultants occur near the base.

In the accident scenarios for Cases 2 and 3, the containment vessel emergency cooling system is activated letting water flow on the top of the containment vessel dome and down the vessel walls to an Elev. 132' 3" to cool the vessel. Tests simulating this scenario showed that the flowing water or wet area covered about 70% of the surface and that the dry areas could have a maximum width of about 15 inches [2.17]. The test analysis also showed a maximum difference in temperature between the wet and dry regions of 68°F.

In Case 2, the temperature difference between the wet and dry zones was assumed to be 80°F, providing some margin above the maximum difference obtained from the test. The test results indicated that the wet and dry regions could be as narrow as 34 in. and 15 in., respectively. However, in this work, alternating strips of wet (68 in. at 200°F) and dry (30 in. at 280°F) regions were used around the circumference as shown in Fig. 2.40. This was the smallest width that can be used due to the limitation of the Fourier subroutine in the BOSOR4 program which can accommodate only a maximum input of a 100 points along the circumference. A uniform temperature of 280°F was employed below Elev. 132' 3". Figures 2.41 and 2.42 indicate the stress resultants in meridional and circumferential directions on the meridians in the center of the dry and wet zones. Figures 2.43 and 2.44 illustrate extreme fiber meridional and circumferential stresses corresponding to the meridian in the center of the dry region. Figures 2.45 and 2.46 illustrate the extreme fiber meridional and circumferential stresses corresponding to a meridian in the center of the wet region. The maximum stresses calculated in both the cases are at the base of the structure and identical to those calculated in Case 1. Note, however, that meridional compression does occur in the dry zone, i.e., a compressive stress resultant of 10.8 k/in. A more comprehensive analysis using a 3-D finite element model with other widths of wet and dry strips is conducted in Ref. [2.18]. In addition, Ref. [2.18] summarizes a solution that utilizes a strength of material approach to calculate the stress induced in two parallel wet and dry strips. The results obtained from the simple model is consistent with the stresses summarized above.

Figure 2.47 illustrates the circumferential variation of temperature used in Case 3 which is similar to Case 2, except it incorporates a temperature gradient through the thickness of 30°F in the dry region of the cylinder. The temperature gradient used herein corresponds to that recorded in the test results summarized in Ref. [2.19]. This case was analyzed to investigate the effects of a through-the-shell-thickness temperature gradient on the meridional and circumferential stress resultants and hence its effects on the containment shell buckling strength. The results of this case was also compared with those of Case 2 above to determine the critical case to be used in the 3-D analysis conducted in Ref. [2.18]. As with Case 2, temperature below Elev. 132' 3" was assumed to be at 280°F. The distribution in Fig. 2.47 can be modeled as a superposition of two analyses. The first, incorporating no temperature gradient through the containment shell walls and the second, incorporating a temperature gradient of 30°F. Figures 2.48 and 2.49 indicate the stress resultants in the meridional and circumferential directions on the meridians at the center of the wet and dry regions, respectively. Figures 2.50 and 2.51 illustrate extreme fiber meridional and circumferential stresses on the meridian in the center of the dry region, respectively. Figures 2.52 and 2.53 illustrate extreme fiber meridional and circumferential stresses on the meridian in the center of the wet region, respectively. The maximum stresses recorded in both Case 2 and 3 are at the base of the structure. Case 3 stresses in the striping region are less than those of Case 2.

2.4 Combination of Stresses

Section 1.3 of SRP Section 3.8.2 [2.2] stipulates that the design loading combinations be in compliance with Subsection NE, Section III, Division 1 of the ASME Code [2.21] and Regulatory Guide 1.57 [2.20]. Table 2.5 defines the load combinations used in the analysis. Tables 2.6 to 2.9 indicate the stress intensities for the load combinations as defined in Table 2.5 as compared to the allowable stress intensities for the Design Conditions and Service Levels A, C, and D as per Subsection NE of the ASME Code [2.3 (Table NE3221.1)]. The Allowable Stresses depend upon the stress classification, i.e., primary or secondary as shown in Table 2.10. Table 2.10 also defines the nomenclature used in Tables 2.6 to 2.9.

2.5 Summary

The axisymmetric stress analysis showed that no violation of the allowable stress intensity occurred.

2.6 References

2.1 Bushnell, D., "BOSOR4 Program for Stress, Buckling and Vibration of Complex Shells of Revolution," Structural Mechanics Laboratory, Lockheed Missiles and Space Co., Inc., Palo Alto, CA (1975).

2.2 "U.S. NRC Standard Review Plan (SRP) Section 3.8.2," Rev. 1 -- July 1981, pp. 3.8.2.9 - 2.8.2.11.

2.3 American Society of Mechanical Engineers, Boiler and Pressure Vessel Code, Section NE3220, 1989.

2.4 Castello, J. E., Orr, R. S., and Mandava, P. R., "Westinghouse AP600 Design Criteria Manual," Document ID:GWC1 001, RVV.0, April 1993.

2.5 Letter to NRC from N. J. Liparulo, "Polar Crane Loads on the Containment Vessel," July 20, 1994.

2.6 L. Greimann et. al., "System 80+TM Containment -- Structural Design Review," NUREG/CR 5957, NRC, Washington, D.C., May 1993.

2.7 Clough, R. W. and Penzien, T., Dynamics of Structures, New York, McGraw Hill, 1964.

2.8 Biggs, J. M., Introduction to Structural Dynamics, New York, McGraw Hill, 1964.

2.9 Venmarcke, E. H., "Structural Response to Earthquakes," Chapter 8, Seismic Risk and Engineering Decisions, B. C. Lominitz and E. Rosenbluth, Editors, Elsevier Publishing Co., 1976.

2.10 Wilson, E. L., Kiureghuian, A., and Bayo, E. P., "A Replacement for the SRSS Method in Seismic Analysis," Earthquake Engineering and Structural Dynamics, University of California, Berkeley, Vol. 9, No. 2, March 1981.

2.11 American Society of Civil Engineers, Manuals and Reports on Engineering Practice No. 58, Structural Analysis and Design of Nuclear Plant Facilities, 1980.

2.12 "Floor Response Spectra at the Base of the Containment Vessel," a Facsimile message from Tom Cheng - U.S. NRC to Lowell Greimann, Ames Laboratory, transmitted on April 19, 1995.

2.13 Lyth, G. R. and Surry, D., "Phase II Wind Tunnel Testing for the Westinghouse AP600 Reactor," Report No. WCAP-13323, May 1992.

2.14 Lyth, G. R. Surry, D., "Phase IVa Wind Tunnel Testing for the Westinghouse AP600 Reactor," Report No. 14068, 1994.

2.15 American Society of Civil Engineers, Minimum Design Loads for Buildings and Other Structures, ASCE 7-88, ASCE, New York, New York. 1994.

2.16 Gilmore, J. E., "AP600 Passive Containment Cooling System -- Phase II -- Test Data Report," WCAP-13296, March 1992.

2.17 "AP600 Standard Safety Analysis Report," document prepared for U.S. NRC, San Francisco Operations Office, Westinghouse Electric Corporation. Revision 3, Sec. 3.8.2.1.1, May 31, 1995.

2.18 L. Greimann et. al., "Three-dimensional Buckling Analysis for the AP600 Standard Plant Containment Vessel," NUREG-CR/6461, final report to NRC, Washington, D.C., publication pending Oct. 1995.

2.19 McDermott, D., "Passive Containment Cooling System," Presented to NRC and Ames Laboratory Personnel, March 28, 1994.

2.20 Regulatory Guide 1.57, "Design Limits and Loading Combinations for Metal Primary Reactor Containment System Components." NRC, Washington, D.C., June 1973.

2.21 American Society of Mechanical Engineers, Boiler and Pressure Vessel Code, Section NE3222, 1989.

This page left intentionally blank.

3. BUCKLING ANALYSIS

3.1 Analysis Approach

The axisymmetric buckling analysis of the AP600 containment vessel was performed by using the BOSOR5 program [3.1]. The BOSOR5 program was developed from the BOSOR4 program and is designed for axisymmetric stress analysis and buckling analyses. In addition, BOSOR5 can handle nonlinear material behavior.

When BOSOR5 is used for buckling analysis, the circumferential variation of the stress resultants is not permitted. Hence, the worst meridian analysis approach is used to analyze a nonsymmetrically loaded shells [3.2 and 3.3]. Sections 1330 and 1720 of ASME Code Case N-284 recommends the assumption of uniform stress distribution around the circumference adopted in this approach [3.4]. In order to identify the worst meridian for the buckling analysis, several meridians must be examined and the worst meridian is identified as the one with the highest stress resultants. In BOSOR4, the analysis is completed by considering the worst meridian stress resultant to be distributed uniformly around the entire circumference. In BOSOR5 direct input of stress resultants is not permitted, and the worst meridian stress resultants must be converted into equivalent axisymmetric pressures for the buckling analysis [3.5 (Appendix C)].

This section summarizes the buckling analysis results for the AP600 containment vessel. The analysis was performed to determine the buckling factors of safety for Design Conditions and Service Levels A, C, and D. The minimum predicted buckling load was determined by introducing geometric imperfections and material nonlinearities into the analysis. The geometric imperfection is modeled as an axisymmetric sinusoidal wave [3.5 (Sec. 3.3 and Sec. A.3.4)] with a wave length, L_K expressed in terms of the radius, r, and thickness of the shell, t, as:

$$L_K = K\sqrt{rt} \tag{3.1}$$

where K is the imperfection wavelength parameter [3.5 (Sec. 3.3)]. An imperfection sensitivity analysis is performed by varying K to achieve the minimum buckling load. A radial imperfection amplitude equals to half the containment wall thickness, i.e., 0.8125 in. was used which corresponds to the ASME Code specified maximum deviation of one shell thickness (1.625 in.) [3.5 (Sec. A.3.4) and 3.6 (Note 7)].

The material imperfections caused by residual stresses were incorporated by using the stress strain curves as shown in Fig. 3.1 or Fig. 3.2. These stress-strain relationships were derived from the plasticity equations in the ASME Code Case N-284 and the material properties of the AP600 containment shell corresponding to temperatures of 280°F and 120°F. The yield strength of the AS537 Class 2 steel to be used in the AP600 containment has a yield strength of 59 ksi and a Young's modulus of 29.23 ksi at a temperature of 120°F and 52.76 ksi and Young's modulus of 27.4 ksi at a temperature of 280°F. These are the temperature relevant to the load combination (Table 2.5).

3.2 Loading and Solution Process

The theory on which the BOSOR [3.1] is based does not exclude the possibility that several values of circumferential wave number, n, may be associated with the minimum buckling loads. Therefore, one must always check if the minimum buckling load is calculated. This can be accomplished by assuming an initial buckling circumferential wave number, NOB and calculate the stability determinate for a sequence of load steps for which a prebuckling stress analyses are carried out. The BOSOR manual [3.1] provides the user with some formula that can be used to approximately estimate this number of circumferential waves. However, it is recommended that several trials must be carried out to investigate the buckling load associated with other assumed values of circumferential waves to insure that the least buckling load has been achieved.

In BOSOR, the load is applied in increments as a load-time relationship. Time is only used to describe the loading sequence as well as the load increment size to be used in the analysis. The buckling analysis consists of prebuckling and eign buckling stages. During the prebuckling stage, an axisymmetric analysis is performed at each load level.

The BOSOR program calculates the stability determinate corresponds to the specified NOB. Buckling occurs when the sign of the stability determinate is changed between two consecutive load steps. In this case, the BOSOR program will calculate the bifurcation buckling loads for a range of circumferential wave numbers that are specified by the user. This will insure calculating the minimum buckling load.

In this work, the critical load, P_{cr}, is defined as the minimum of the load at which instability occurs or the load at which an axisymmetric collapse occurs. The latter is the load corresponding to a circumferential wave number equal to zero. The ratio, λ, of the critical load to the applied load is used herein as an indication of the buckling factor of safety.

The different stresses to be considered in the buckling analysis are the nonaxisymmetric stresses due to the crane loading and seismic loading and the axisymmetric stresses due to the self weight of the structure, external and internal pressures and temperature loads. As mentioned in Sec. 3.1, BOSOR5 does not permit circumferential variations in stress resultants. Hence, the stress resultants on the worst meridian are considered to be uniform around the circumference. A set of equivalent loads must be generated which produce axisymmetric stress resultants equal to those on the worst meridian [3.5 (Appendix C)].

For the crane loading under operating conditions, the 10° Azimuth was determined to be the worst meridian as shown in Fig. 2.8 and Fig. 2.9. A set of equivalent axisymmetric ring loads were generated by considering the stress resultants caused by the crane loads at discrete points and converting them into ring loads. These equivalent ring loads are applied at discrete points on the containment vessel shell. Figures 3.3 and 3.4 are a comparison between the stress resultants on the worst meridian and those produced by the equivalent ring loads. The sinusoidal type variation in Fig. 3.4 is caused by the sinusoidal geometric imperfection. The self weight of the containment vessel was also modeled by a set of ring loads. These loads were generated by considering the weight density of the segment and the contributory area at each mesh point.

For the seismic loading, the equivalent axisymmetric pressures were determined with meridional and circumferential stress resultants in either: (1) compression and tension, respectively, or (2) tension and compression, respectively. Both the meridional and circumferential stresses can not be in compression at the same time since this would be incompatible with the modal quantities. For example, Fig. 3.5 illustrates that the meridional and circumferential stress resultants for the first horizontal mode of vibration are different in sign. The sinusoidal type variation of the circumferential stress resultants in Fig. 3.5 is caused by the sinusoidal geometric imperfection. The equivalent axisymmetric pressures are generated by software that was developed by the authors. This software was also used to determine the equivalent pressures for the wind lateral load (Sec. 2.3.5).

Based on the relevant Load Combinations (Table 2.3), the self weight, internal or external pressure and temperature loads are added to the equivalent axisymmetric pressures and input directly into BOSOR5 for analysis.

3.3 Design Conditions and Level A Service Limits

(a) Load Combinations DG1 and DBA1

Load Combination DG1 and DBA1 both consist of internal pressure of 45 psig and a nominal temperature of 280°F (Table 2.5). As discussed earlier (Sec. 2.3.6), the temperature loading for Load Combination DBA1 was idealized by three cases.

(1) Case 1, Uniform temperature

For the uniform temperature case (Case 1), Fig. 3.6 indicates the meridional (N_1) and circumferential (N_2) stress resultants from an elastic analysis corresponding to a load multiplier of 1.0. Two zones of compressive stress can be identified: the first at the knuckle region of the top ellipsoidal head caused primarily by internal pressure and the second at the base caused by constricted thermal expansion.

The perfect containment vessel was analyzed by considering the self weight of the structure and crane in addition to internal pressure and temperature loads. The material stress strain curve corresponding to a temperature of 280°F is used (Fig. 3.2). The analysis illustrated that gross tensile yielding in the cylindrical region was reached at a load multiplier of 3.12. The deformed shape of the containment vessel is as shown in Fig. 3.7. The analysis was repeated with a sinusoidal imperfection with a peak to trough amplitude of 1.625 in. and a wavelength of 139.7 in. corresponding to an imperfection wave length parameter, K, of 4 (Eq. 3.1). The load multiplier associated the gross yielding mode was 3.1. Hence, the gross yielding mode not sensitive to imperfections.

To investigate the possibility of buckling of the AP600 upper ellipsoidal head, the containment vessel head was isolated from the cylindrical portion and analyzed for two loadings: internal pressure alone and the DBA1 loading combination. The axisymmetric model of the top ellipsoidal head is shown in Fig. 3.8. The model consists of 5 segments and 74 elements. This corresponds to the mesh used in all analyses of the containment vessel. The head is restrained in all directions except in the radial direction at the base. For the internal pressure only case, an elastic-perfectly plastic stress strain curve (σ_y = 60,000 psi and E = 29,500,000 psi) was used and a perfect geometry was assumed. Buckling of the head was detected at an internal pressure of 171 psig. The number of circumferential waves in the buckled shape, n, was 33. A mesh sensitivity study was performed by considering two more models of the head, with twice (148) and four times (296) the number of elements. No significant change was observed in the buckling load. The buckled shape of the head is shown in Fig. 3.9. From Fig. 3.9, the wavelength of the buckle corresponds to an imperfection wavelength parameter, K, of approximately 10.4 (Eq. 3.1).

The analysis (elastic - perfectly plastic material) was repeated by considering sinusoidal imperfections with the wave lengths ranging from 70.4 in. (K of 2.0) to 498.7 in.(K of 14.0). The minimum buckling load was determined to be 164 psig corresponding to a K of 13.5.

The isolated upper ellipsoidal head was further analyzed for the DBA1 loading combination. The material stress strain curve corresponding to a temperature of 280°F (Fig. 3.2) was used. A perfect geometry was initially assumed. The buckling factor of safety was determined to be 3.62. The buckled shape of the head is as shown in Fig. 3.10. The number of circumferential waves in the buckled mode, n, was 35. The analysis was repeated with a sinusoidal imperfection of wave length 480.5 in. (K of 13.5) yielding a minimum buckling factor of 3.52 with the number of circumferential waves in the buckled mode, n, equal to 35. Hence, it can be concluded that geometric imperfection has an insignificant effect on the head buckling strength.

In order to investigate the buckling of the lower ellipsoidal head due to the restraint offered by the base under temperature loading, it was isolated from the cylindrical portion and analyzed under the DBA1 loading combination. Two different material properties were considered: elastic and the stress strain curve in Fig. 3.2. The axisymmetric model of the lower ellipsoidal head is shown in Fig.

3.11. The meridional stress resultant of 17600 lb/in applied at the top of the model corresponds to 45 psig internal pressure. The top of the model was restrained against rotation and radial movements.

For the elastic case, a perfect geometry was initially assumed. Buckling of the lower head was detected at a load multiplier of 9.0. The buckled shape of the structure is shown in Fig. 3.12 with the number of circumferential waves, n, equal to 80. The wavelength of the buckle corresponds to an imperfection wavelength parameter, K, of 4.0 (Eq. 3.1). The elastic analysis was repeated by performing a sensitivity study with regard to wavelength. The minimum buckling load multiplier was determined to be 8.6, corresponding to a wavelength of 160.3 in. (K of 4.5).
The isolated lower ellipsoidal head was further analyzed using the stress strain curve in Fig. 3.2. Initially, a perfect geometry was assumed. No buckling was detected before a gross yielding at the containment base was reached at a load multiplier of 5.30. The analysis was repeated by incorporating the geometric imperfection and by performing a sensitivity study with regard to wavelength. The minimum load multiplier was determined to be 4.9, corresponding to a wavelength of 160.3 in. (K of 4.5) and was associated with gross yield at the base of the containment vessel. The deformed shape of the head is as shown in Fig. 3.13.

In summary, the minimum factor of safety for load combinations DBA1 and DG1 was 3.10 and was associated with the general tensile yield of the cylinder. The maximum effective uniaxial surface strain corresponding to this factor was 0.387%. The two factors of safety associated with the upper and lower ellipsoidal heads were 3.52 and 4.90, respectively, and do not control.

(2) Case 2 and Case 3 (Temperature Striping Conditions)

The results of the stress analysis due to striping is discussed in Sec. 2.3.6. Compressive meridional (N_1) stress resultants of Case 2 and Case 3 are compared in Fig. 3.14. From the figures, it can be concluded that Case 2 is conservative and bounds Case 3 results. An axisymmetric buckling analysis of these cases is not reasonable, although it could be performed by the worst meridian approach, i.e., by assuming that the compressive stresses in the dry region exist uniformly around the circumference. Since the stresses vary quite rapidly from the dry meridian to the wet meridian, the analysis would be too conservative. Buckling of the containment under striping will be addressed in Ref. [3.7] with the three-dimensional model.

(b) Load Combinations DG2 and DBA2

Load Combinations DG2 and DBA2 both consist of an external pressure of 2.5 psig and a nominal temperature of 120°F (Table 2.5). The minimum buckling factor of safety is determined to be 3.03 corresponding to an imperfection wave length of 139.7 in. (K=4.0). The buckled shape of the containment vessel is shown in Fig. 3.15. Buckling occurs between the upper and lower stiffeners with the number of circumferential waves, n, equal to 14.

The pressure associated with buckling is 3.03 times 2.5 psig or 7.58 psig. Using ASME Code case N-284 [2.3], the predicted buckling pressure is equal to the classical buckling pressure (9.50 psig) times the capacity reduction factor (0.8) times the plasticity reduction factor (1.0) or 7.60 psig. This compares favorably.

(c) Load Combination OC1

The Load Combination OC1 consists of internal pressure of 1.0 psig, temperature of 120°F and lateral load due to a design wind velocity of 110 mph. The minimum factor of safety is determined to be 7.10 and was controlled by gross yield at the base. This was corresponding to an imperfection wave length of 108.3 in. (K of 3). The deformed shape of the structure is shown in Fig. 3.16.

3.4 Level C and Level D Service Limits

Level C and Level D have the same load combinations as per SRP Section 3.8.2 [3.8] (Table 2.5) but different allowable factors of safety (Table 1.2). As Level C has a larger factor of safety requirement, it will control over Level D. The analysis for the cases involving seismic loading was performed with the meridional stress resultants in compression and the circumferential stress resultants in tension (Sec. 3.2).

(a) Load Combination OC2

The Load Combination OC2 consists of internal pressure of 1.0 psig, temperature of 120°F and SSE loading. The minimum factor of safety was determined to be 3.8 corresponding to an imperfection wave length of 125.2 in. (K of 3.5) and was controlled by gross yielding at the containment base . The deformed shape of the structure is shown in Fig. 3.17.

(b) Load Combination OC3

The Load Combination OC3 consists of internal pressure of 1.0 psig, temperature of 120°F and lateral load due to a tornado of design wind velocity of 300 mph. The minimum factor of safety is determined to be 5.20 corresponding to an imperfection wavelength of 125.2 in. (K of 3.5). This was controlled by gross yielding at the containment base. The deformed shape of the structure is shown in Fig. 3.18.

(c) Load Combination DBA3

The Load Combination DBA3 consists of internal pressure of 45.0 psig, temperature of 280°F and SSE loading. The minimum buckling factor of safety is determined to be 3.20 corresponding to an imperfection wave length of 125.2 in. (K of 3.5). This was controlled by gross yielding in the region of the cylindrical portion. The deformed shape of the structure is shown in Fig. 3.19.

(d) Load Combination DBA4

The Load Combination DBA4 consists of external pressure of 3.0 psig, temperature of 120°F and SSE loading. The minimum buckling factor of safety is determined to be 2.02 corresponding to an imperfection wave length of 139.7 in. (K of 4). For this controlling load case, the variation of the effective uniaxial strain at the extreme fiber at the El. 100.0' is shown in Fig. 3.20. Note that the effective strain is well above the proportional limit. Hence, the buckling of the containment vessel is not elastic. The buckled shape of the containment vessel is shown in Fig. 3.21. The number of circumferential waves in the buckled shape, n, is 13. The buckled shape indicates that the buckling is local in nature and is affected by the presence of the stiffeners.

3.5 Summary of Buckling Analysis

The allowable factors of safety against buckling prescribed in Section NE 3222.2 of the ASME Code are listed in Table 1.2. The calculated buckling factors of safety are summarized in Table 3.1. The buckling factors of safety for all Design Conditions and Service Levels A, C, and D satisfy the requirements as prescribed in Section NE 3222.2 of the ASME Code, except for Load Combination DBA4. The calculated factor of safety for Service Level C, Load Combination DBA4, is 2.02 which does not satisfy NE 3222.2. All load combinations satisfy the ASME Code Case N-284 criteria. Regulatory Guide 1.57 is also satisfied.

3.6 References

3.1 Bushnell, D., "BOSOR5 Program for Buckling of Elastic-Plastic Complex Shells of Revolution Including Large Deflections and Creep," Structural Mechanics Laboratory, Lockheed Missiles and Space Co., Inc., Palo Alto, CA.

3.2 Bushnell, D., "Plastic Buckling of Various Shells," Joint ASCE/ASME Mechanics Conference, Boulder, CO, June 21-29, 1981.

3.3 Bushnell D., and Smith, S., "Stress and Buckling on Nonuniformally Heated Cylindrical and Conical Shells," AIAA Journal, 9(12), pp. 2314-2321, Dec. 1971.

3.4 "American Society of Mechanical Engineering, Boiler and Pressure Vessel Code Case N-284," Supplement #2 to Nuclear Code Book, 1980.

3.5 L. Greimann et. al., "System 80^{+TM} Containment -- Structural Design Review," NUREG/CR 5957, Washington, D.C., May 1993.

3.6 Regulatory Guide 1.57, "Design Limits and Loading Combinations for Metal Primary Reactor Containment System Components." NRC, Washington, June 1973.

3.7 L. Greimann et. al., "Three-dimensional Buckling Analysis for the AP600 Standard Plant Containment Vessel," NUREG-CR/6461, final report to NRC, Washington, D.C., publication pending Oct. 1995.

3.8 "U.S. NRC Standard Review Plan (SRP) Section 3.8.2," Rev. 1 -- July 1981, pp. 3.8.2.9 - 2.8.2.11.

4. SEISMIC LIMIT ANALYSIS

There is a small probability that the containment vessel could experience seismic loading beyond the SSE. The containment vessel seismic performance, beyond the design earthquake, was evaluated by increasing the seismic loading beyond SSE with constant sustained loads such as dead weights.

4.1 Loading and Solution Process

The loading and solution process for the buckling analysis of the containment vessel is summarized in Section 3.2. The buckling factor, Λ, is defined as the ratio between the SSE loads and the seismic loads which cause buckling. The dead load, including the crane, is also applied and held constant. No other loads are applied. Hence, the net load on the structure, L, is the sum of factored SSE loads and the dead load (including crane), D.

$$L = D + \Lambda\,(SSE) \tag{4.1}$$

4.2 Buckling Analysis

The containment vessel is initially loaded with SSE loading and the dead weight of the structure. Geometric imperfections are introduced into the analysis and an imperfection sensitivity analysis is performed by varying the imperfection wavelength parameter, K (Eq. 3.1). The imperfection is modeled as a sinusoidal wave with a radial imperfection amplitude of 0.8125 in. The material stress strain curve in Fig. 3.1 was used. The seismic loading was increased by the factor, Λ, until buckling occurred at a load multiplier of 4.60 with an imperfection wavelength of 139.7 in. (K of 4). The variation of the effective uniaxial strain at the extreme fiber at the Elev. 100.0 ft. is shown in Fig. 4.1. The buckled shape of the containment vessel is shown in Fig. 4.2. The number of circumferential waves in the buckled shape, n, is 16. The buckled shape indicates that the buckling is local in nature and occurs between the base and the lower stiffener.

This page left intentionally blank.

5. SUMMARY AND CONCLUSIONS

5.1 Summary

The objective of the present work is to review the design adequacy of the Westinghouse AP600 Containment vessel. An analysis was performed to check stress levels against the ASME Code requirements. The adequacy of the structure design against buckling was reviewed using finite difference analysis software for axisymmetric shells.

The Westinghouse AP600 Containment vessel is a cylindrical steel shell structure with an inner radius of 65 ft. and a wall thickness of 1.625 in. The cylindrical vessel is topped by an ellipsoidal head. The bottom is enclosed by another ellipsoidal head embedded into a concrete foundation at base. The cylindrical portion of the containment vessel is provided with two T-ring stiffeners and one box-girder stiffener. A crane bridge and a trolley, for fuel handling purposes, are mounted on the box-girder stiffener. Two equipment hatches and two personnel locks constitute the major penetrations located at different elevations in the containment vessel. The containment air baffle, walkway, HVAC duct, cable trays, concrete on external stiffener and the containment vessel recirculation unit platform constitute the major appurtenances. The material used in the construction is Type SA 537 class 2 steel.

SRP 3.8.2 stipulates that the design and analysis procedures be in compliance with the ASME Code and Regulatory Guide 1-57. Loadings on the structure include dead loads inclusive of crane loads, wind and tornado loads, internal and external pressures, temperature, and seismic loading in the form of earthquake spectra. SRP 3.8.2 further prescribes the load combinations pertaining to Design Conditions and Service Limits A, C, and D as classified by the ASME Code. Section NE3222.1 of the Code establishes the admissible factors of safety against buckling for Design Conditions and Service Levels A, C, and D.

The numerical analysis was performed with the BOSOR4 and BOSOR5 finite difference software. The Westinghouse AP600 Containment vessel was modeled as an axisymmetric shell consisting of different segments and mesh points. The starting and ending of each segment in the cylindrical portion of the containment were dictated by the locations of the penetrations, the location of the stiffeners and the appurtenances. The additional mass of the penetrations and the appurtenance was smeared around the circumference.

The stresses due to the individual loads were computed using the stress analysis option in BOSOR4. The nonsymmetric loadings were modeled using the Fourier expansion option in BOSOR4. Wind pressures were identified based on the absolute maximum values recorded in the test reports supplied by the Westinghouse Corporation and were modeled in the form of axisymmetric uniform suction and nonaxisymmetric net lateral load on the structure. The seismic loading to the structure was in the peak-broaden form of the earthquake response spectra supplied by the Westinghouse through the NRC channels.

The modal stress quantities were combined by the SRSS method. Seismic stresses for several meridians were compared to select the controlling meridian for the seismic case. The stresses from individual loads and seismic event were combined according to SRP 3.8.2 into stress intensities and were found to satisfy the allowable limits.

The buckling analysis, for each individual load combination, was accomplished using the BOSOR5 program. The buckling assessment was performed by using the worst meridian assumption; that is, the stresses on the most highly stressed meridian were assumed to exist uniformly around the circumference. Since BOSOR5 does not accept stress quantities for input, the SRSS stress quantities due to earthquake and the stresses due to wind and tornado loads were transformed into equivalent axisymmetric pressures. The material nonlinearities were incorporated using a stress-strain constitutive relationship derived from the equations for the plasticity reduction factor given in ASME Code Case N-284. The effects of the residual stresses were incorporated using a reduced proportional limit.

In general, the predicted buckling load for a structure is evaluated as a load multiplier or a factor of safety times the applied loads. Since the structure is imperfection sensitive, sinusoidal imperfections were introduced in the analysis. The imperfection parameters were governed by the ASME Code tolerance values. The amplitude of the imperfection was equal to the maximum allowed ASME tolerance. Sensitivity of the buckling load multiplier with regard to the imperfection wavelength was studied to identify the critical imperfection configuration. The calculated minimum factors of safety values were 3.03 (design conditions and Level A service limits) and 2.02 (Levels C and D), respectively. The former corresponds to load combination DG2 or DBA2 (external pressure of 2.5 psig and temperature of 120°F) and the latter to the load combination DBA4 (external pressure of 3.0 psig, temperature of 120°F and SSE).

The seismic limit analysis of the structure was also performed. The dead load was held constant. The seismic loading was increased until buckling occurred at a load multiplier of 4.60.

5.2 Conclusions

On the basis of the analyses performed herein, the following can be concluded:

(1) Based on the stress analysis, all stress intensities were below the allowable limit, as specified in Section NE3221 of the code.

(2) The predicted minimum buckling factor of safety is 3.03 for Design Conditions and Service Level A and 2.02 for Service Levels C and D. The calculated factors of safety do not satisfy the requirements of NE3222.1. They satisfy Regulatory Guide 1.57 and Code Case N-284.

(3) A seismic margin limit of 4.60 was predicted.

These values are conservative because:

(a) The analysis was performed using a two-dimensional axisymmetric code, with the stresses assumed to be uniform around the circumference and equal to their maximum value.

(b) The imperfection, based on the ASME Code recommended tolerances, was also assumed to be axisymmetric.

(c) The material model was assumed to have a reduced proportional limit at 0.55 times the yield stress to account for residual stresses.

5.3 Recommendations

In order to gain further understanding of the buckling of the AP600 steel containment, the following recommendations are made:

(1) The behavior of the structure needs to be examined using a three-dimensional finite element code. Most of the conservative assumptions listed above can be relaxed only if a complete three-dimensional model is studied. However, a three-dimensional analysis would required more computational effort.

(2) In a three-dimensional code, nonaxisymmetric imperfections depicting a state nearer to true fabricated shells can be represented. However, a representative imperfection shape must be established using Code specified tolerances, measured insitu imperfections or randomly introduced imperfections.

(3) To ascertain actual shell failure, i.e., containment leakage, a study of the post buckling behavior would be necessary. The extent and magnitude of post buckling strains could be compared to strain failure criteria to predict shell failure. The extent of the buckling mode (local versus general) could be predicted.

This page left intentionally blank.

Table 1.1 Weight of the AP600 Attachments

Attachment	Weight (lbs)	Location	
		From Elev.	To Elev.
Air baffle	410,845	142'	241'
Walkway	25,000	162'	-
HVAC Duct	44,761	190'	-
HVAC Duct	13,239	205' 4"	-
HVAC	51,000	155'	192'
Cable Trays	72,000	152'	160'
Containment Recirculation Unit	82,300	162'1"	
Concrete on External Stiffener	78,500	132'3"	

Table 1.2 Factors of Safety for ASME Service Limits

Service Limit	Factor of Safety		
	NE-3222.2	Regulatory Guide 1.57*	Case N-284
Design Condition	3.0	---	2.0
Levels A & B	3.0	---	2.0
Level C	2.5	2	1.67
Level D	2.0	2	1.3

*Does not explicitly identify the service limit except as being associated with the loading causing the largest compressive stress.

Table 2.1 Mass Density of the Shell Segments Used in the BOSOR Models

Segment	Elevation		Mass Density x 10^{-3} lb. sec^2/in.
	From	To	
1	100' 0'	104' 1 1/2"	0.738
2	104' 1 1/2"	114' 7"	1.01938
3	114' 7"	120' 10"	0.8384
4	120' 10"	133' 2 2/3"	0.738
5	133' 2 2/3"	143' 9 3/4"	1.03947
6	143' 9 3/4"	155' 10 3/4"	1.0439
7	155' 10 3/4"	170' 0"	1.154738
8	170' 0"	186' 2"	0.87456
9	186' 2"	202' 5"	0.97136
10	202' 5"	208' 5"	0.8449
11	208' 5"	218' 8 1/2"	0.8449
12	218' 8 1/2"	231' 2 1/2"	0.8449
13	231' 2 1/2"	243' 8 1/2"	0.8449
14	243' 8 1/2"	254' 1/8"	0.738
15	254' 1/8"	256' 4"	0.738
16 (1)	132' 3"	132' 3"	1.92552
17 (2)	131' 4"	132' 6"	0.738
18 (3)	170' 0"	170' 0"	0.738
19 (4)	169' 6"	170' 6"	0.738
20 (5)	208' 5"	208' 5"	0.738
21 (6)	202' 5"	202' 5"	0.738
22 (7)	202' 5"	208' 5"	3.9839
23 (8)	202' 5"	208' 5"	0.2000
24 (8)	202' 5"	208' 5"	0.2000
25 (9)	130' 5"	131' 9"	0.0500

(1) Web of stiffener at Elev. 132.25'.
(2) Flange of stiffener at Elev. 132.25'.
(3) Web of stiffener at Elev. 170'.
(4) Flange of stiffener at Elev. 170'.
(5) Top flange of crane girder.
(6) Bottom flange of crane girder.
(7) Web beneath the rail.
(8) Ficticious ring for crane girder radial stiffeners.
(9) Ficticious ring beneath the external T-ring stiffener at Elev. 132' 3".

Table 2.2 Effective Modal Mass Computation - Perfect Shell (Vertical Modes)

Mode	Frequency (Hz)	Generalized Mass (GM)	Participation Factor, Γ	Effec. Mass ($GM * \Gamma^{2)}$	% of Total Mass
1	13.61	9597.0	0.0	0.0	0.0
2	16.16	3314.0	1.956	12679.20	71.63
3	21.82	479.2	0.651	203.20	1.15
4	23.04	254.0	0.819	170.30	0.96
5	23.64	1251.0	0.032	1.30	0.01
6	23.66	46.2	0.541	13.53	0.08
7	24.44	112.6	1.084	132.31	0.75
8	24.72	244.8	0.496	60.22	0.34
9	25.53	89.6	0.834	62.30	0.35
10	26.52	113.7	1.282	186.90	1.06

Table 2.3 Effective Modal Mass Computation - Perfect Shell (Horizontal Modes)

Mode	Frequency (Hz)	Generalized Mass (GM)	Participation Factor, Γ	Effec. Mass ($GM * \Gamma^{2}$)	% of Total Mass
1	6.77	7411.0	1.356	13626.90	76.98
2	19.31	3420.0	0.702	1686.80	9.53
3	23.13	140.7	0.880	108.88	0.62
4	23.62	971.5	0.563	307.72	1.74
5	23.97	67.3	0.019	0.02	0.00
6	24.47	204.2	1.085	240.39	1.36
7	24.76	139.0	0.168	3.90	0.02
8	25.00	150.6	1.046	164.80	0.93
9	25.68	143.2	0.400	22.90	0.13
10	26.72	149.4	0.322	15.50	0.09

Table 2.4 Pressure Coefficients [2.15 (Appendix C; Case 20)]
(Wind Azimuth 315°, Level 5)

Tap	Max. Coef.	Min. Coef.	Mean Coef.	Max. absolute value of Pressure (psig) (Wind @110 mph)	Max. absolute value of Pressures (psig) (Wind @300 mph)
141 (55°)	-0.40	-3.12	-1.60	-0.84	-2.60
142 (10°)	-0.39	-2.94	-1.49	-0.79	-2.45
143 (325°)	1.81	-0.20	0.68	-0.05	-0.16
144 (280°)	1.01	-1.38	-0.14	-0.37	-1.15
145 (235°)	-0.99	-3.66	-2.13	-1.00	-3.10
146 (190°)	-0.09	-2.18	-0.86	-0.59	-1.83
147 (145°)	-0.04	-2.79	-0.70	-0.75	-2.33
148 (100°)	-0.02	-2.90	-0.75	-0.78	-2.42

Table 2.5 Load Combinations as per S.R.P 3.8.2

ASME Limits	Design Conditions		Level A			Level C and Level D			
Load Combinations as per S.R.P.3.8.2*	DG1	DG2	OC1	DBA1	DBA2	OC2	OC3	DBA3	DBA4
Dead Load (D)	X	X	X	X	X	X	X	X	X
Live Load (L)	X	X	X	X	X	X	X	X	X
Operating conditions:									
$P_o = 1.0$ psig $T_o = 120^oF$			X			X	X		
Wind @ 110 mph			X						
Accident Conditions:									
$P_a = 45$ psig $T_a = 280^oF^{\#}$	X			X				X	
$P_a = -2.5$ psid $T_a = 120^oF$		X			X				
$P_a = -3.0$ psid $T_a = 120^oF$									X
S.S.E						X		X	X
W_T @ 300 mph							X		

*DG1= Design Conditon 1; DG2 = Design Condition 2; OC1 = Operating Condition 1; OC2 = Operating Condition 2; OC3 = Operating Condition 3; DBA1 = Design Basis Accident 1; DBA2 = Design Basis Accident 2; DBA3 = Design Basis Accident 3; DBA4 = Design Basis Accident 4.

#Includes temperature profiles Case 1, Case 2 and Case 3. [Sec. 2.3.6]

Table 2.6 Design Conditions

SRP Reference Number	Load Combination	Design Allowable Stress Intensity Limit			Maximum Calculated Stress	
		Type	Limit	Value (psi)	Value (psi)	Elev. (ft)
(ii)	DG1	P_L	1.1 S_{mc}	24,200	22,596	+214
(ii)	DG2	P_m	1.0 S_{mc}	22,000	2,457	+103

Table 2.7 Level A Service Limits

SRP Reference Number	Load Combination	Design Allowable Stress Intensity Limit			Maximum Value as per Stress Analysis	
		Type	Limit	Value	Value (psi)	Elev. (ft)
(iii)(a)(1)	OC1	P_m	1.0 S_{mc}	22,000	2,683	+104
(iii)(a)(1)	OC1	P_L+P_b+Q	3.0 S_{m1}	80,100	21,894	+100
(iii)(a)(2)		Not applicable				
(iii)(a)(3)						
(iii)(a)(3)	DBA1	P_L	1.1 S_{mc}	24,200	22,596	+214
(iii)(a)(3)						
(iii)(a)(3)	DBA1	P_L+P_b+Q	3.0 S_{m1}	80,100	77,517	+100
	DBA2	P_m	1.0 S_{mc}	22,000	2,457	+103
	DBA2	P_L+P_b+Q	3.0 S_{m1}	80,100	21,405	+100

Table 2.8 Level C Service Limits

SRP Ref. Number	Load Combination	Design Allowable Stress Intensity Limit (psi)			Maximum Value as per Stress Analysis	
		Type	Limit	Value (psi)	Value (psi)	Elev. (ft)
(iii)(c)(2)	OC2	P_m	1.0 S_y	59,000	12,799	100
(iii)(c)(2)	OC3	P_m	1.0 S_y	59,000	4,433	103
(iii)(c)(1)	DBA3	P_m	1.0S_y	52,760	22,878	214
(iii)(c)(1)	DBA4	P_m	1.0S_y	59,000	13,454	100

Table 2.9 Level D Service Limits

SRP Ref. Number	Load Combination	Design Allowable Stress Intensity Limit (psi)			Maximum Value as per Stress Analysis	
		Type	Limit	Value (psi)	Value (psi)	Elev. (ft)
(iii)(d)(1)	DBA3	P_m	S_f	47,600	22,878	214
(iii)(d)(1)	DBA4	P_m	S_f	47,600	13,454	100

Table 2.10 Nomenclature

P -	Stress Intensity (difference between the algebriacally largest and smallest principal stresses, twice the maximum shear stress).
P_m -	General primary membrane stress intensity (average stress across an entire section of a vessel. Not self limiting. Gross deformation occurs if this stress exceeds yield. An example is general membrane stress in a cylinder or sphere with internal pressure. Temperature stresses are <u>not</u> included. Therefore, the temperature is set equal to zero in Tables 2.5 to 2.8 in those cases for which P_m is checked. These stresses are checked at the shell middle surface).
Q -	Secondary stress intensity (Self-limiting. An example is the stresses due to the bending stress resultants M_1, M_2, M_{12} for pressure or seismic loading. All thermal stresses are secondary. Hence, for those cases in Table 2.5 to 2.8 for which primary plus secondary stresses are checked, the temperature is at the operating or accident level. These stresses are checked at the shell surface).
P_L -	Local primary membrane stress intensity. (A stressed region may be considered local if the distance over which the membrane stress intensity exceeds 1.1 S_{mc} does not extend in meridional direction more than $(rt)^{1/2}$. Typically self-limiting like a secondary stress but redistribution takes place only after large deformations. An example is the local membrane stress near a gross structural discontinuity such as shell intersections at the springline or at a penetration. Membrane stresses near the base of the containment may be considered in this category).
P_b -	Primary bending stress intensity (same as P_m except bending stress. An example is the center of a flat plate with lateral pressures).
S_y -	Yield stress, ASME Table I.2.0: 60,000 psi @ T=0°F; 52,760 psi @ T=280°F; 59,000 psi @ T=120°F.
S_{mc} -	Allowable stress intensity, ASME Table I-10.0: 22,000 psi.
S_{ml} -	Allowable stress intensity, ASME Table I-1.0: 26,700 psi.
S_f -	Allowable stress intensity, 85% of the allowable membrane stress intensity specified in Appendix F: 47,600 psi
D -	Dead loads.
L -	Live loads including all loads resulting from platform flexibility and deformation, and crane loading if applicable, equal to zero for this containment.

	Table 2.10 (Continued)
T_o -	Thermal effects and loads during startup, normal operating or shutdown conditions, based on the most critical transient or steady-state condition.
R_o -	Pipe reactions during startup, normal operating or shutdown conditions, based on the most critical transient or steady-state condition, equal to zero for this containment.
P_o -	External pressure loads resulting from pressure variation either inside or outside containment.
E' -	Loads generated by the safe shutdown earthquake including sloshing effects, if applicable.
P_a -	Pressure load generated by the postulated pipe break accident including P_o, pool swell and subsequent hydrodynamic loads. For this containment, accidental spray actuation is included in this category.
T_a -	Thermal loads under thermal conditions generated by the postulated pipe break accident including T_o, pool swell, and subsequent hydrodynamic reaction loads. For this containment, accidental spray actuation is included in this category.
R_a -	Pipe reactions under thermal conditions generated by the postulated pipe break accident including R_o, pool swell, and subsequent hydrodynamic reaction loads, equal to zero for this containment.
P_s -	All pressure loads which are caused by the actuation of safety relief valve discharge including pool swell and subsequent hydrodynamic loads, equal to zero for this containment.
T_s -	All thermal loads which are generated by the actuation of safety relief valve discharge including pool swell and subsequent hydrodynamic thermal loads, equal to zero for this containment.

Table 3.1 Buckling Factors of Safety

S.R.P. Reference Number	Load Combination	Factor of Safety	Buckling Location
DESIGN CONDITIONS			
(ii)	DG1	3.10	General tensile yield in the Cylinder
(ii)	DG2	3.03	Buckling between upper and lower stiffeners
LEVEL A SERVICE LIMITS			
(iii)(a)(1)	OC1	7.10	Gross Yield near the base.
(iii)(a)(2)	Not applicable		-
(iii)(a)(3)	DBA1	3.10	General tensile yield in the Cylinder
(iii)(a)(3)	DBA2	3.03	Buckling between upper and lower stiffeners
LEVEL C SERVICE LIMITS			
(iii)(c)(1)	DBA3	3.20	Gross yield at base
(iii)(c)(1)	DBA4	2.02	Between base and lower stiffener
(iii)(c)(2)	OC2	3.80	Gross yield near the base.
(iii)(c)(2)	OC3	5.20	Gross yield near the base.
LEVEL D SERVICE LIMITS			
(iii)(d)(1)	DBA3	3.20	Gross yield at base.
(iii)(d)(1)	DBA4	2.02	Between base and lower ring.

This page left intentionally blank.

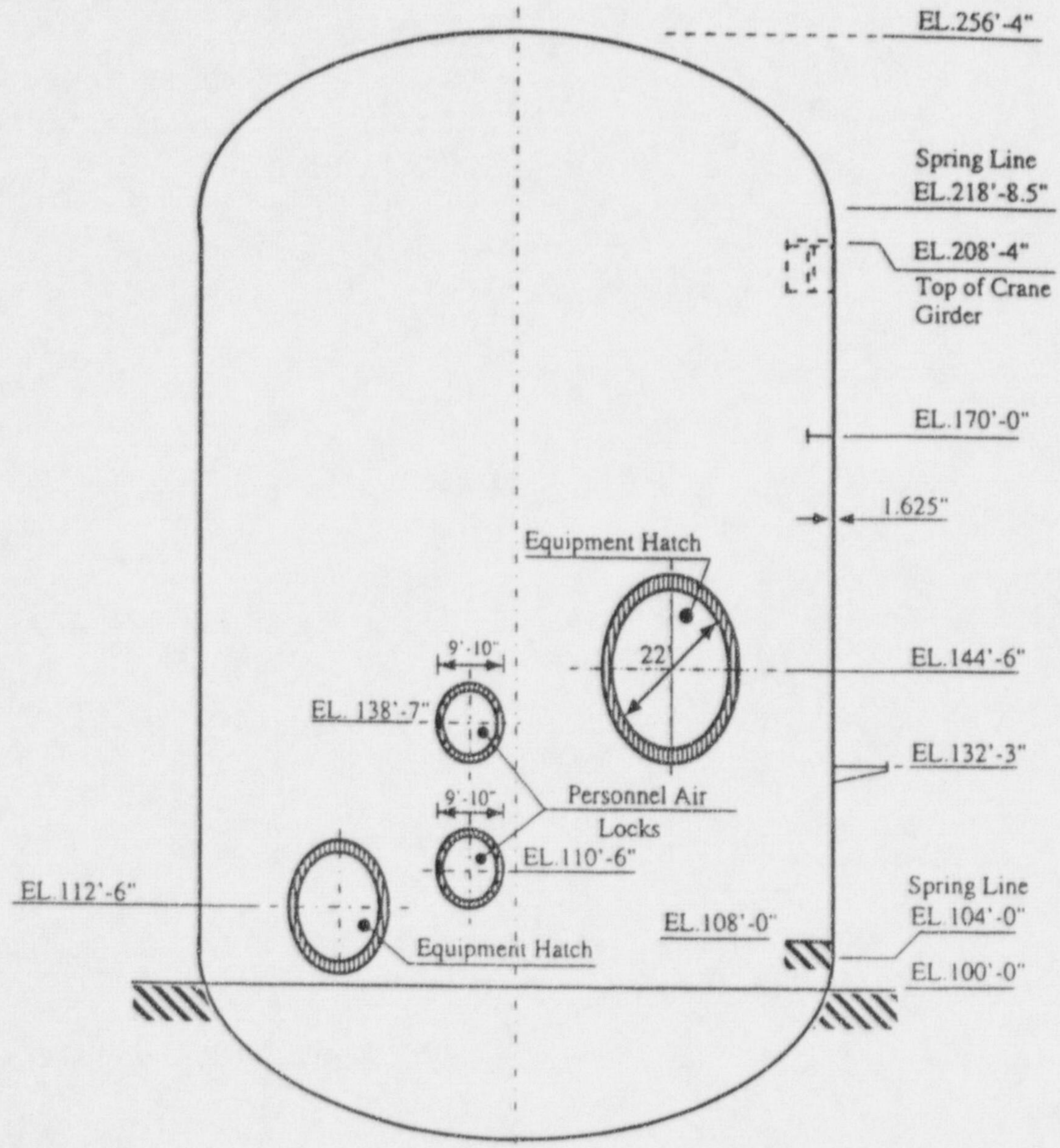

Fig. 1.1 Elevation of AP600 Steel Containment (Penetration Shown Distorted)

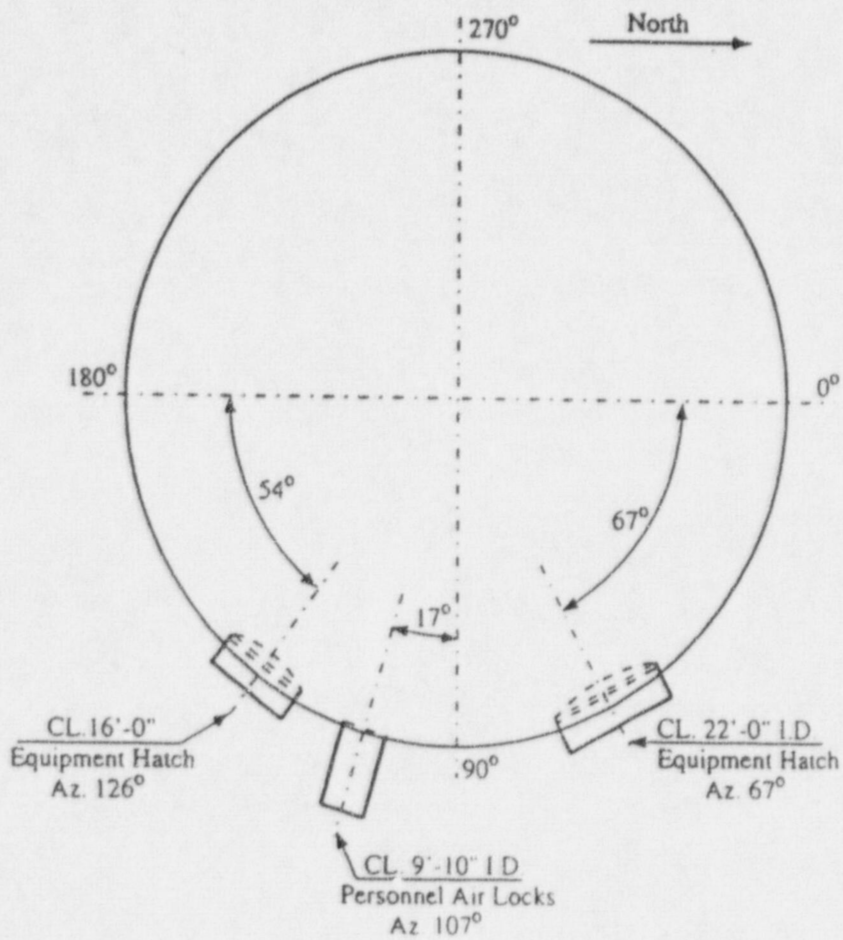

Fig. 1.2 Orientation of Major Penetrations

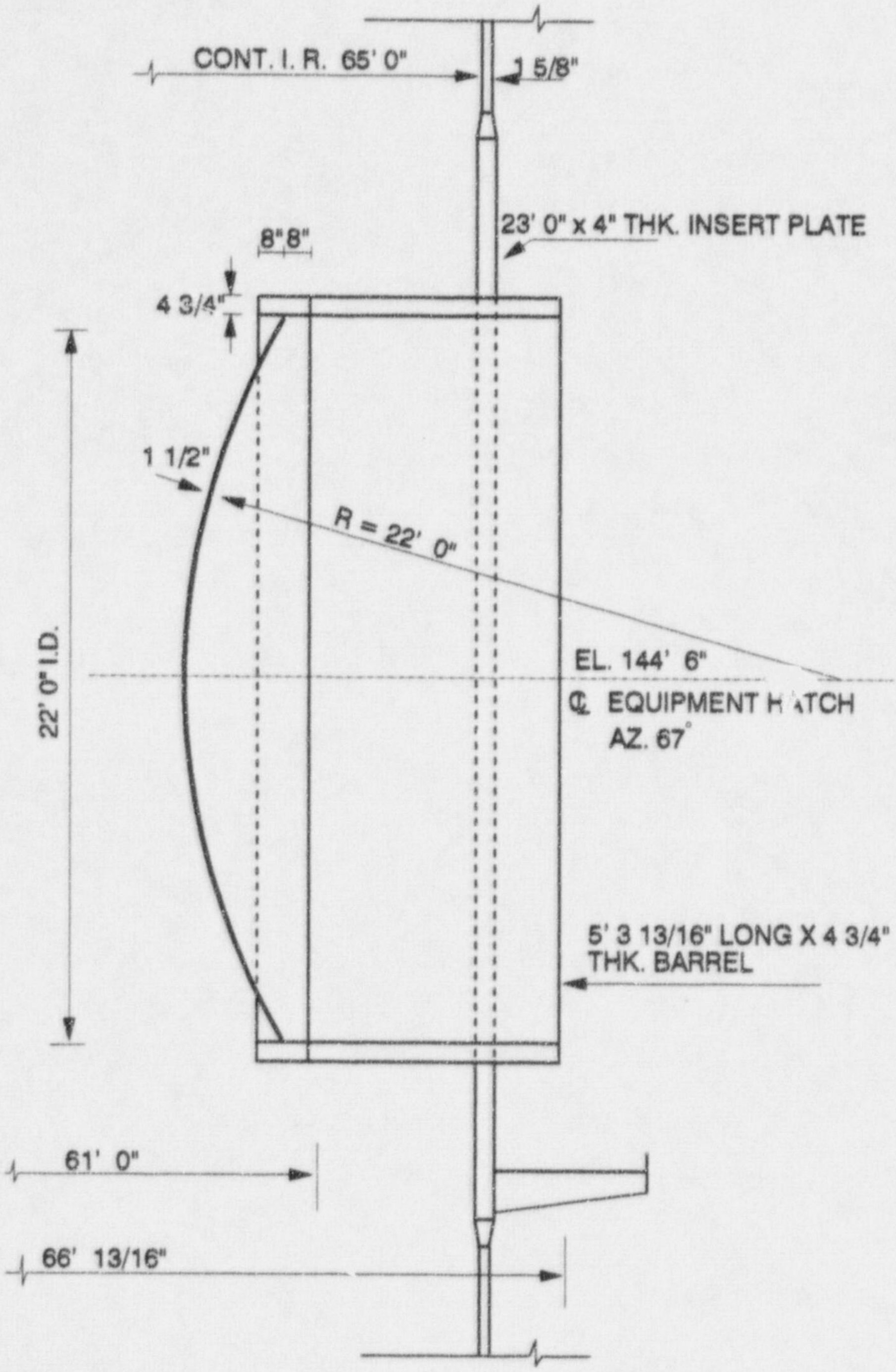

Fig. 1.3 Details of the 22 ft. Diameter Equipment Hatch

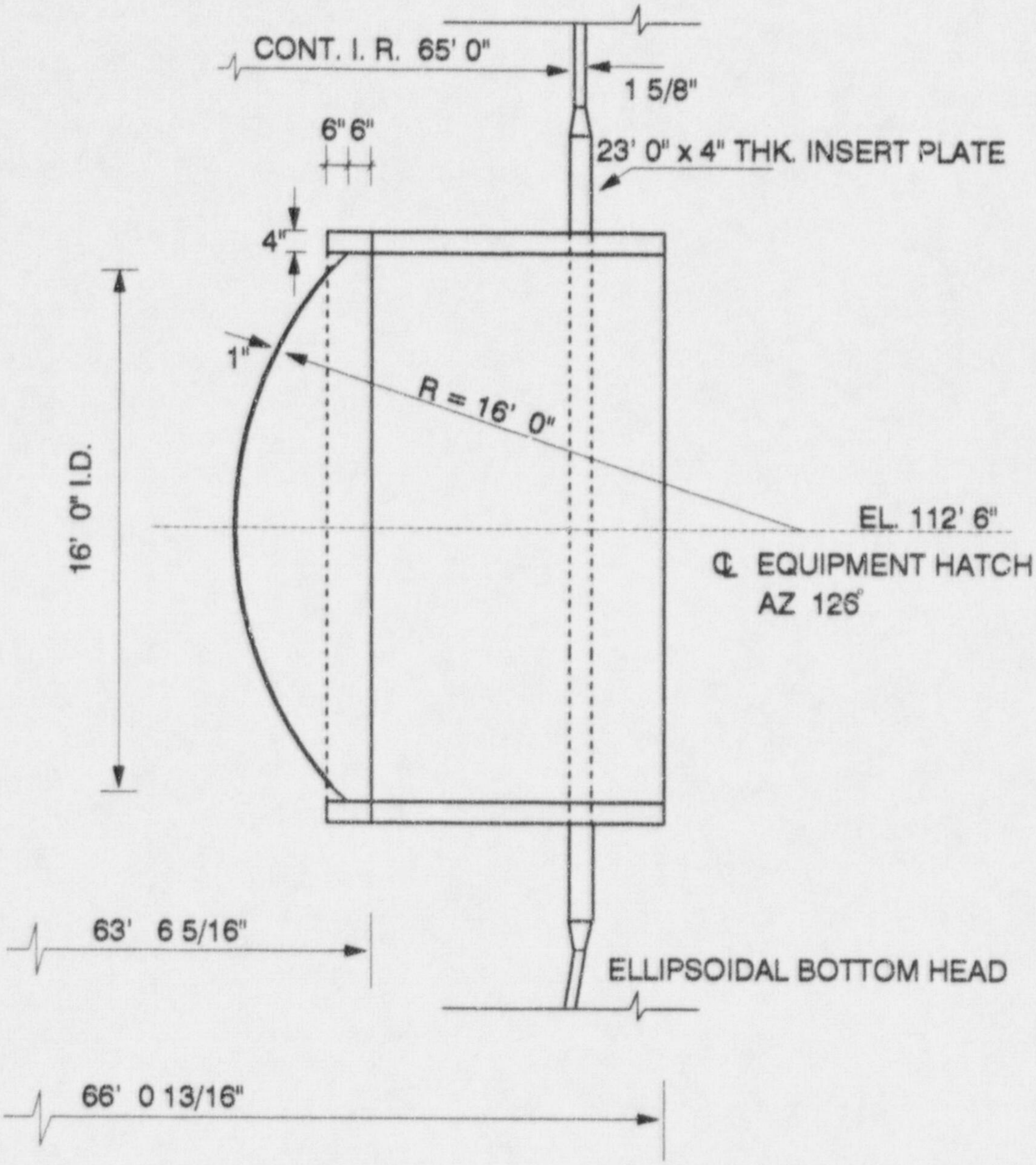

Fig. 1.4 Details of the 16 ft. Diameter Equipment Hatch

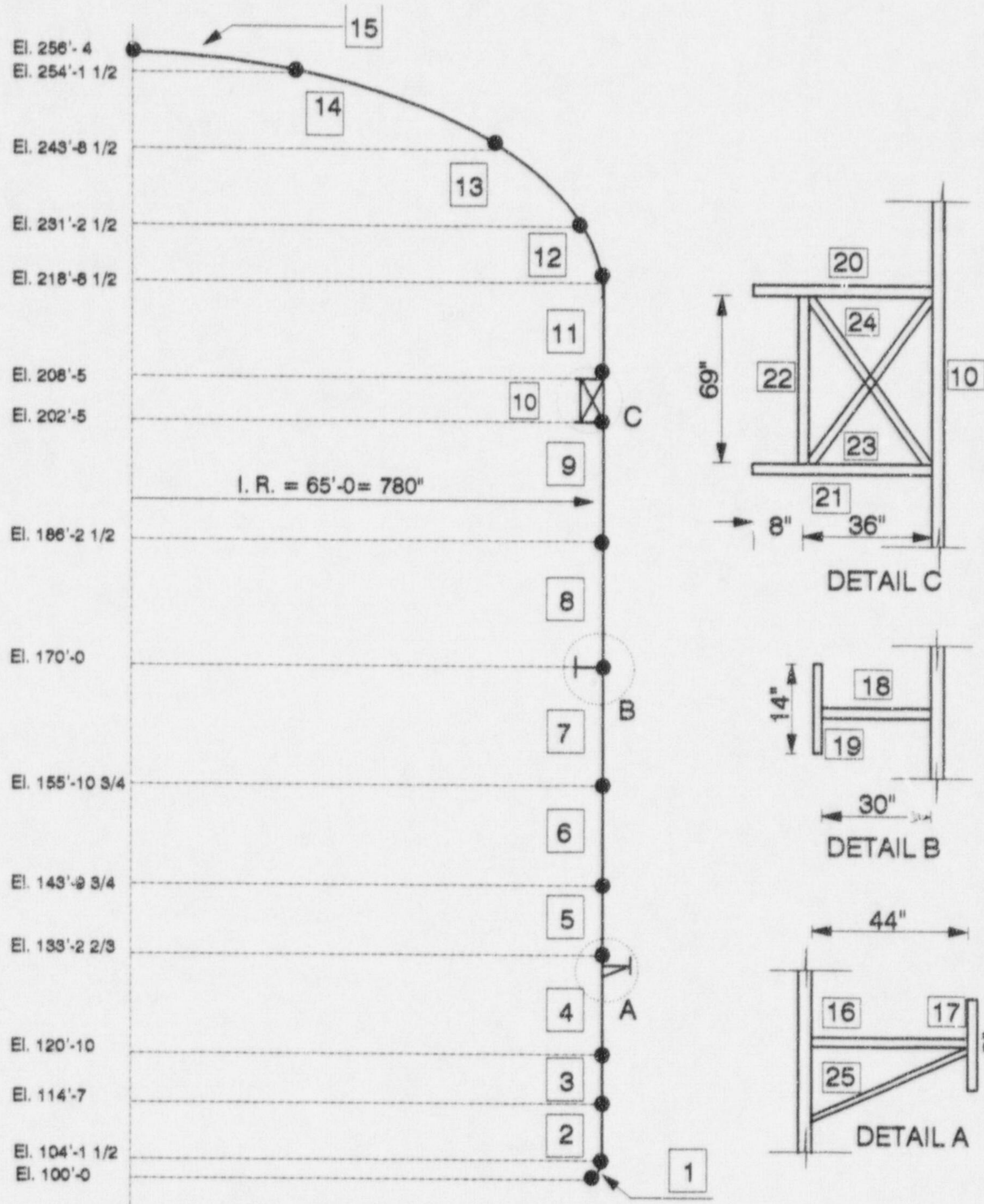

Segment No.	1	2	3	4	5	6	7	8	9	10	11	12	13	14	15
No. of Mesh Pt.	6	8	5	10	9	10	11	12	12	5	8	11	11	21	21

□ Segment No.
● Segment ends

No. of mesh points for segments 16 through 25 equal to 5 points.
Segments 23,24 and 25 represent web stiffeners.
Fixed support condition was assumed at the base

Fig. 2.1 Axisymmetric Model of AP600 Steel Containment

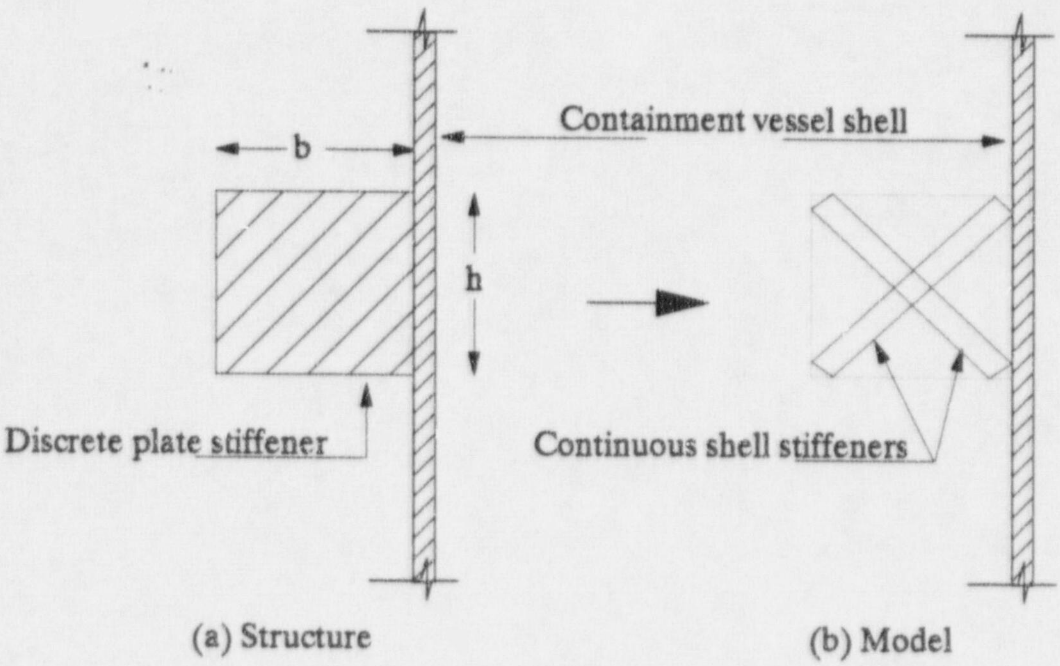

Fig. 2.2 Modeling of the Crane Girder

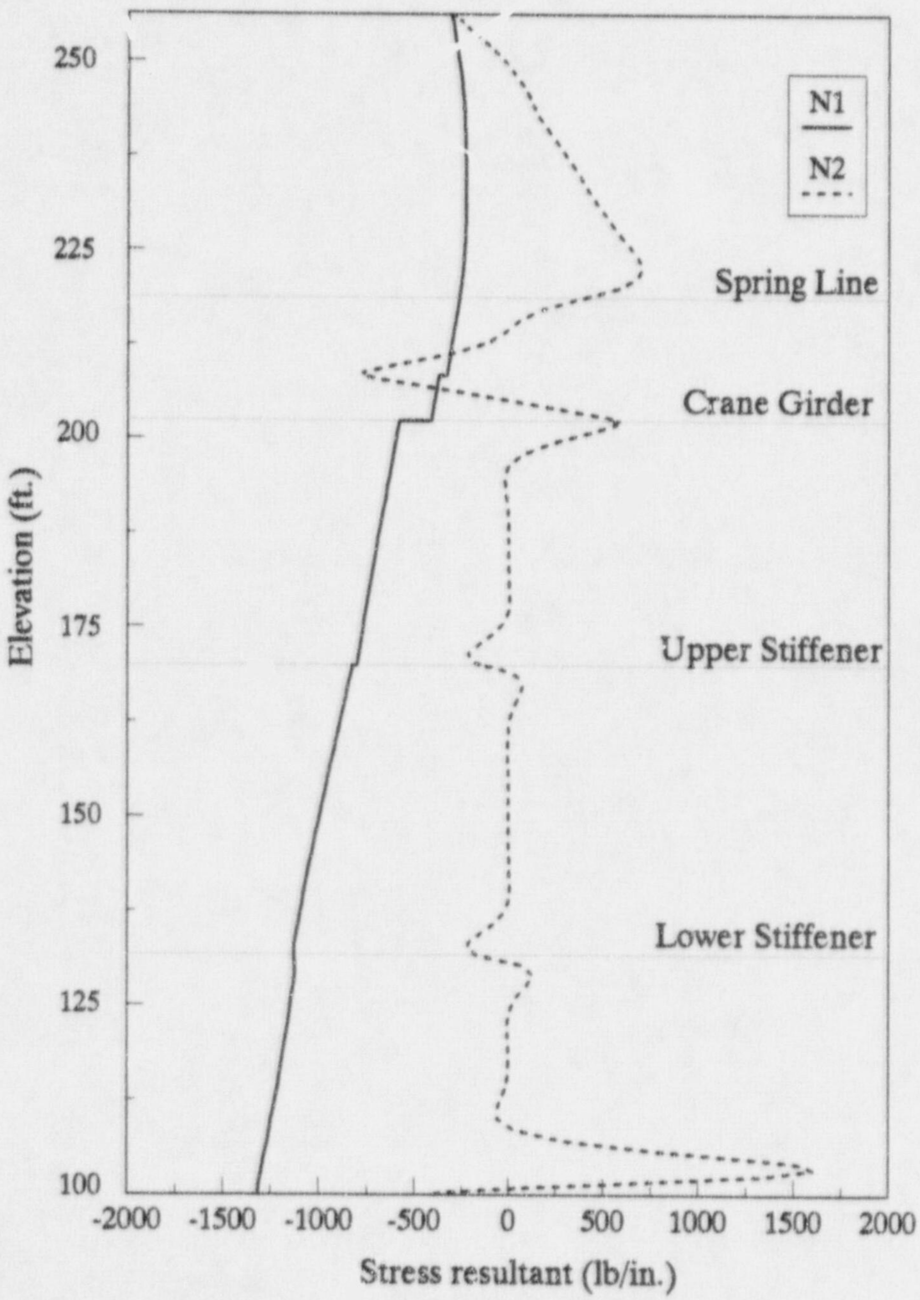

Fig. 2.3 Meridional (N_1) and Circumferential (N_2) Stress Resultants due to the Containment Self Weight

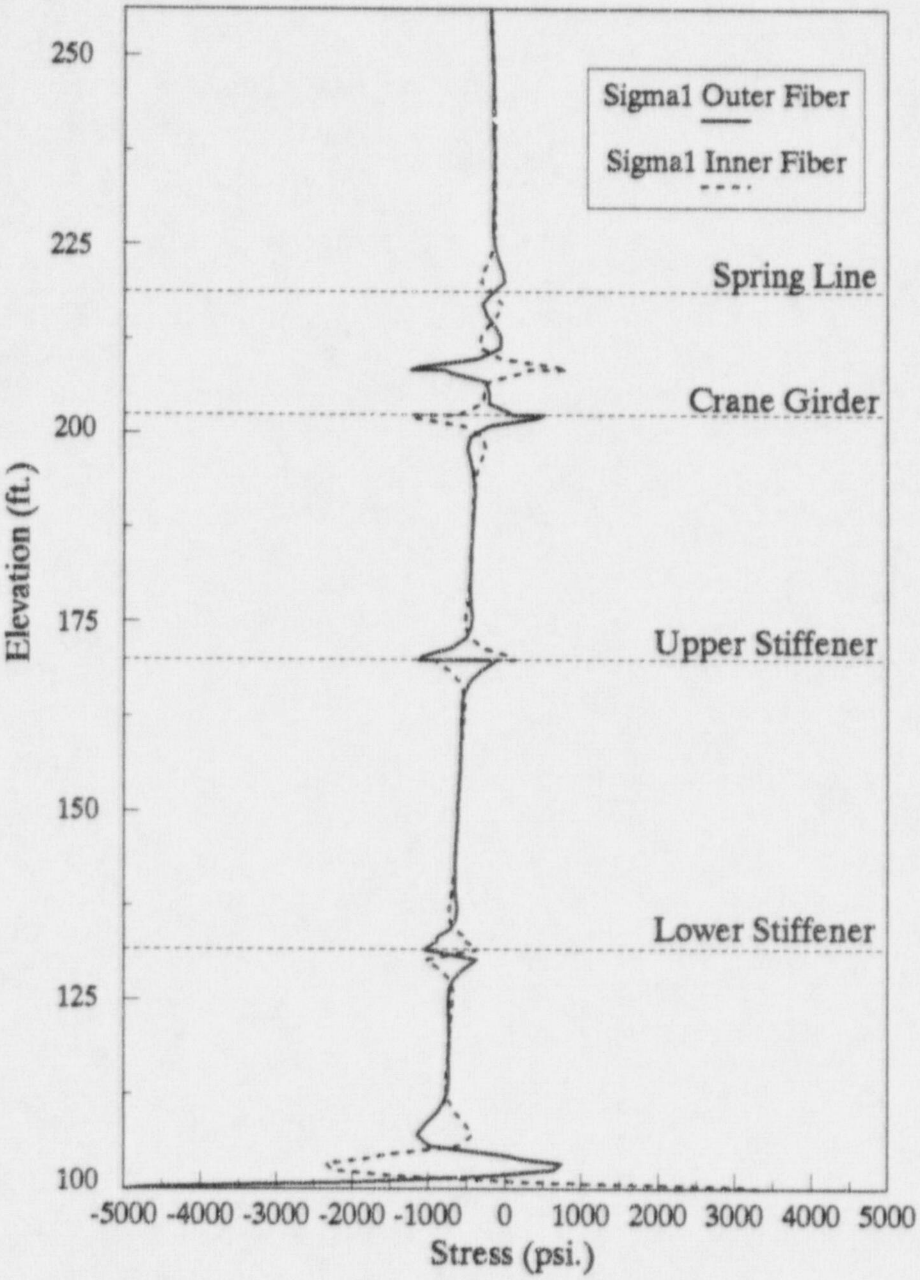

Fig. 2.4 Extreme Fiber Meridional ($Sigma_1$) Stresses due to Containment Self Weight

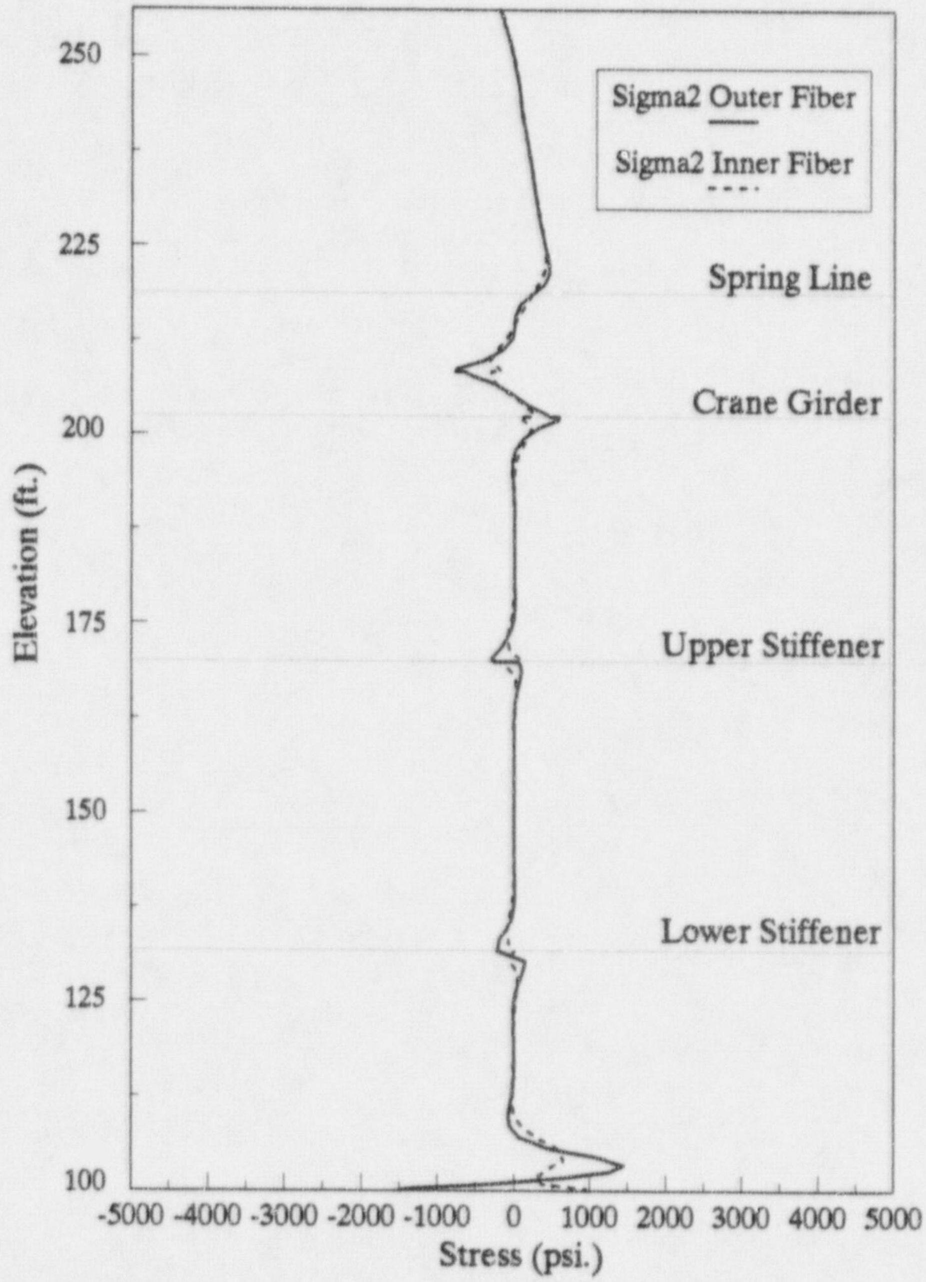

Fig. 2.5 Extreme Fiber Circumferential ($Sigma_2$) Stresses due to Containment Self Weight

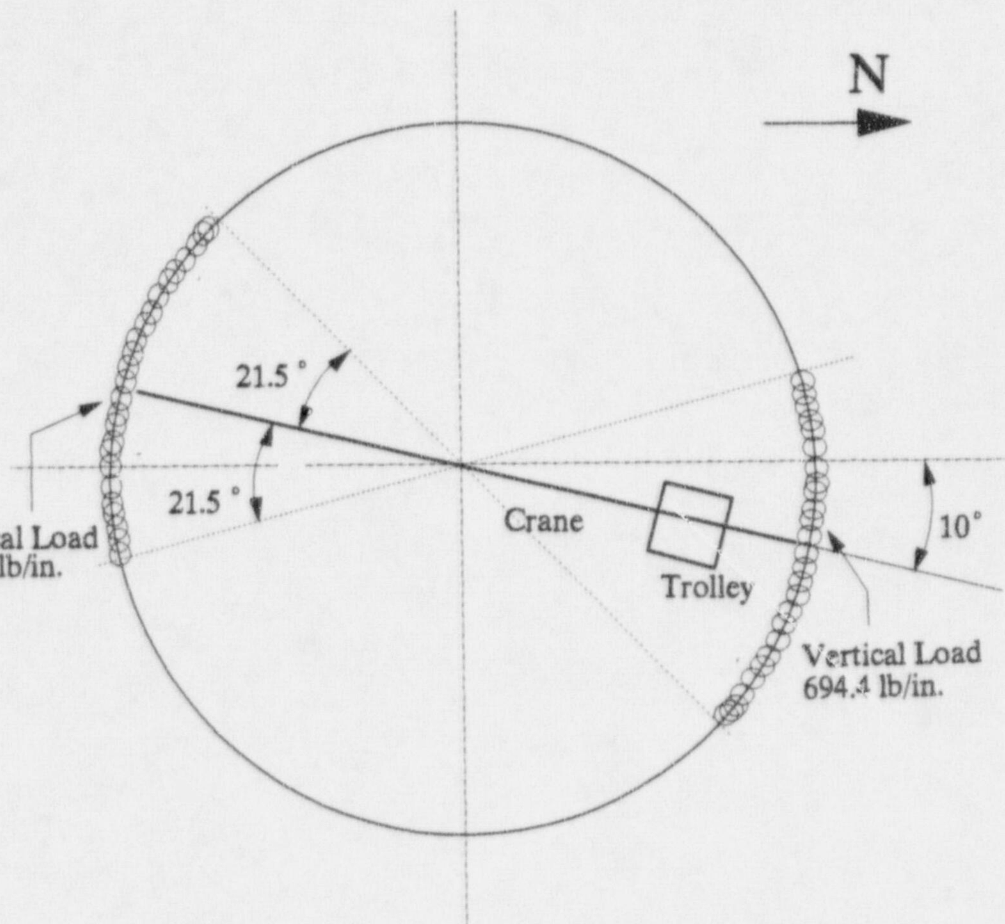

Fig. 2.6 Plan View of the Containment with Trolley Parked for Plant Operating Condition

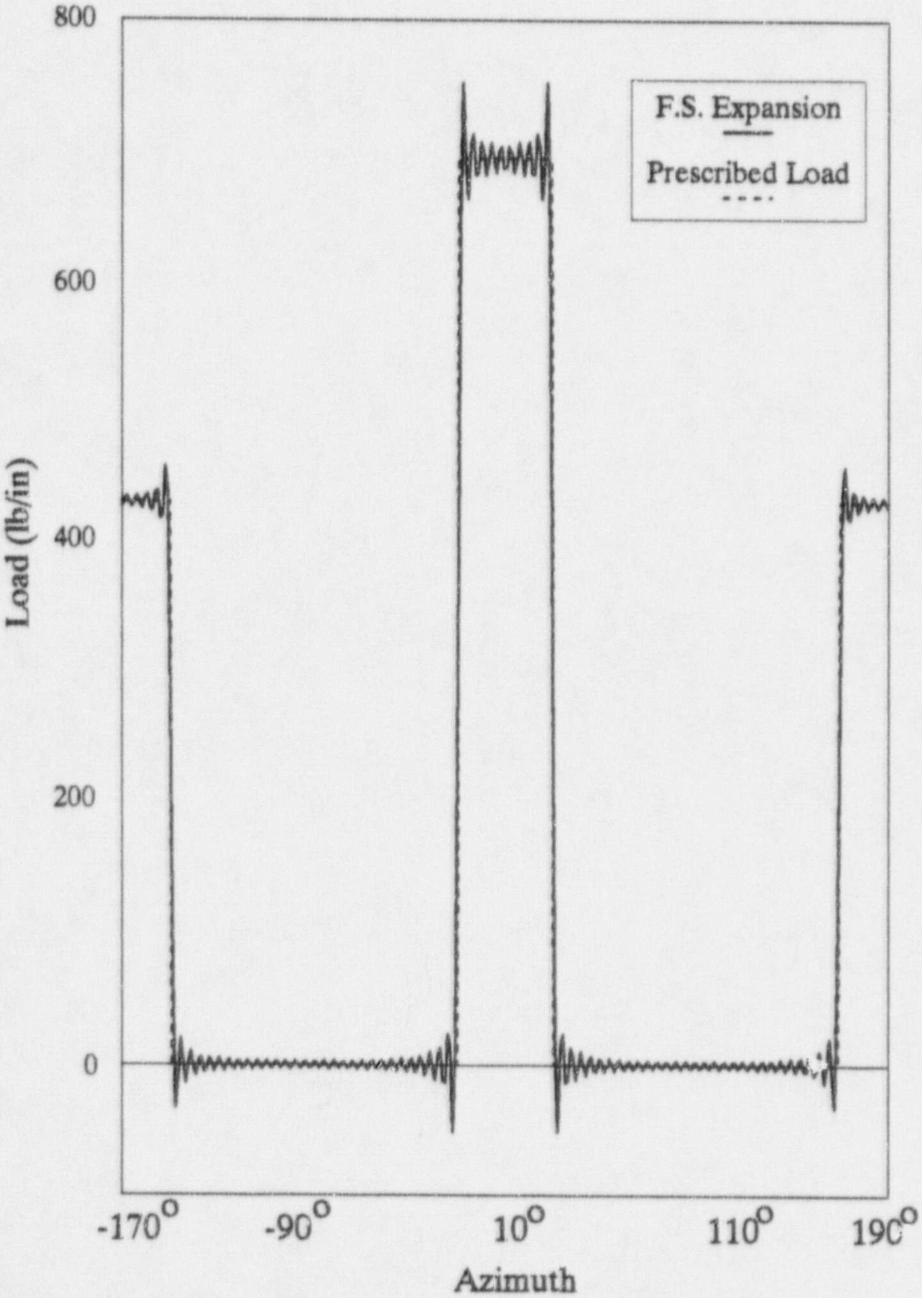

Fig. 2.7 Comparison of the Prescribed Crane Loading and Fourier Series Expansion

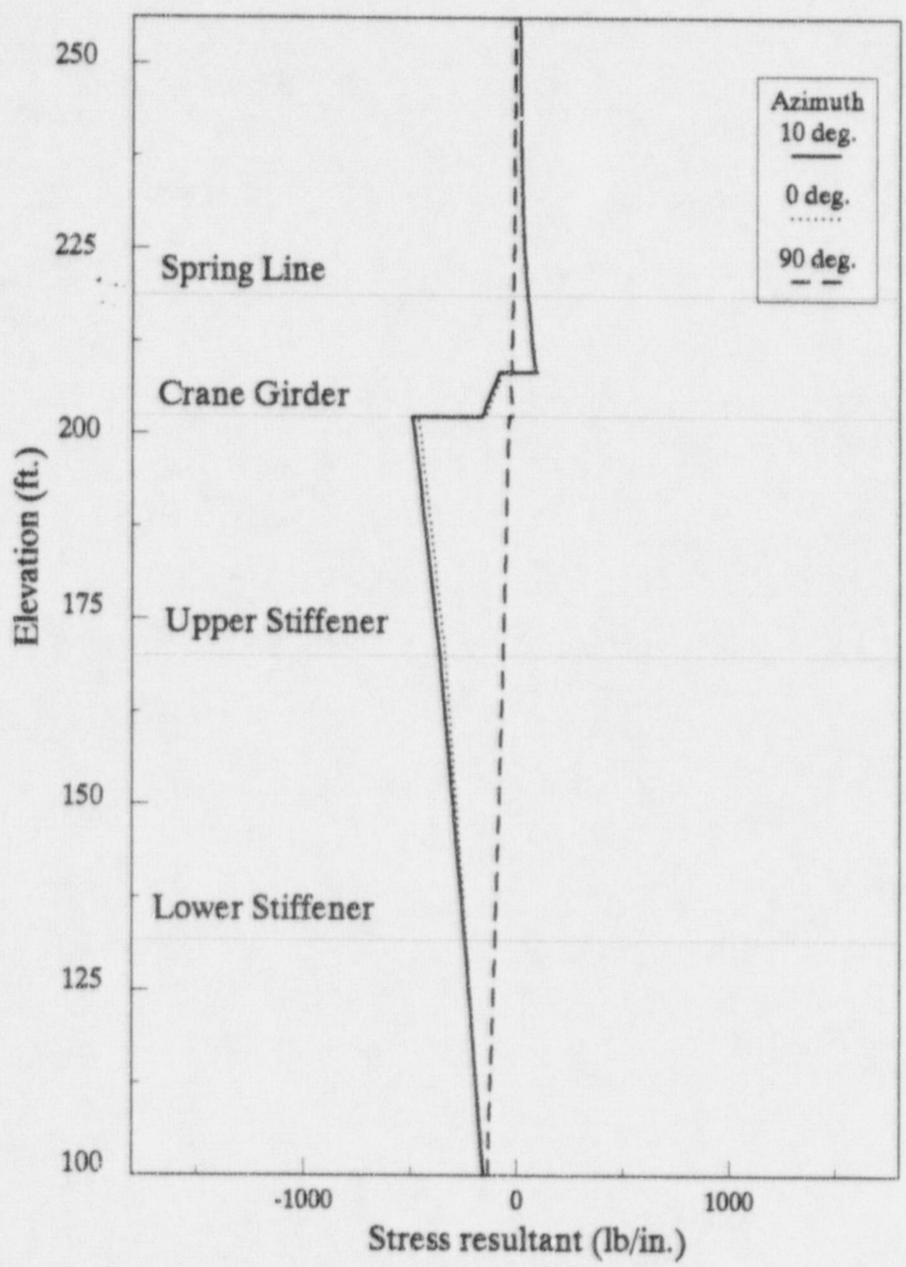

Fig. 2.8 Comparison of Meridional (N_1) Stress Resultants due to Crane Dead Load

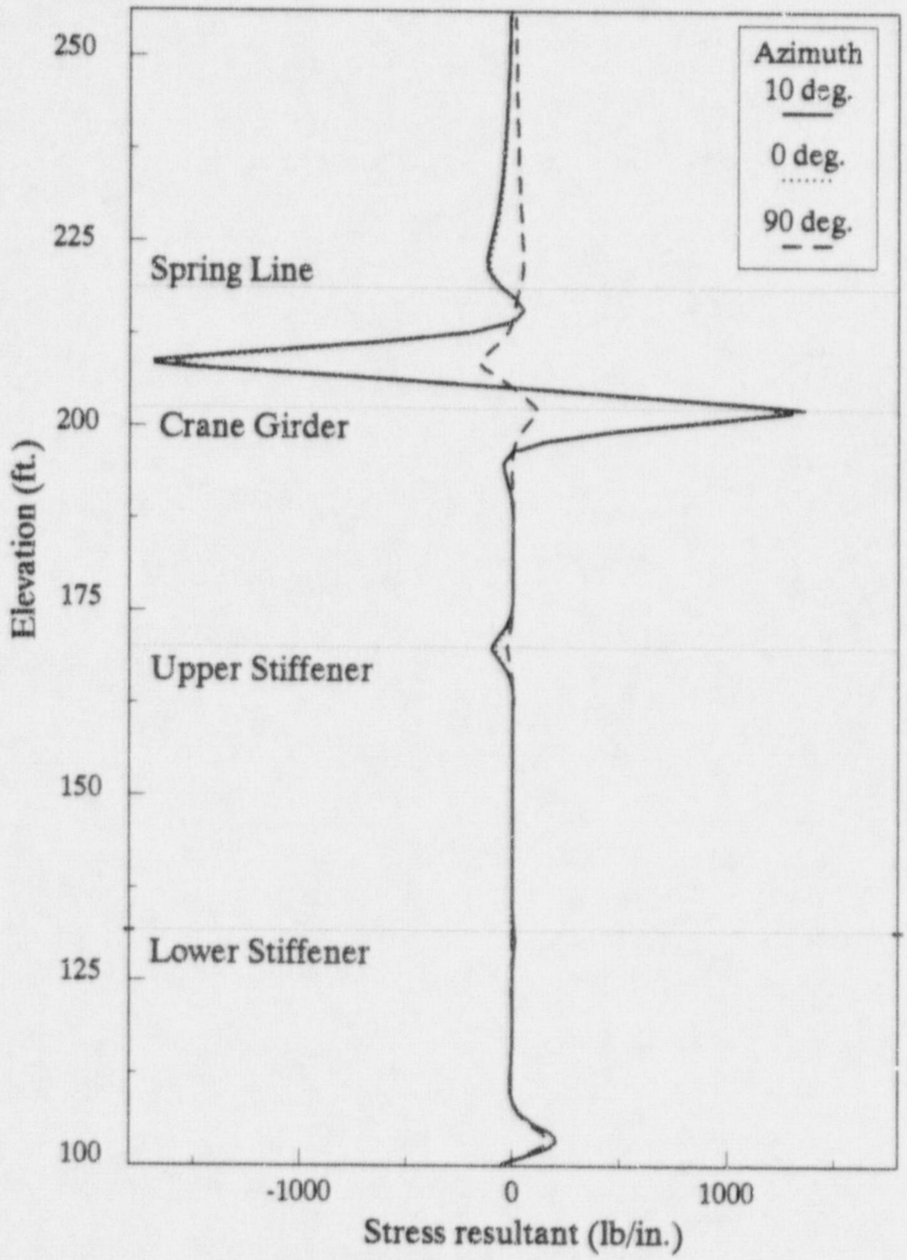

Fig. 2.9 Comparison of Circumferential (N_2) Stress Resultants due to Crane Dead Load

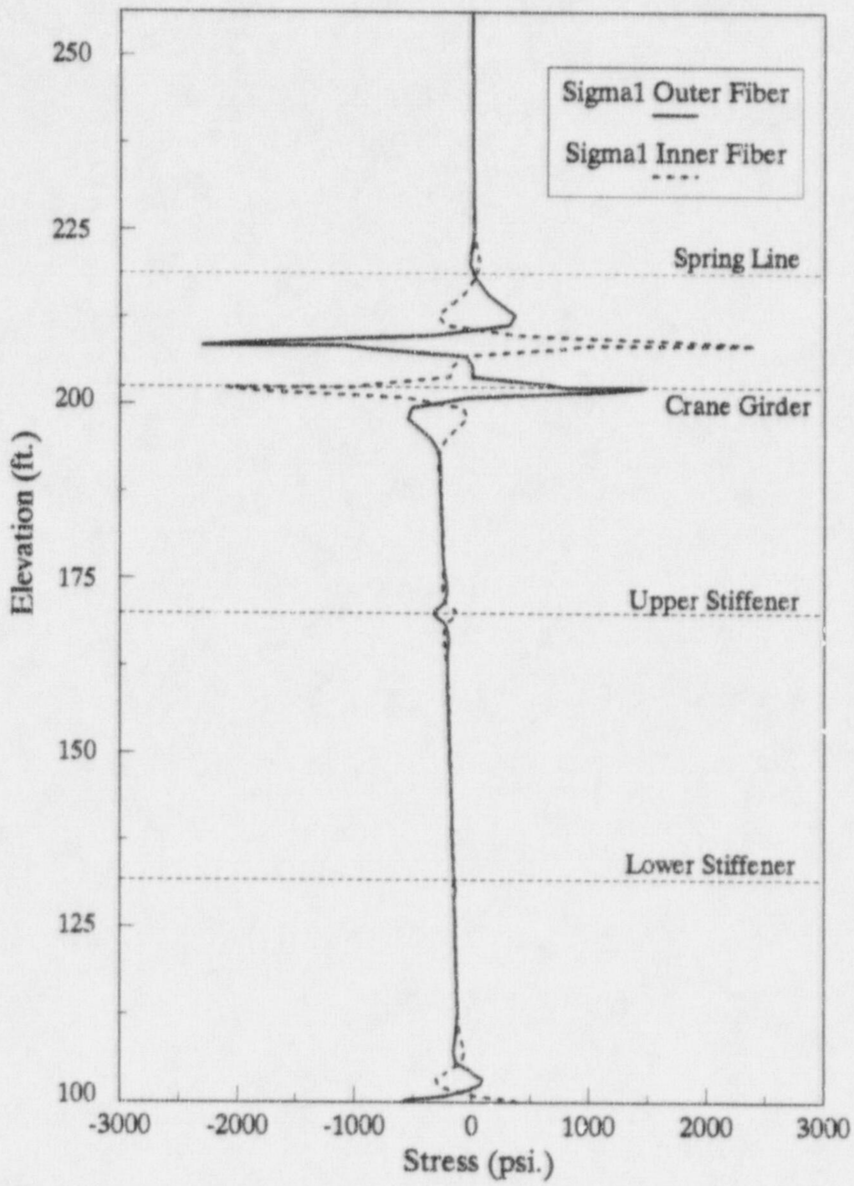

Fig. 2.10 Extreme Fiber Meridional ($Sigma_1$) Stresses due to Crane Dead Load at 10° Azimuth

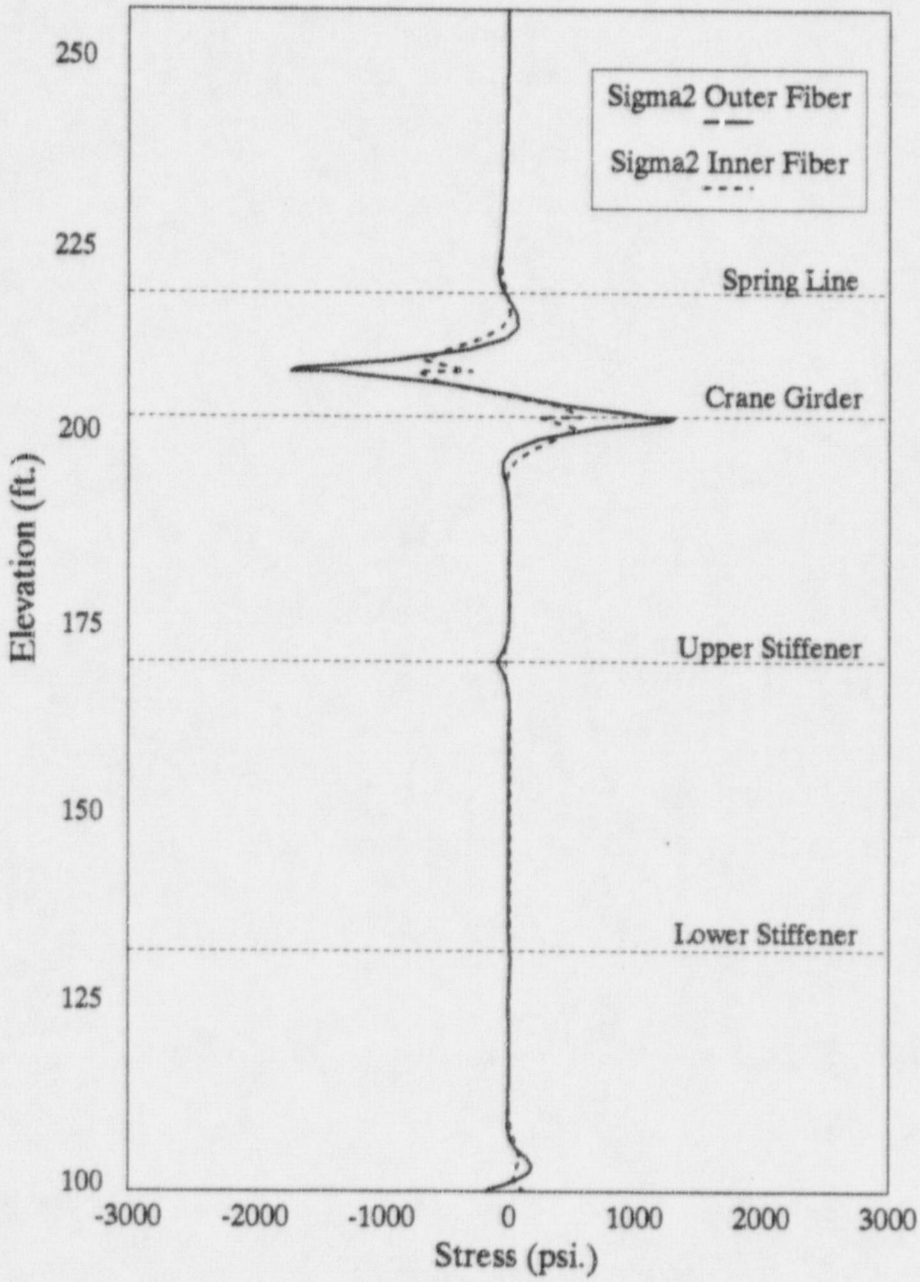

Fig. 2.11 Extreme Fiber Circumferential ($Sigma_2$) Stresses due to Crane Dead Load at 10° Azimuth

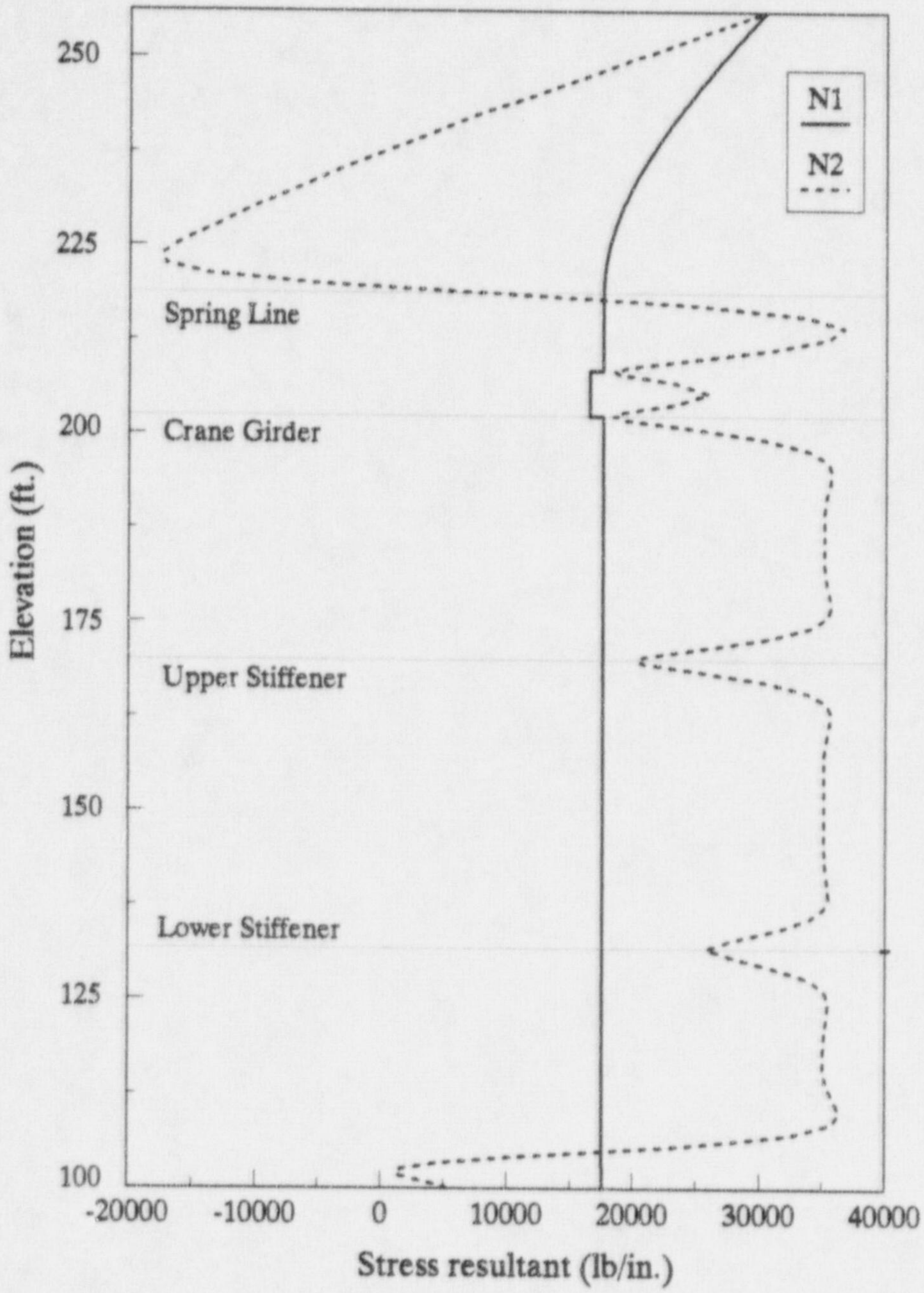

Fig. 2.12 Meridional (N_1) and Circumferential (N_2) Stress Resultants due to Internal Pressure of 45 psig

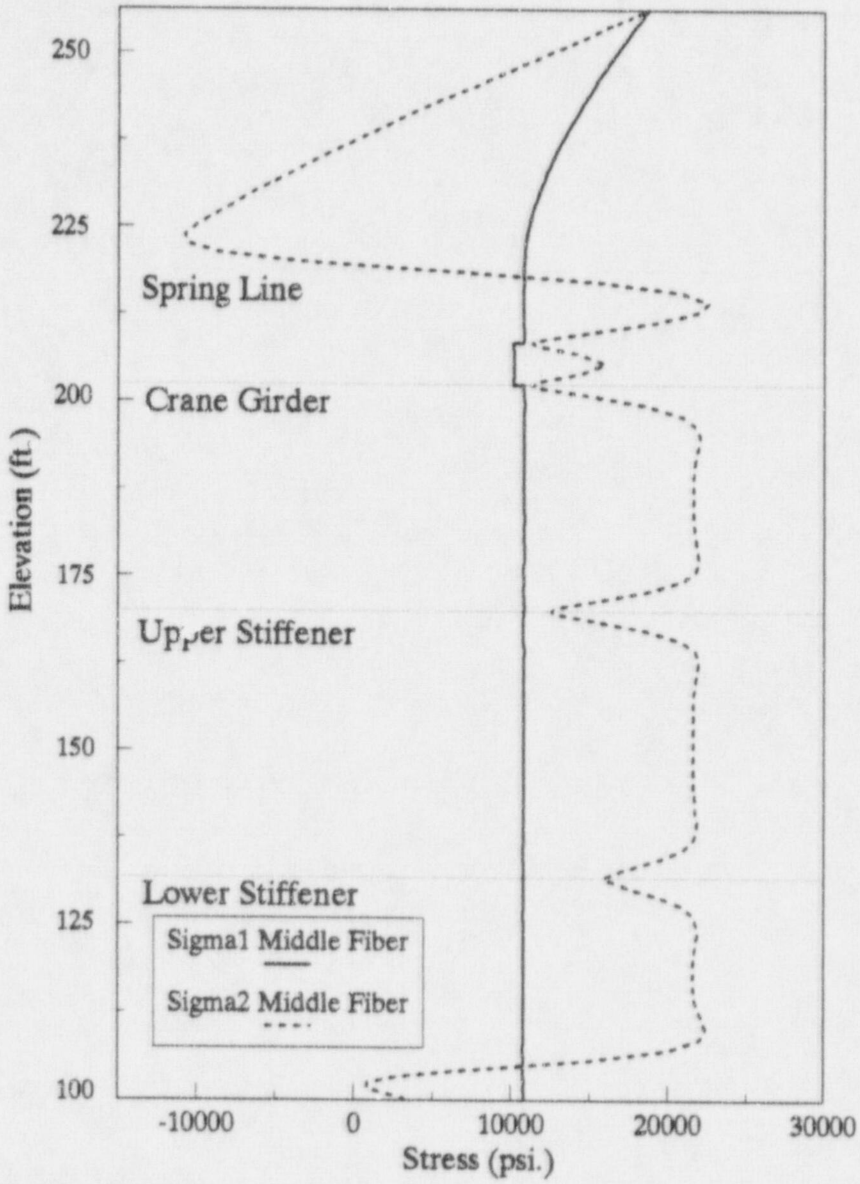

Fig. 2.13 Middle Surface Meridional (Sigma$_1$) Stresses and Circumferential (Sigma$_2$) Stresses due to Internal Pressure of 45 psig

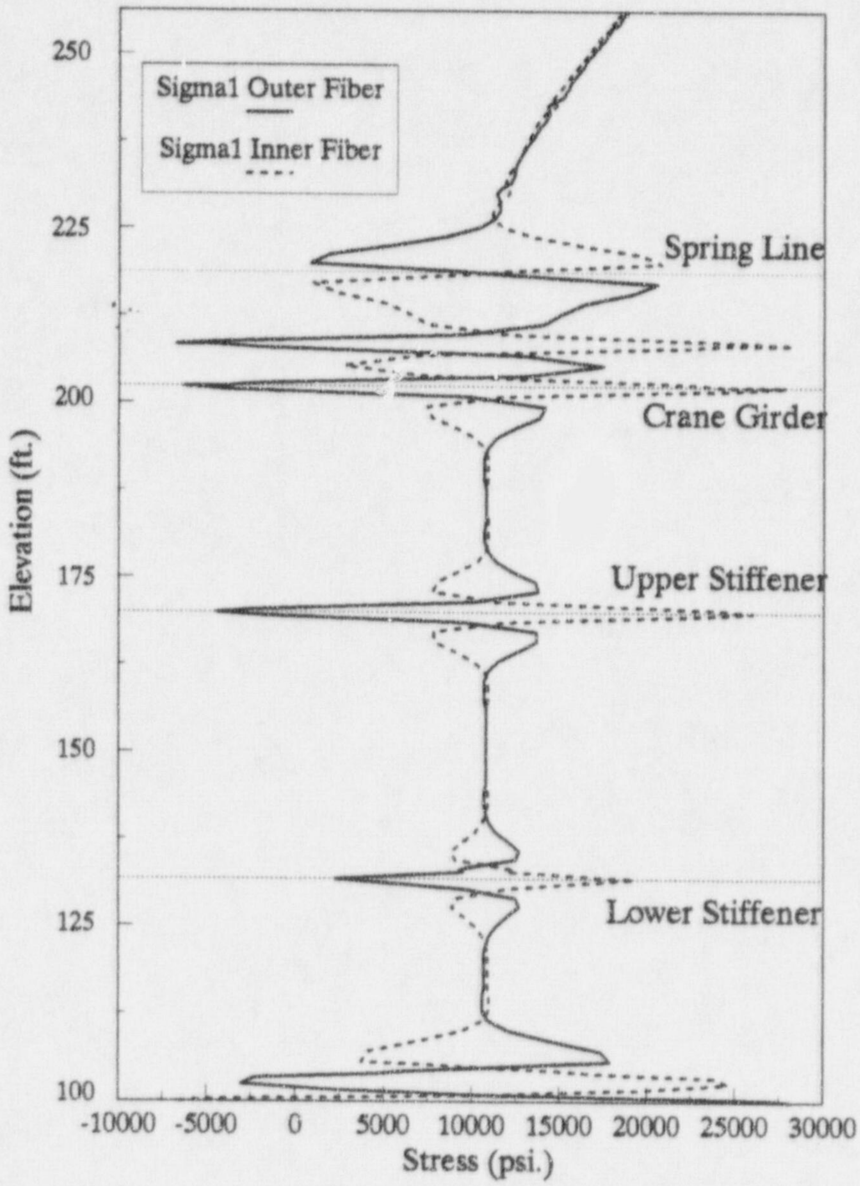

Fig. 2.14 Extreme Fiber Meridional ($Sigma_1$) Stresses due to Internal Pressure of 45 psig

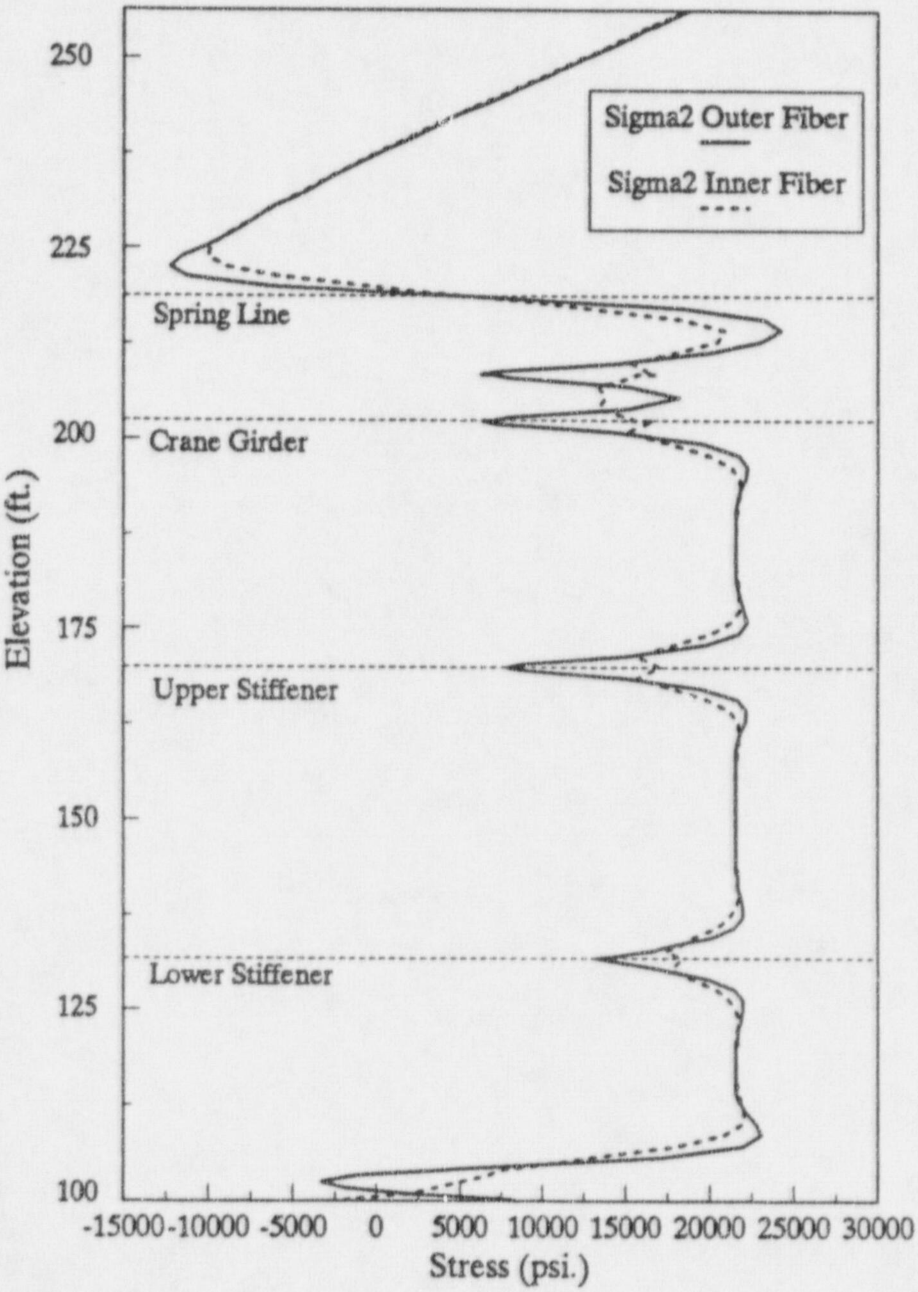

Fig. 2.15 Extreme Fiber Circumferential (Sigma$_2$) Stresses due to Internal Pressure of 45 psig

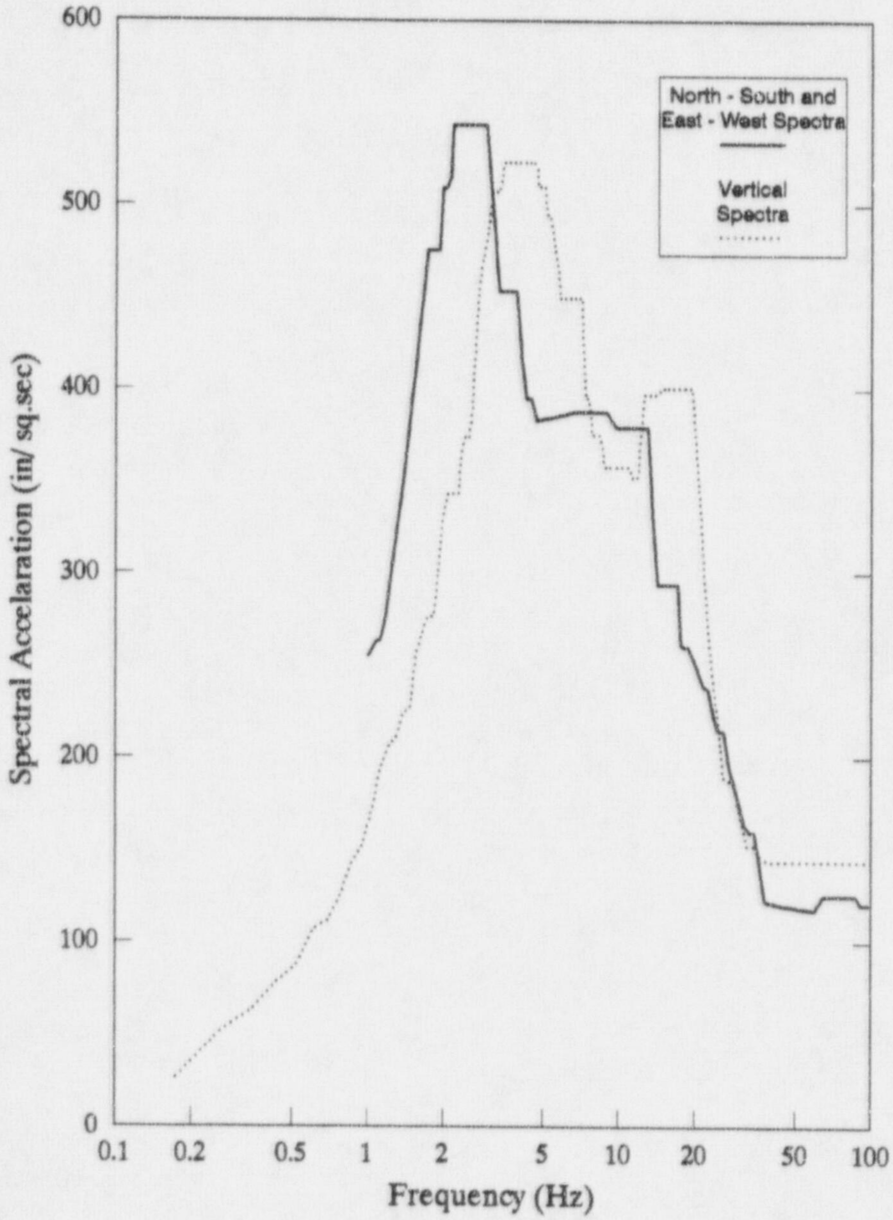

Fig. 2.16 SSE Response Spectra (4% Damping)

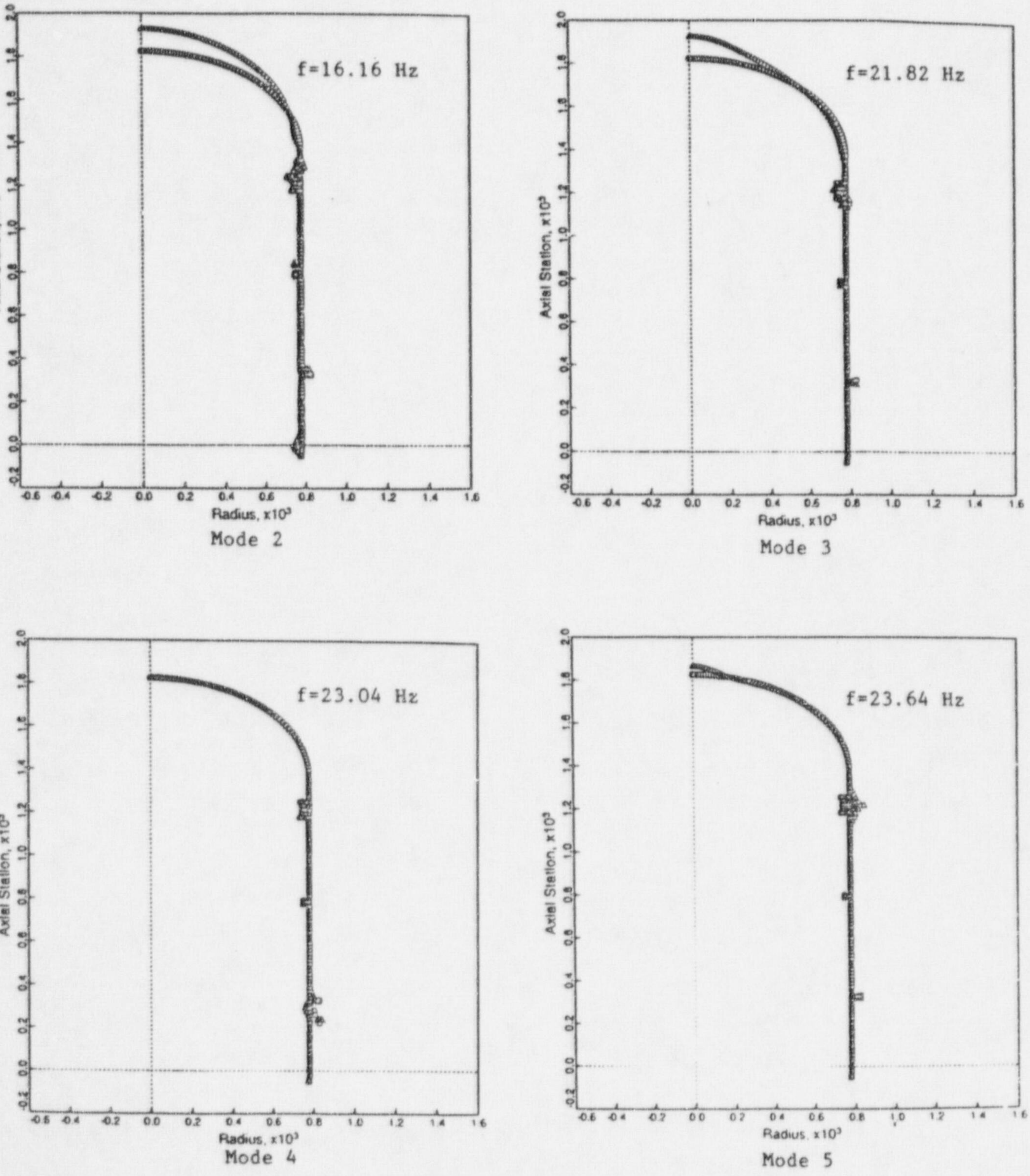

Fig. 2.17 Vibration Modes in the Vertical Direction

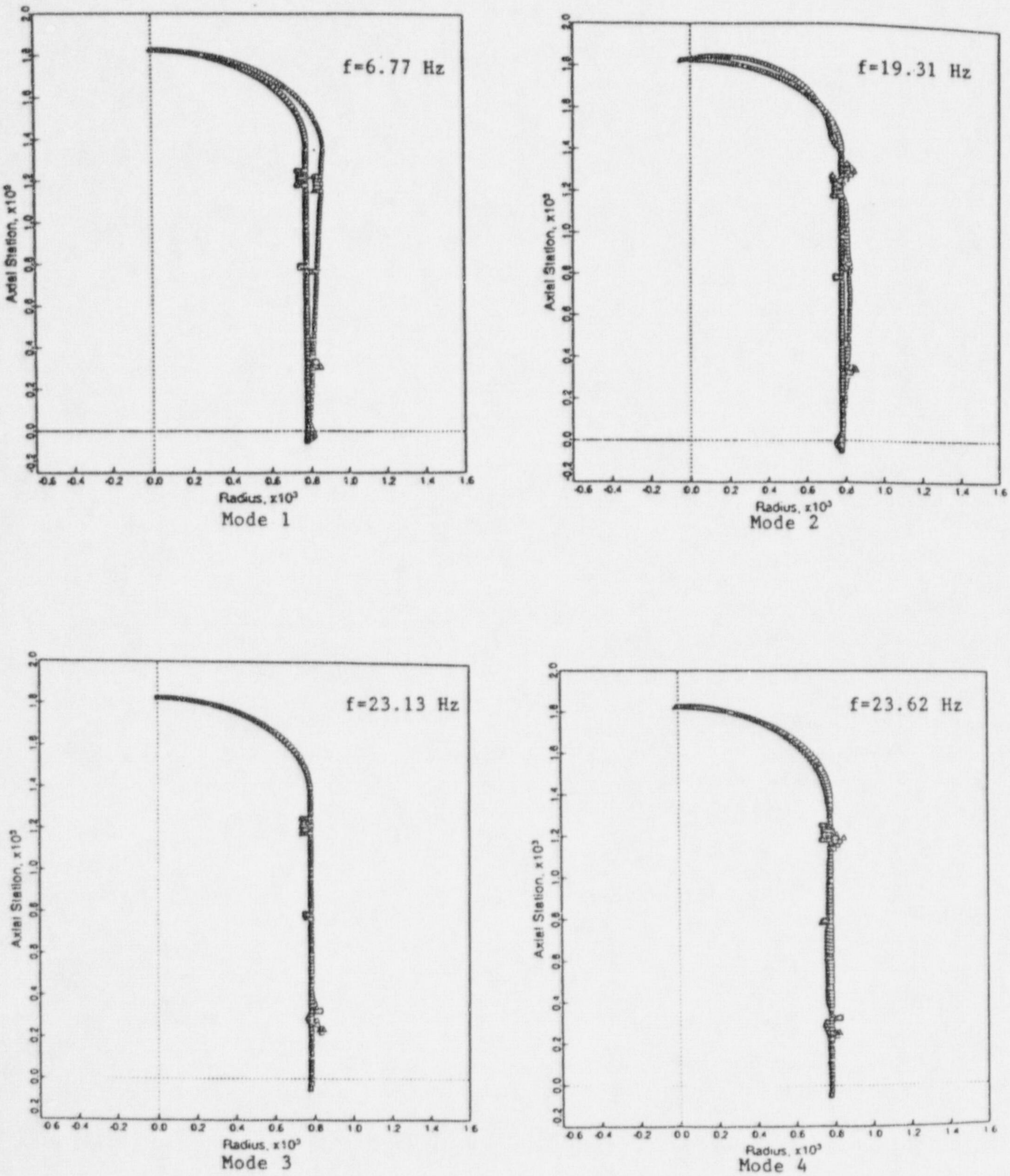

Fig. 2.18 Vibration Modes in the Horizontal Direction

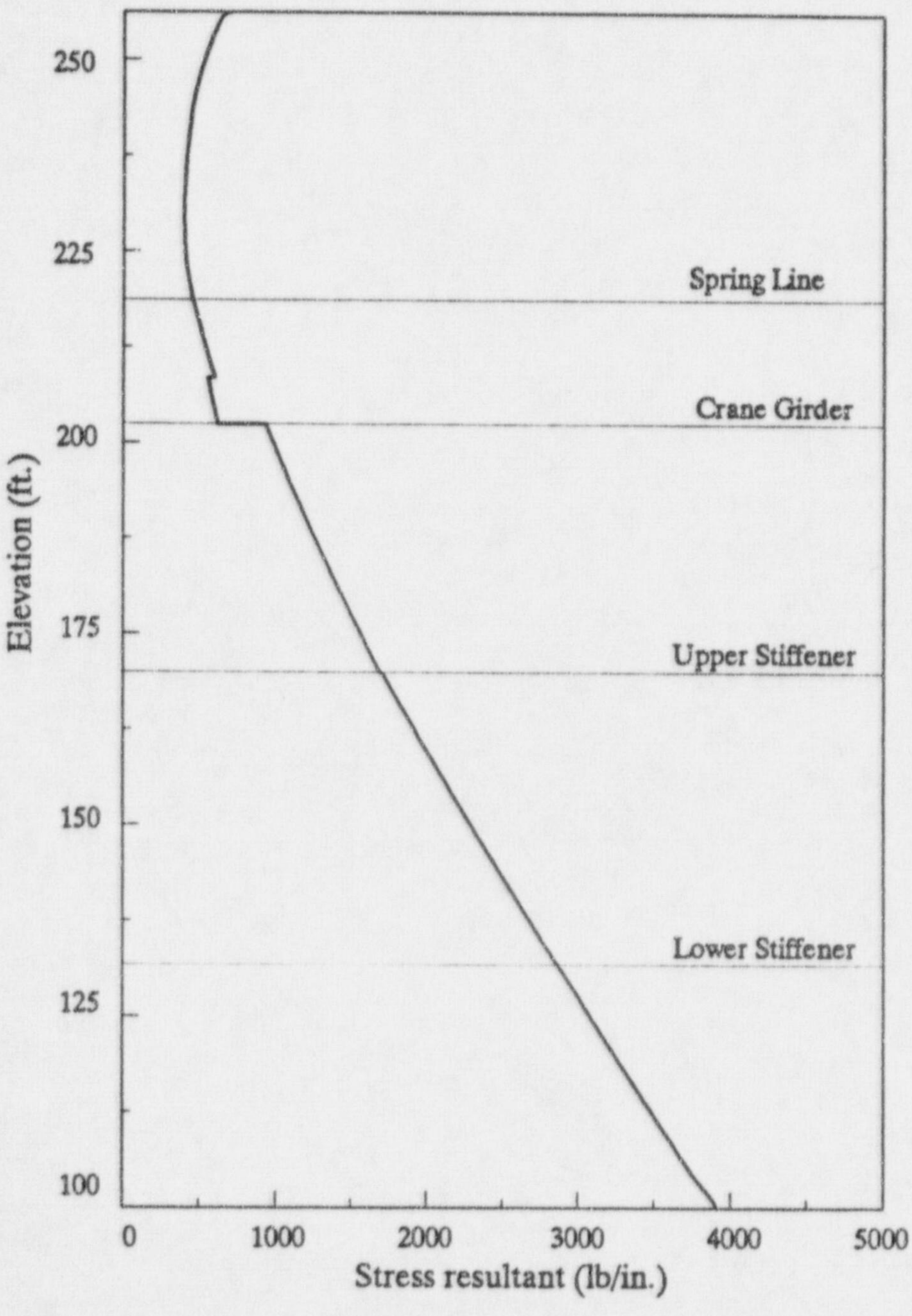

Fig. 2.19 SRSS Meridional (N_1) Stress Resultants

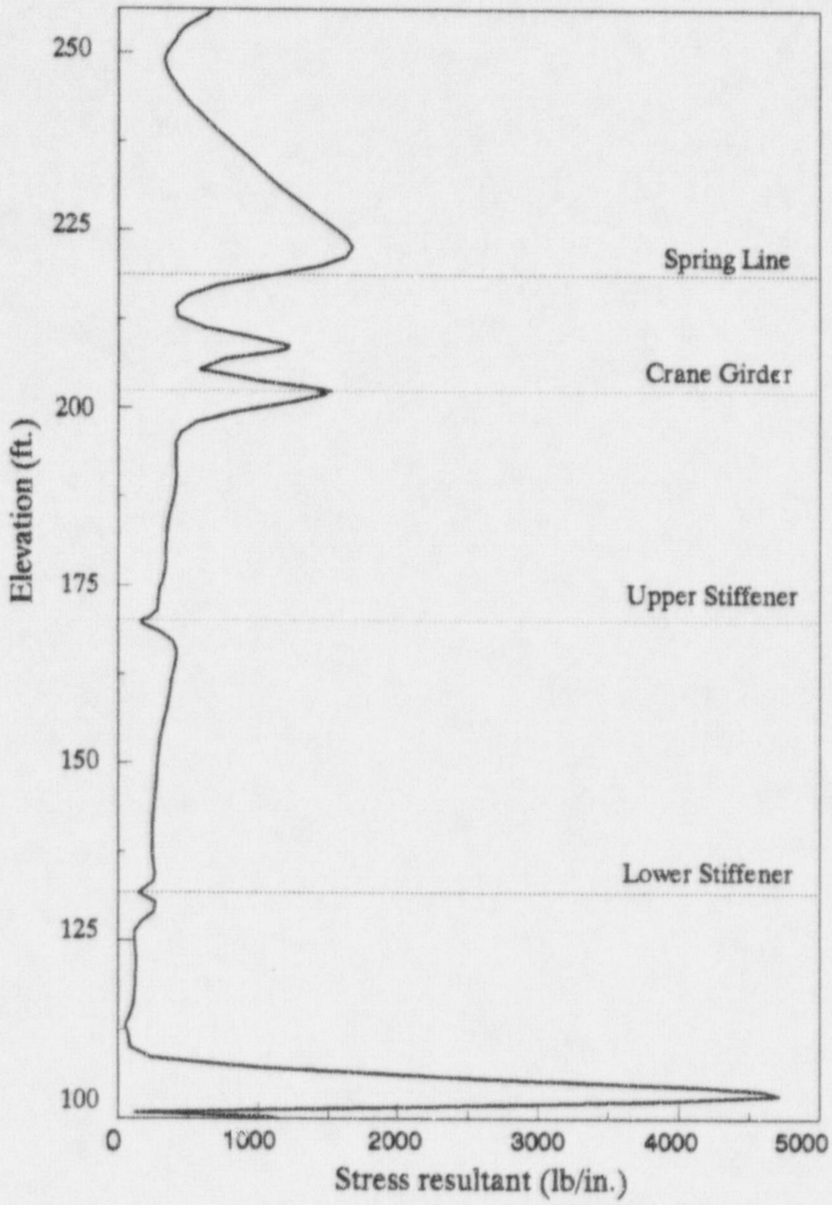

Fig. 2.20 SRSS Circumferential (N_2) Stress Resultants

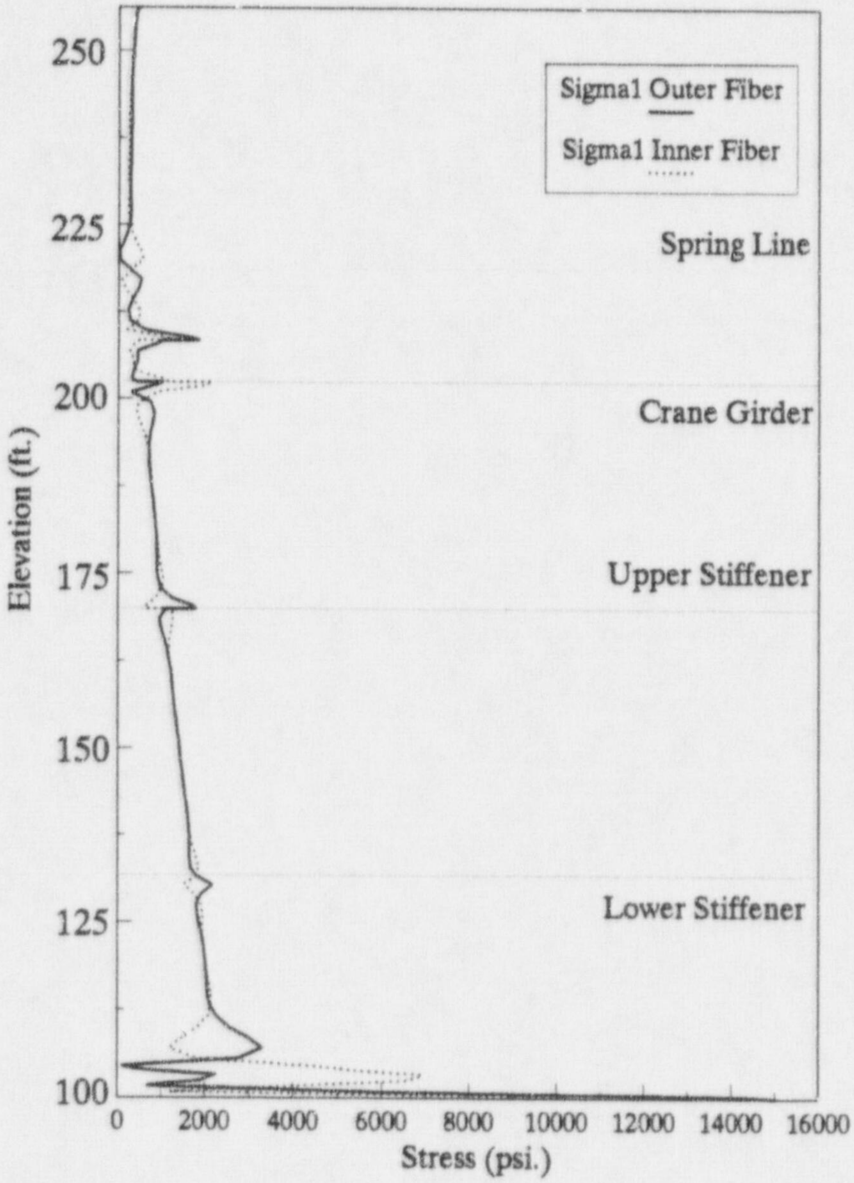

Fig. 2.21 Extreme Fiber SRSS Meridional (Sigma$_1$) Stresses

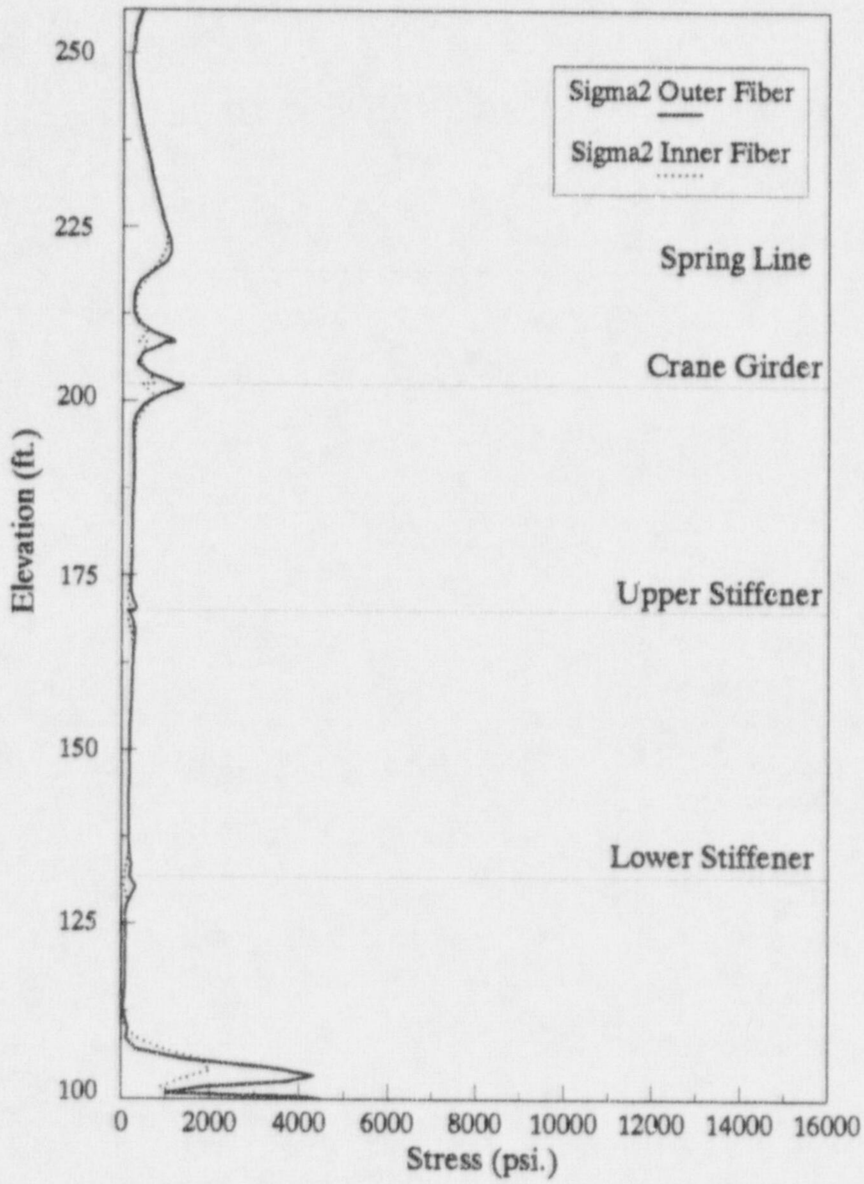

Fig 2.22 Extreme Fiber SRSS Circumferential ($Sigma_2$) Stresses

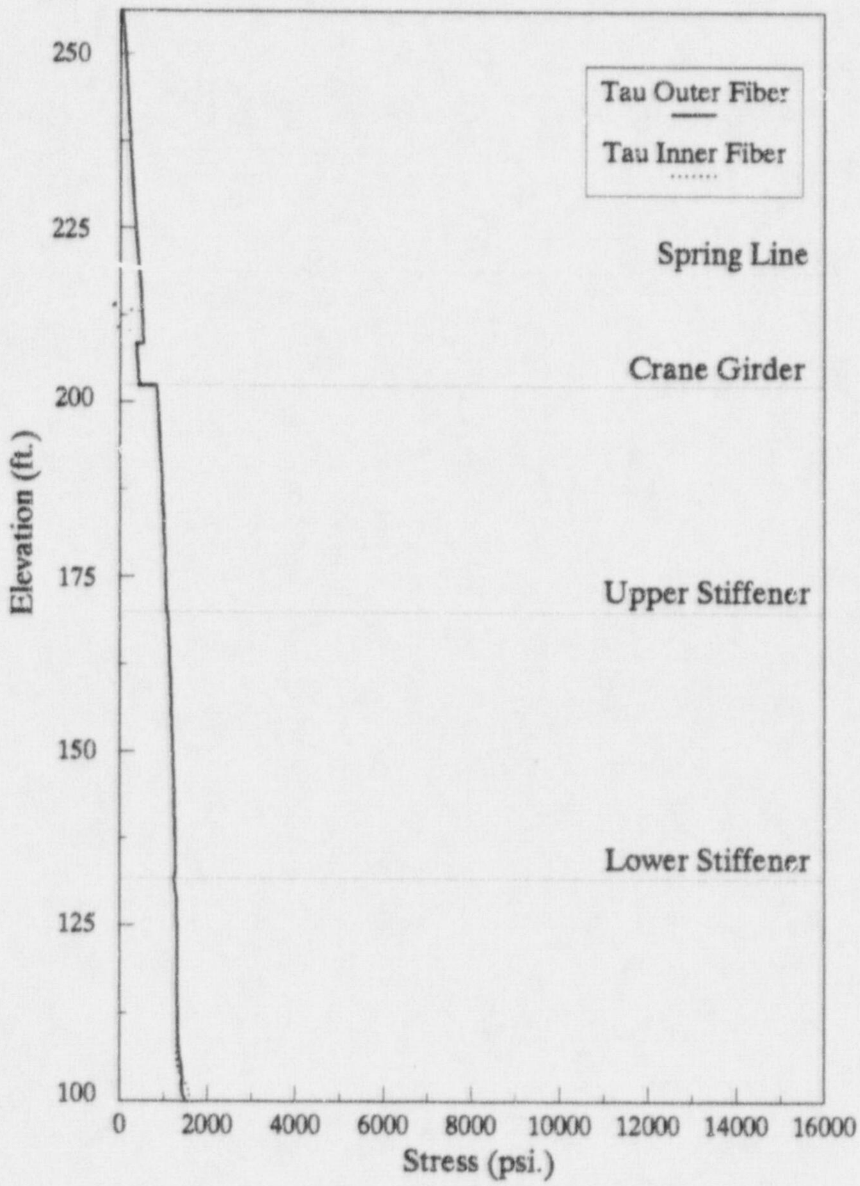

Fig. 2.23 Extreme Fiber SRSS Shear (Tau) Stresses

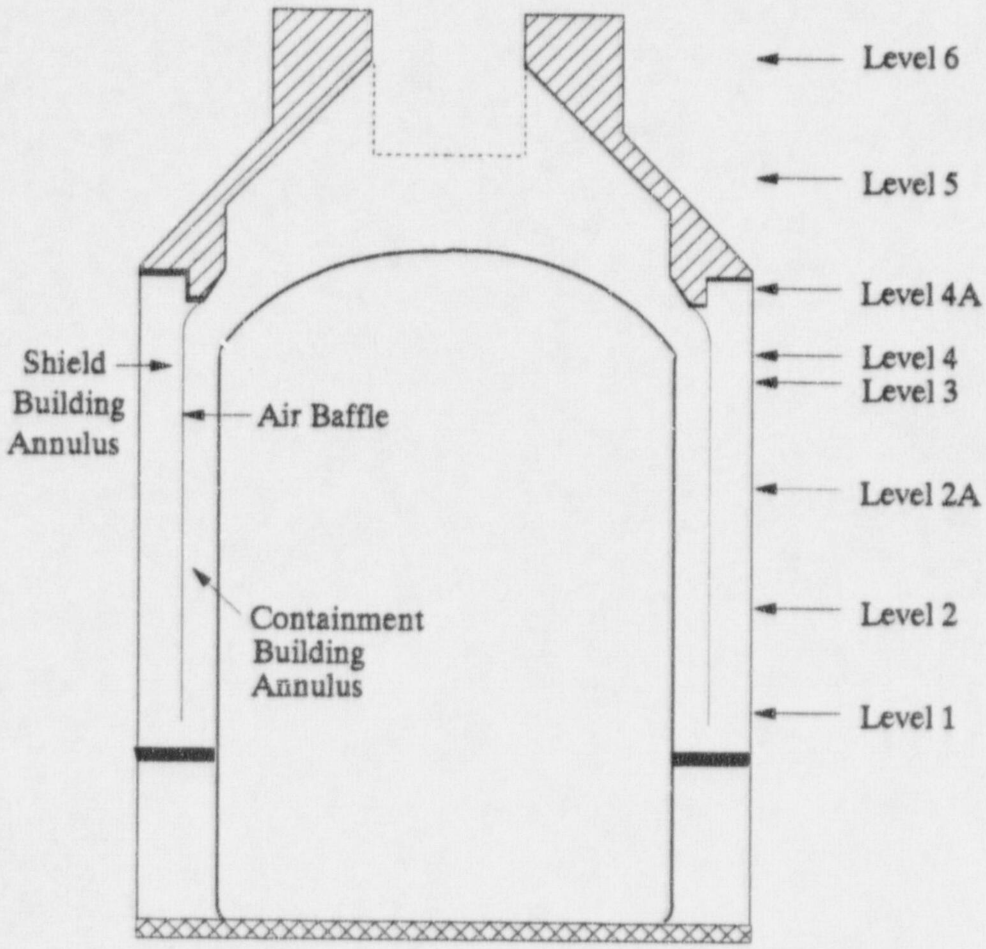

Fig. 2.24 Cross Sectional Elevation of AP600 Containment Indicating Location of Pressure Taps for Wind Pressure Coefficient Measurement

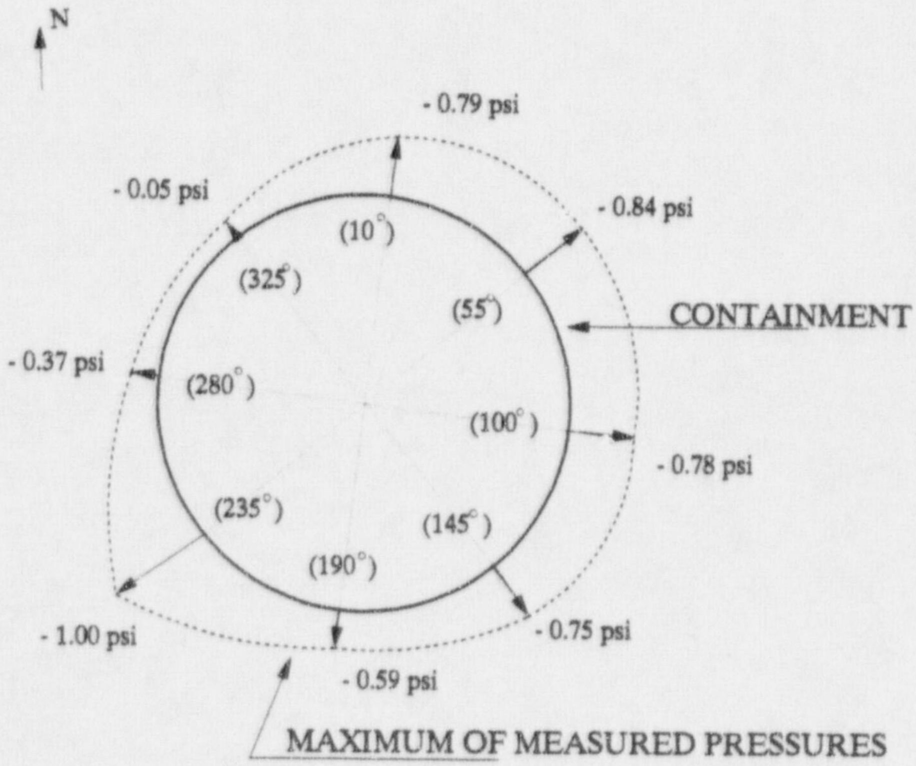

Fig. 2.25 Pressure Distribution Corresponding to Measured Maximum Absolute Value Pressure Coefficients at Level 5 [2.13]

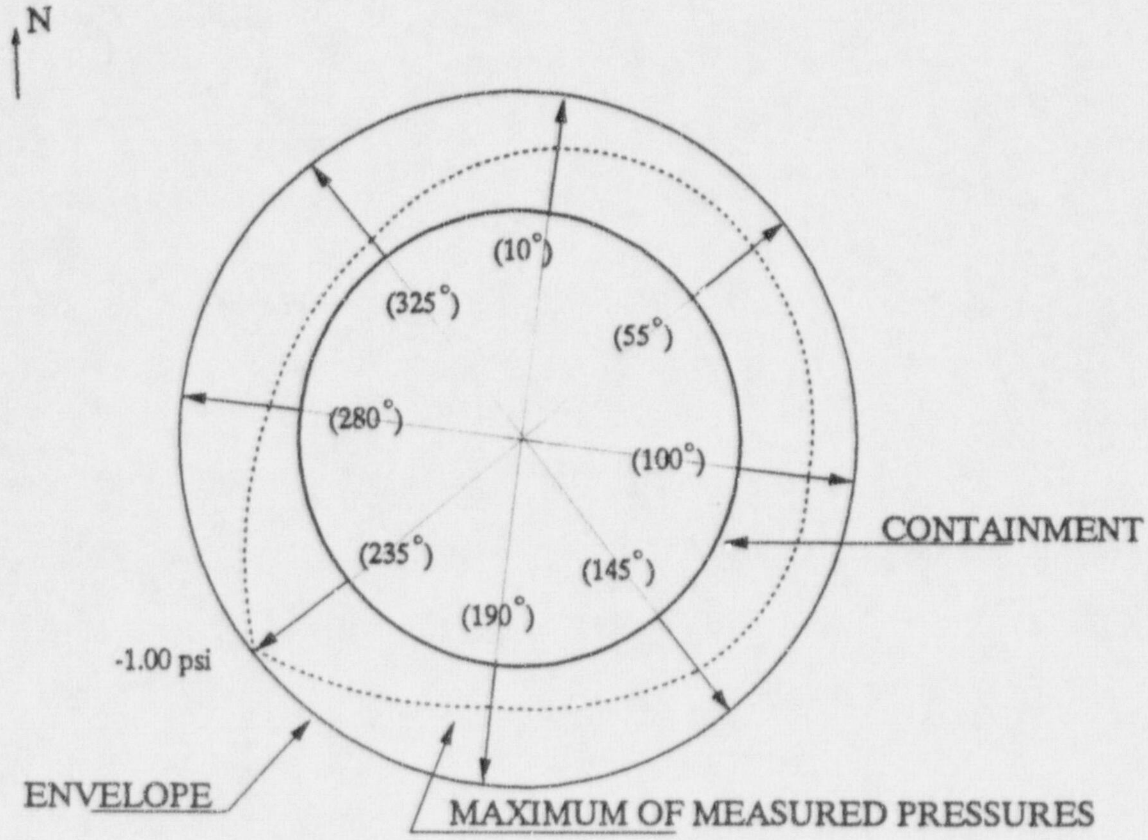

Fig. 2.26 Enveloped Pressure Distribution (Uniform Wind Suction)

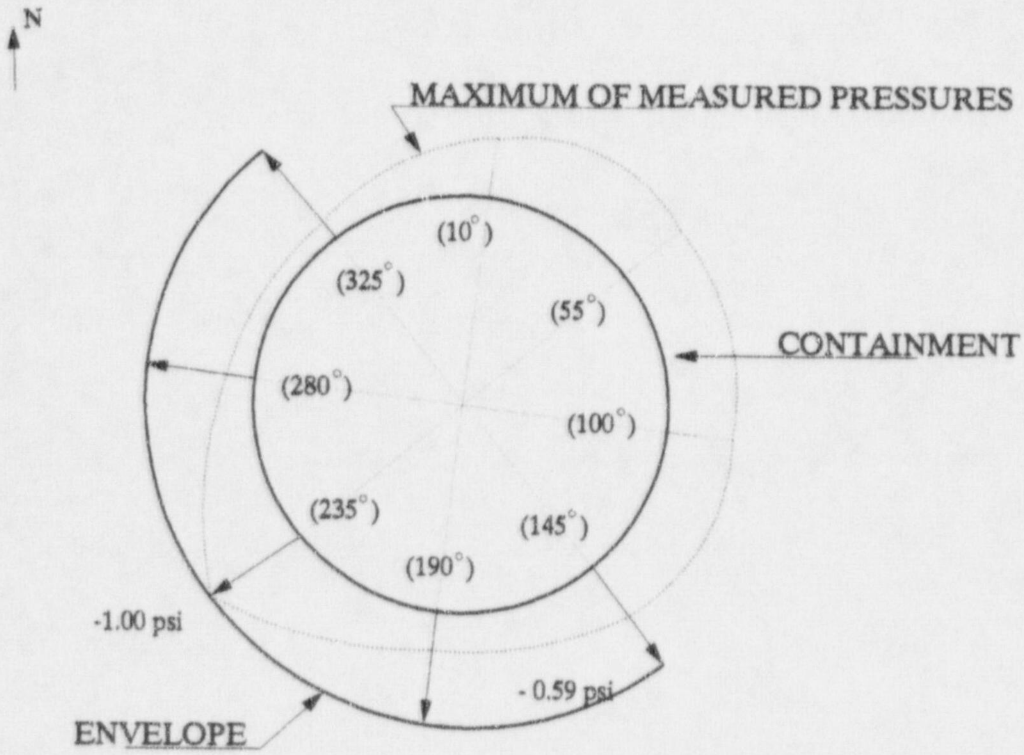

Fig. 2.27 Enveloped Pressure Distribution (Wind Lateral Load)

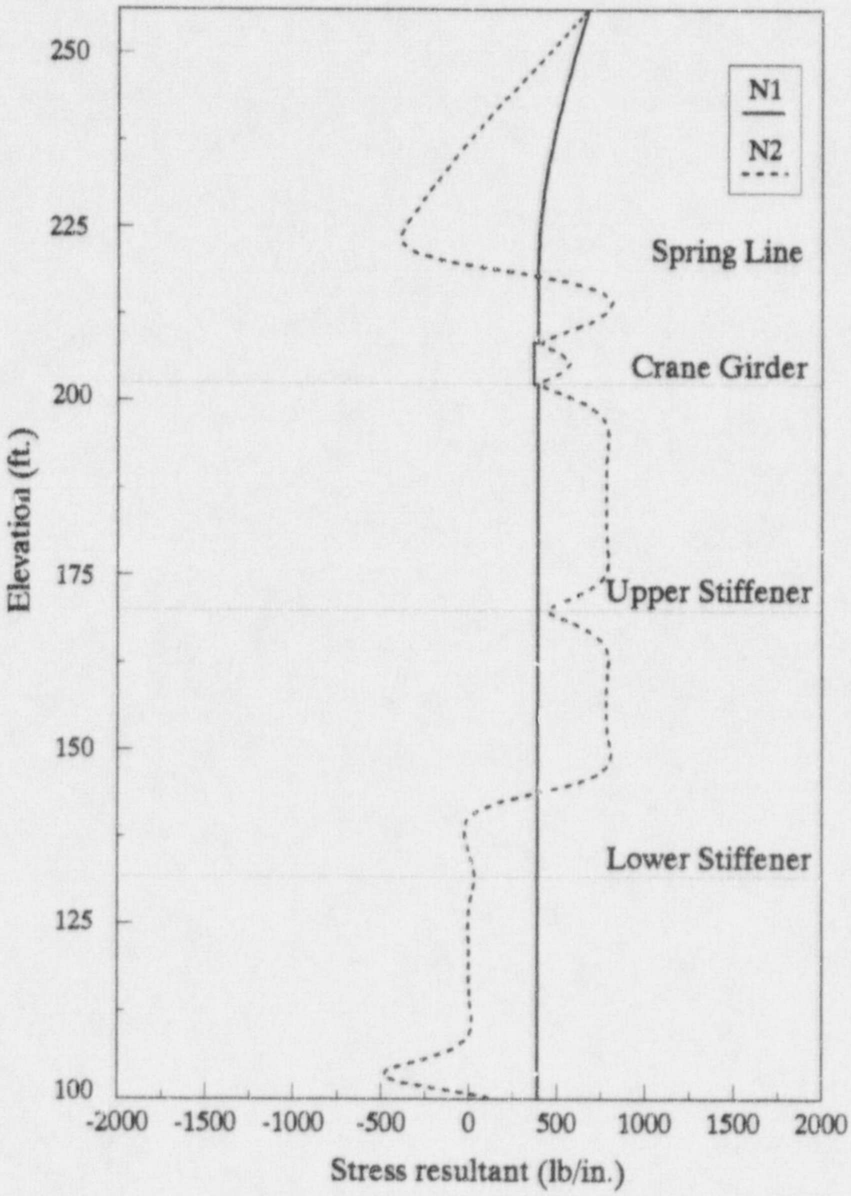

Fig. 2.28 Meridional (N_1) and Circumferential (N_2) Stress Resultants due to Uniform Wind Suction of 1.0 psig

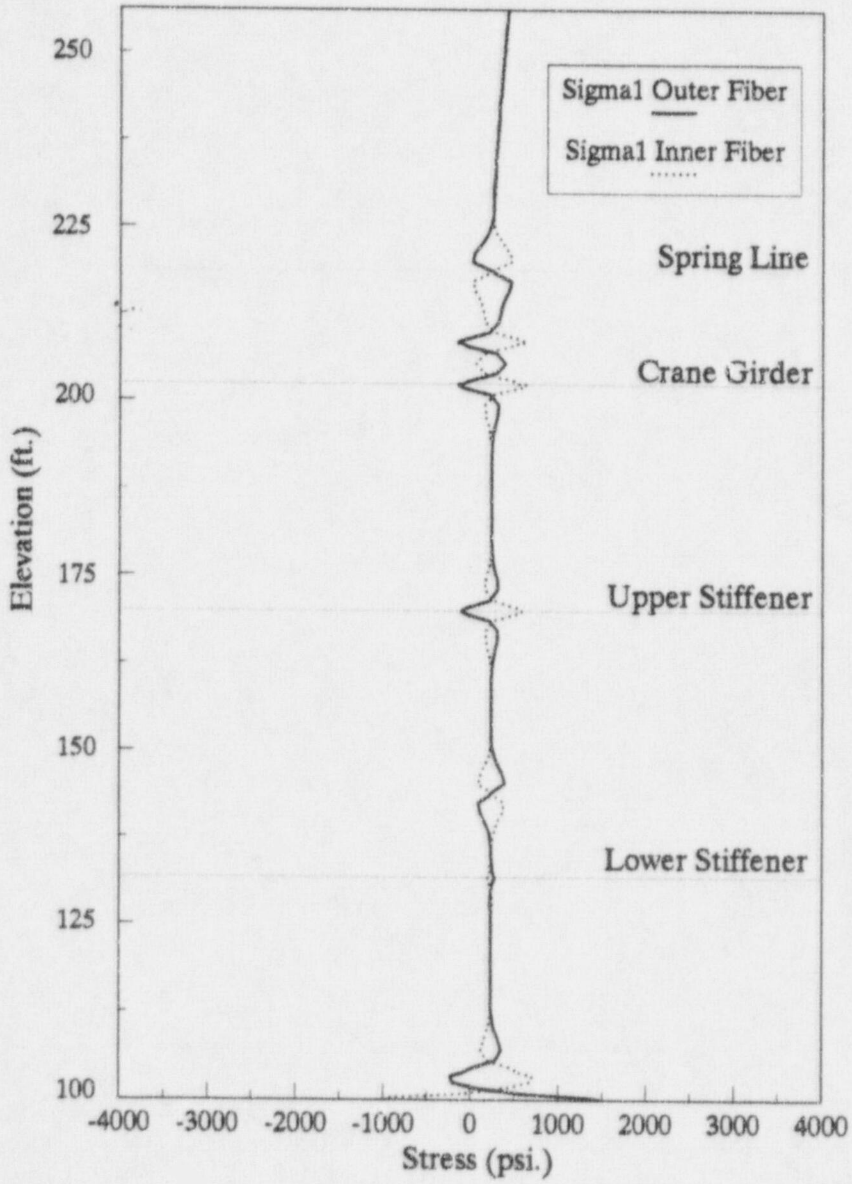

Fig. 2.29 Extreme Fiber Meridional ($Sigma_1$) Stresses due to Uniform Wind Suction of 1.0 psig

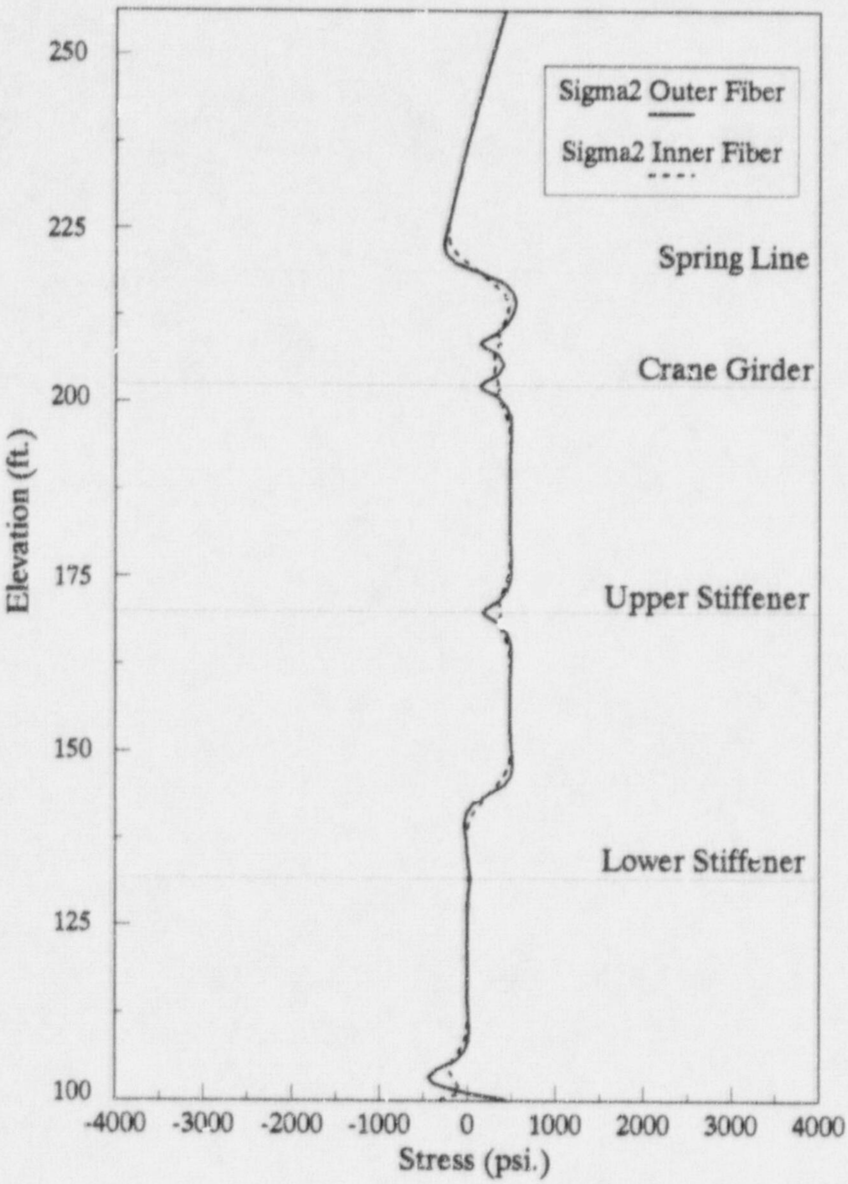

Fig. 2.30 Extreme Fiber Circumferential ($Sigma_2$) Stresses due to Uniform Wind Suction of 1.0 psig

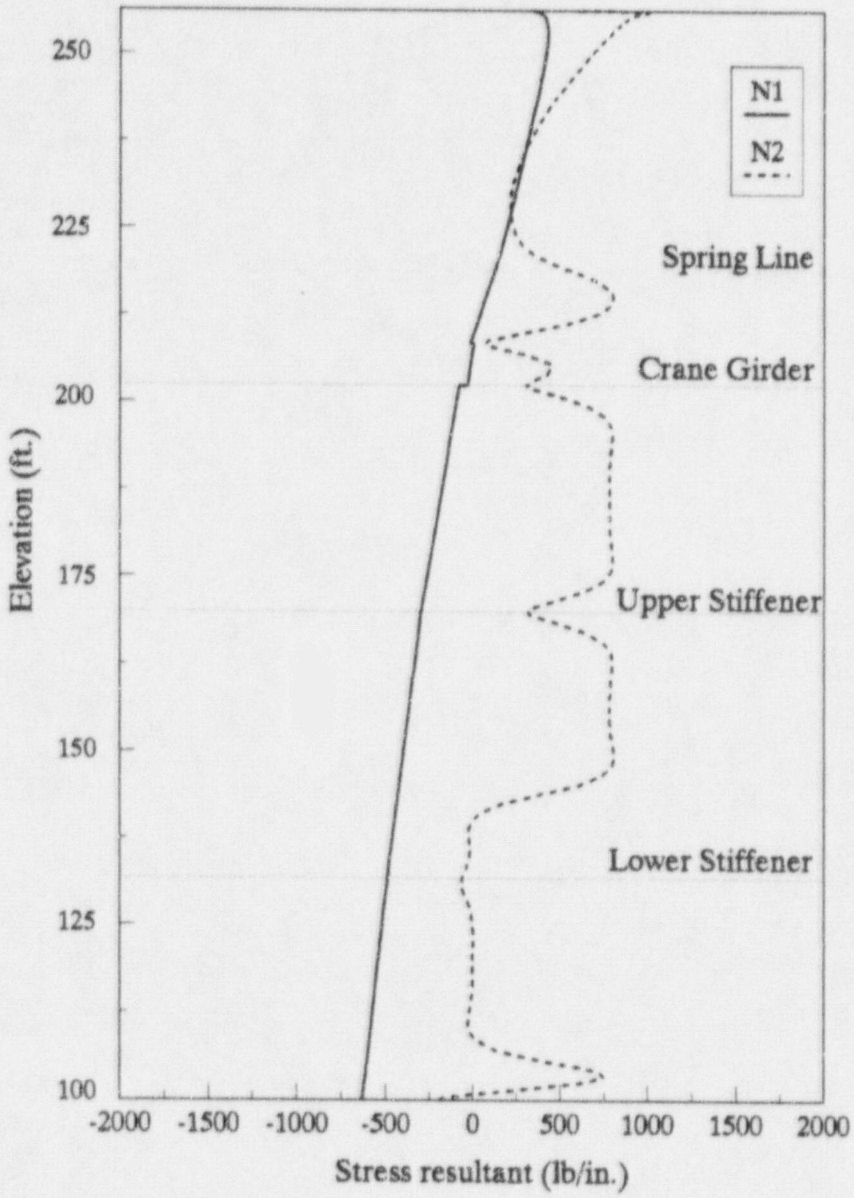

Fig. 2.31 Meridional (N_1) and Circumferential (N_2) Stress Resultants on the 235° Azimuth due to Enveloped Wind Lateral Load (1.0 psig)

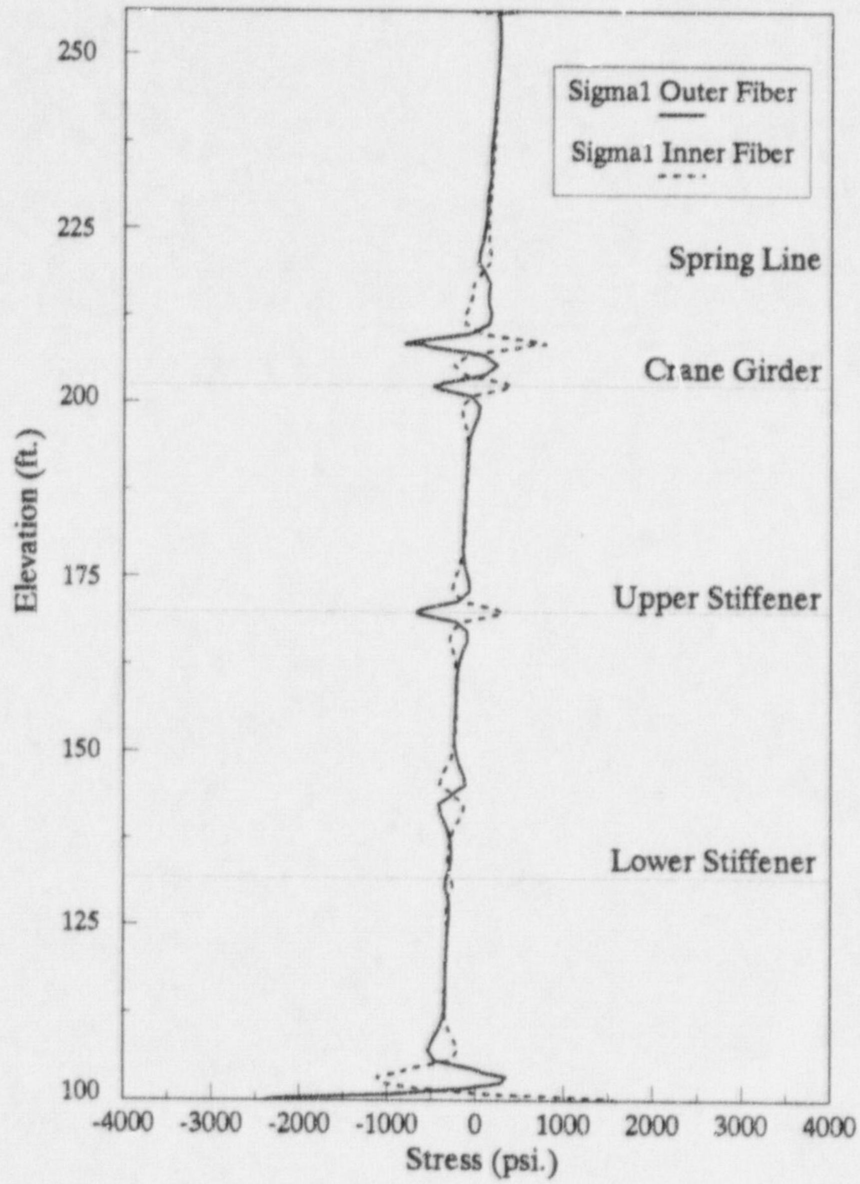

Fig. 2.32 Extreme Fiber Meridional (Sigma$_1$) Stresses on the 235° Azimuth due to Enveloped Wind Lateral Load (1.0 psig)

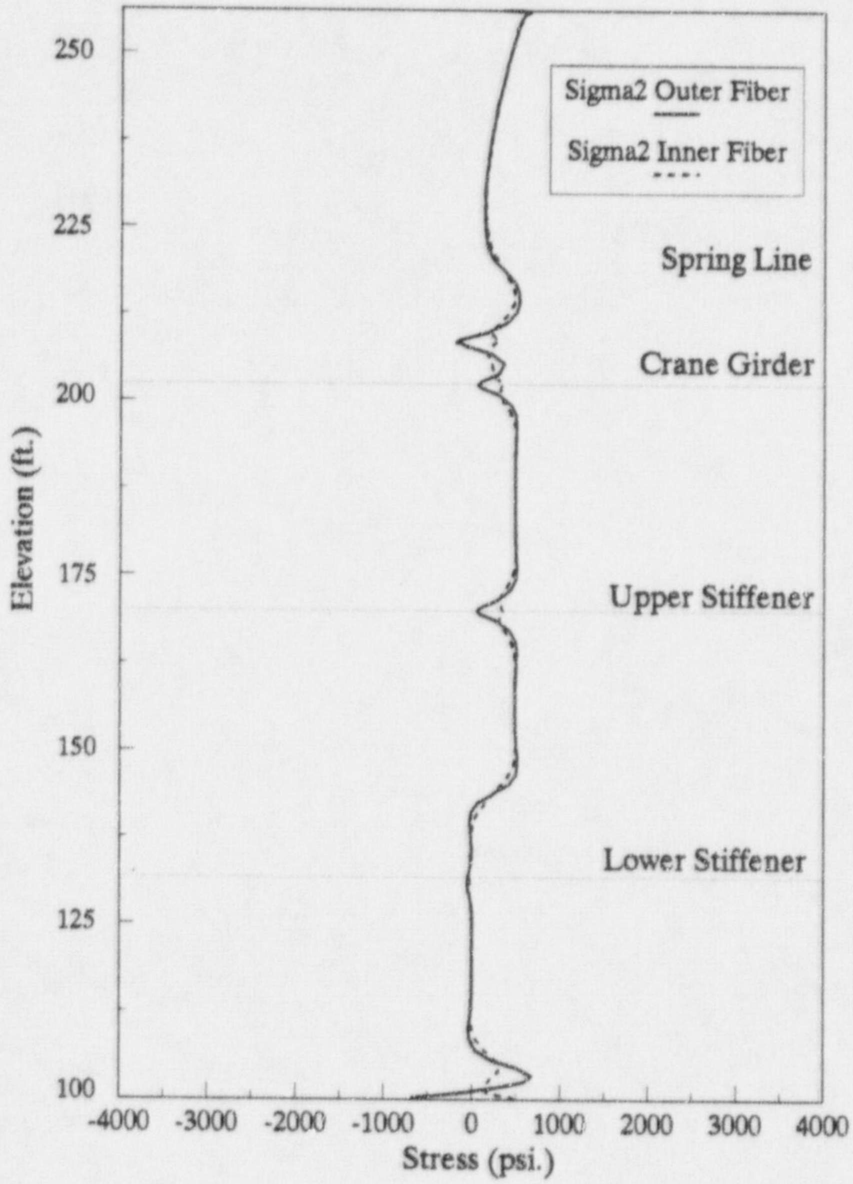

Fig. 2.33 Extreme Fiber Circumferential ($Sigma_2$) Stresses on the 235° Azimuth due to Enveloped Wind Lateral Load (1.0 psig)

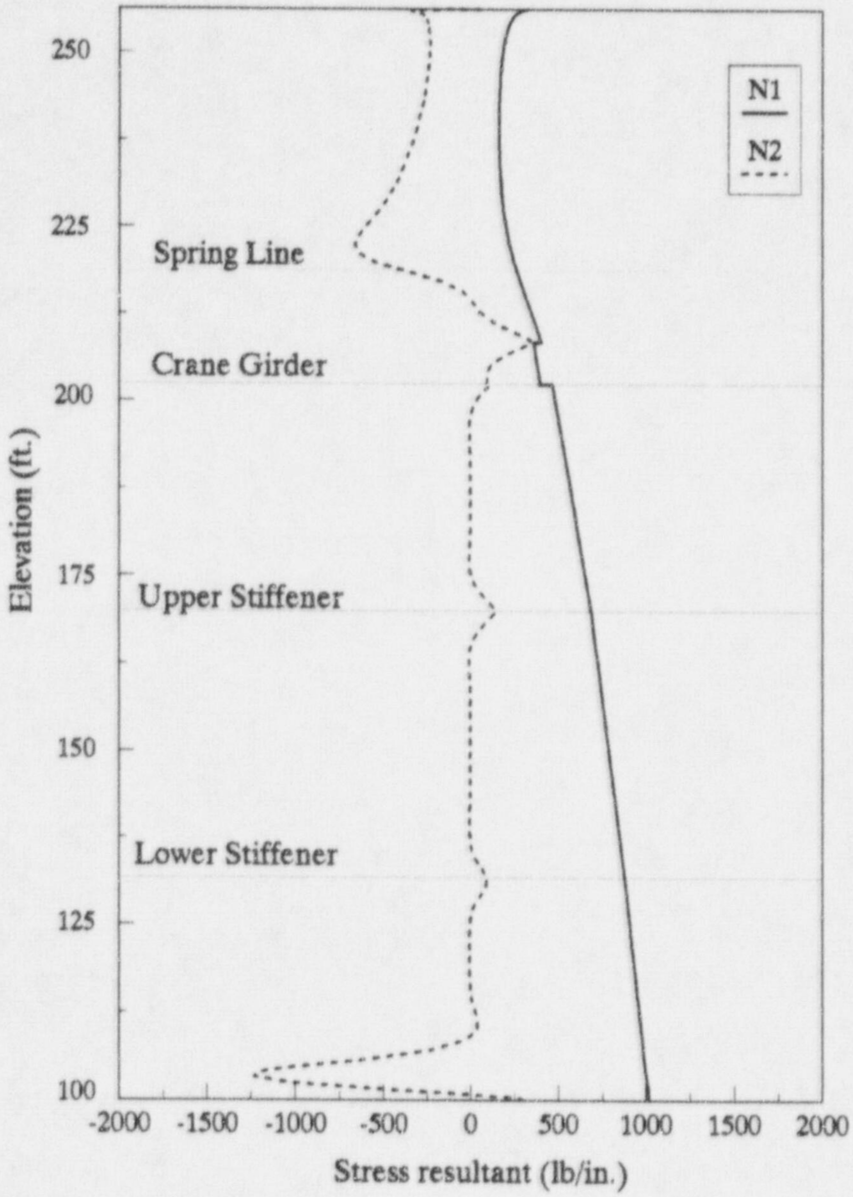

Fig. 2.34 Meridional (N_1) and Circumferential (N_2) Stress Resultants on the 55° Azimuth due to Enveloped Wind Lateral Load (1.0 psig)

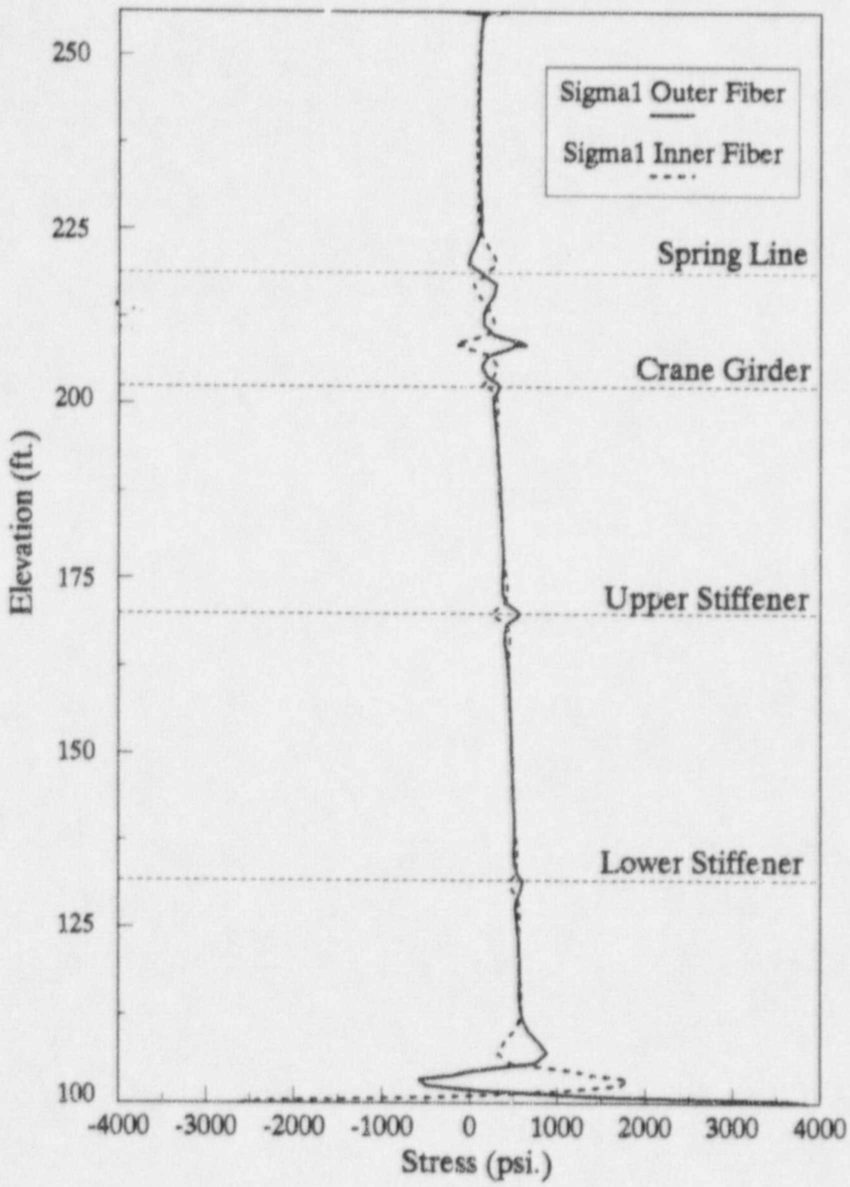

Fig. 2.35 Extreme Fiber Meridional ($Sigma_1$) Stresses on the 55° Azimuth due to Enveloped Wind Lateral Load (1.0 psig)

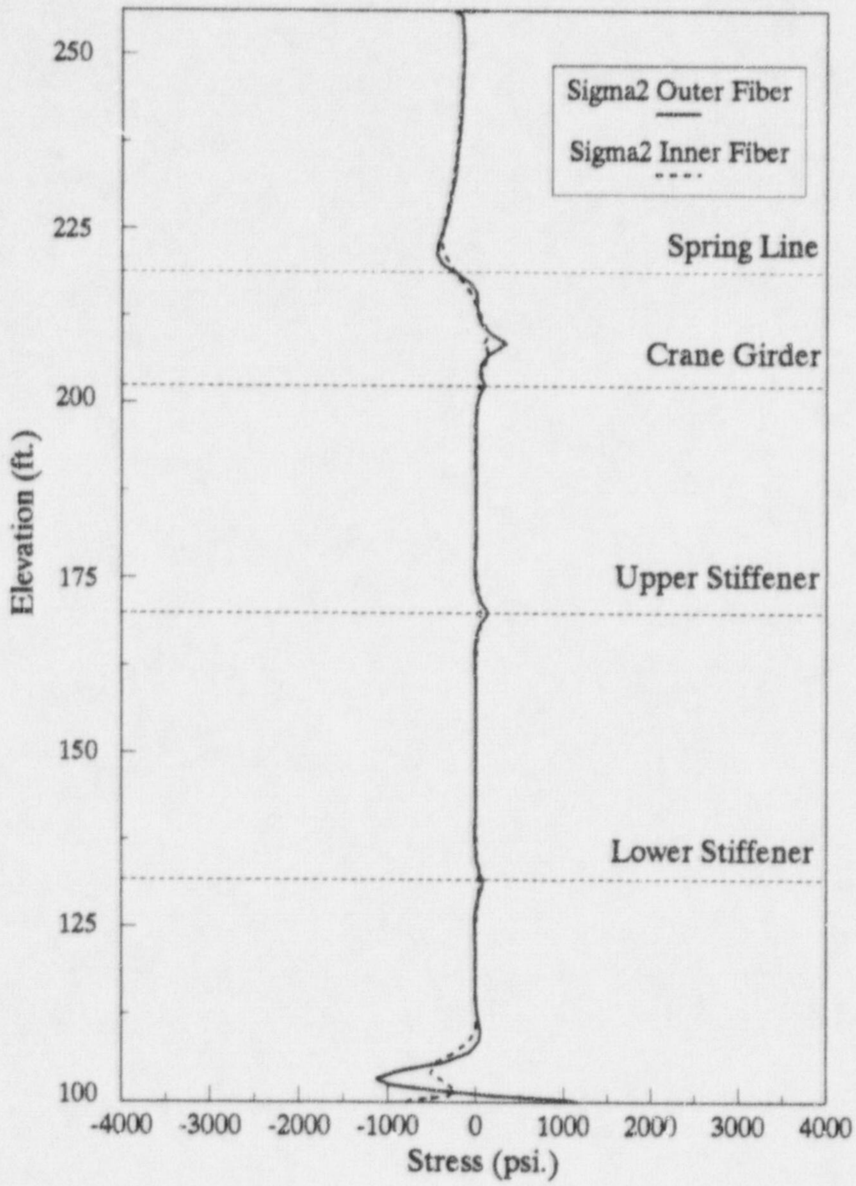

Fig. 2.36 Extreme Fiber Circumferential ($Sigma_2$) Stresses on the 55° Azimuth due to Enveloped Wind Lateral Load (1.0 psig)

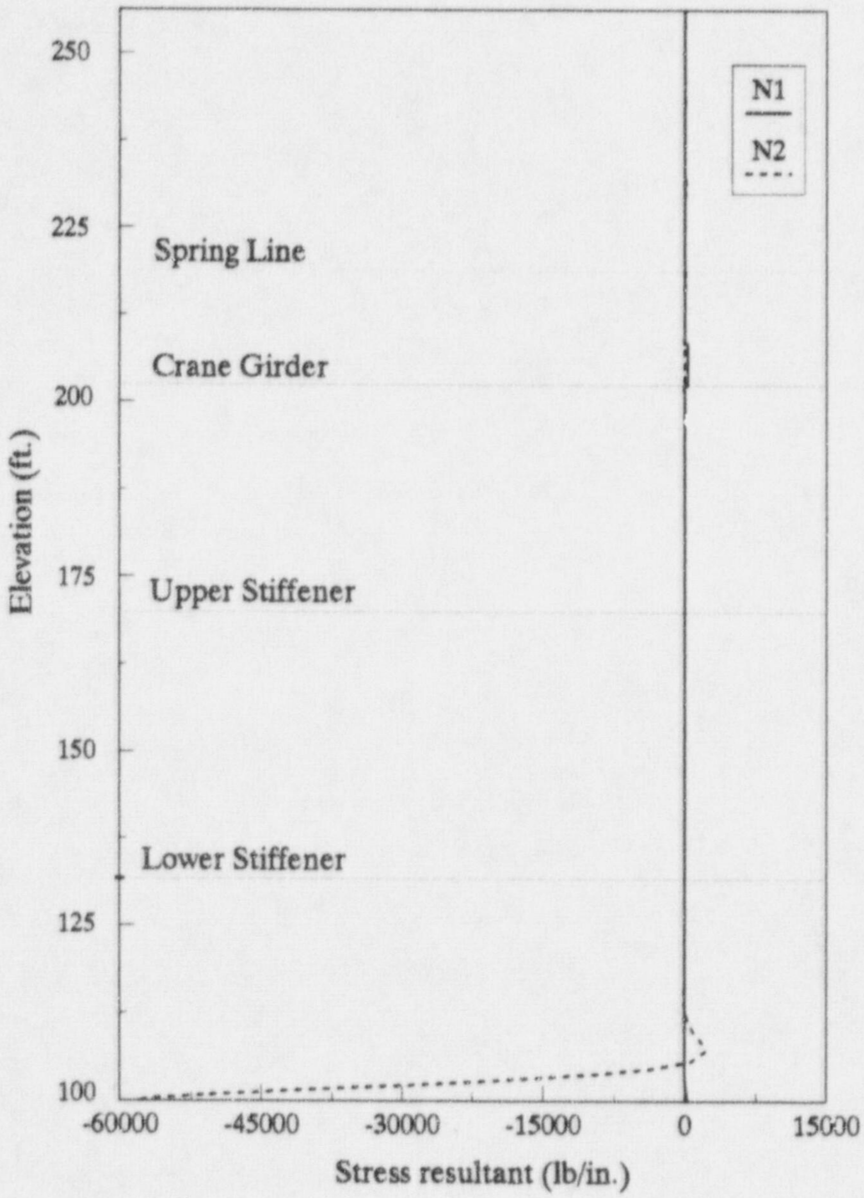

Fig. 2.37 Meridional (N_1) and Circumferential (N_2) Stress Resultants due to Case 1 Temperature Loading

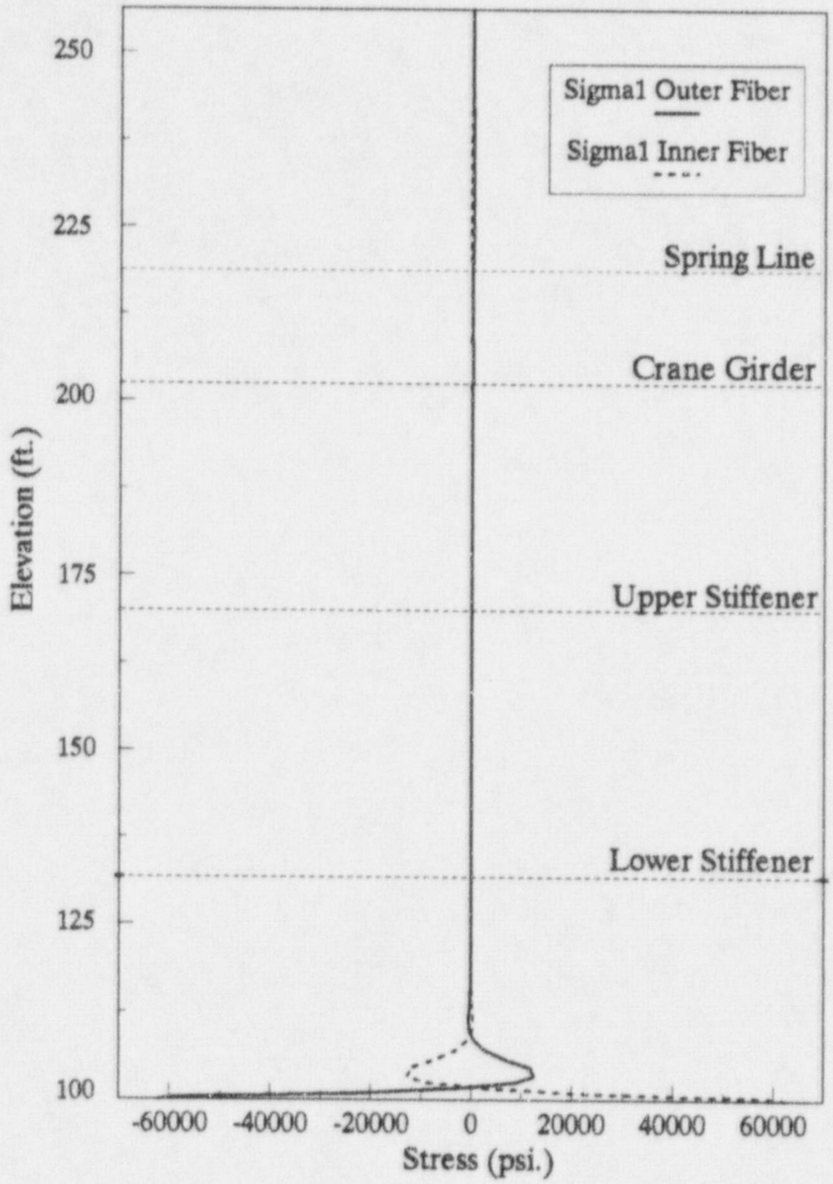

Fig. 2.38 Extreme Fiber Meridional (Sigma$_1$) Stresses due to Case 1 Temperature Loading

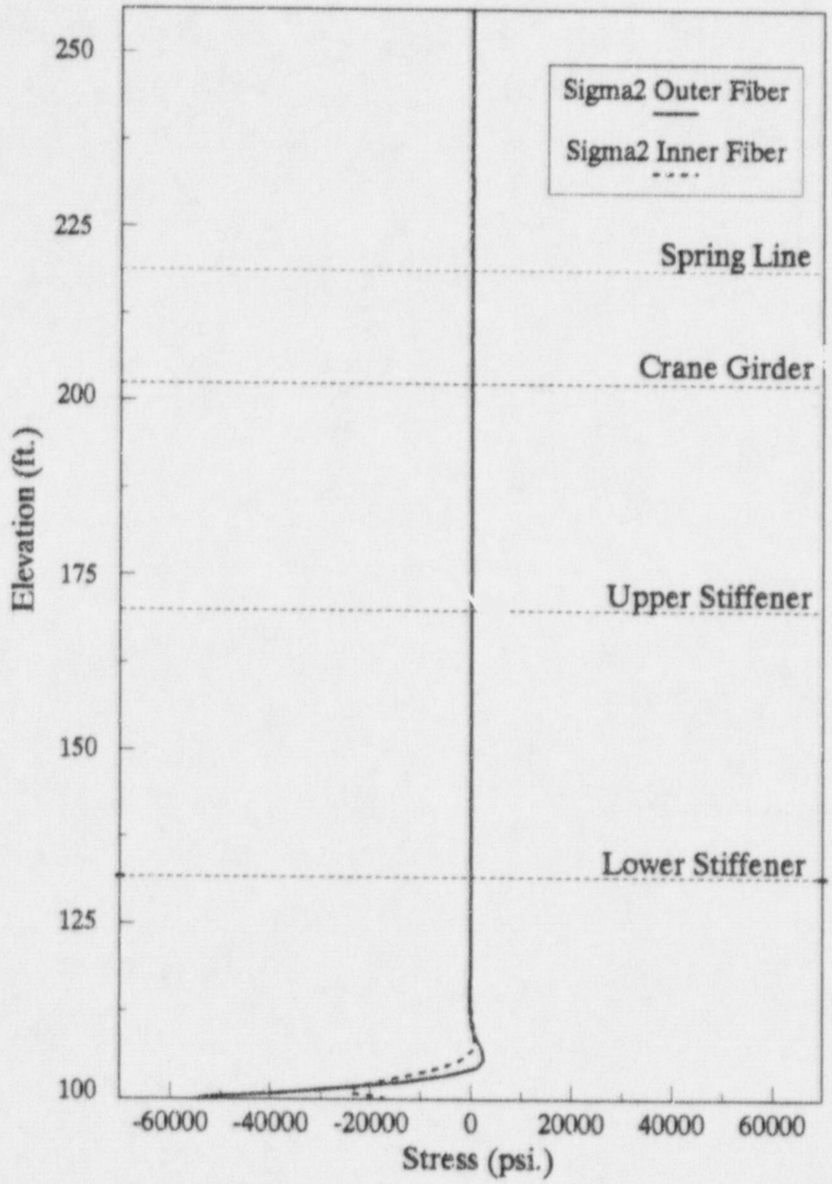

Fig. 2.39 Extreme Fiber Circumferential (Sigma$_2$) Stresses due to Case 1 Temperature Loading

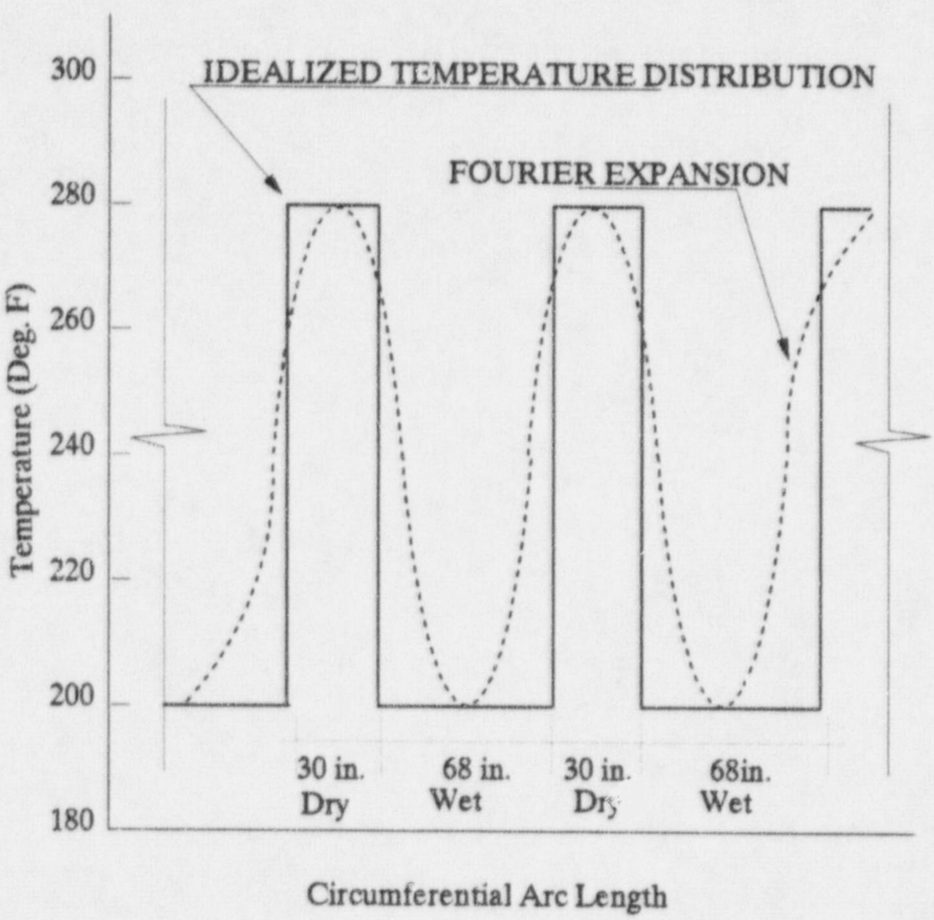

Fig. 2.40 Case 2 Temperature Loading Above Elevation 132' 3"

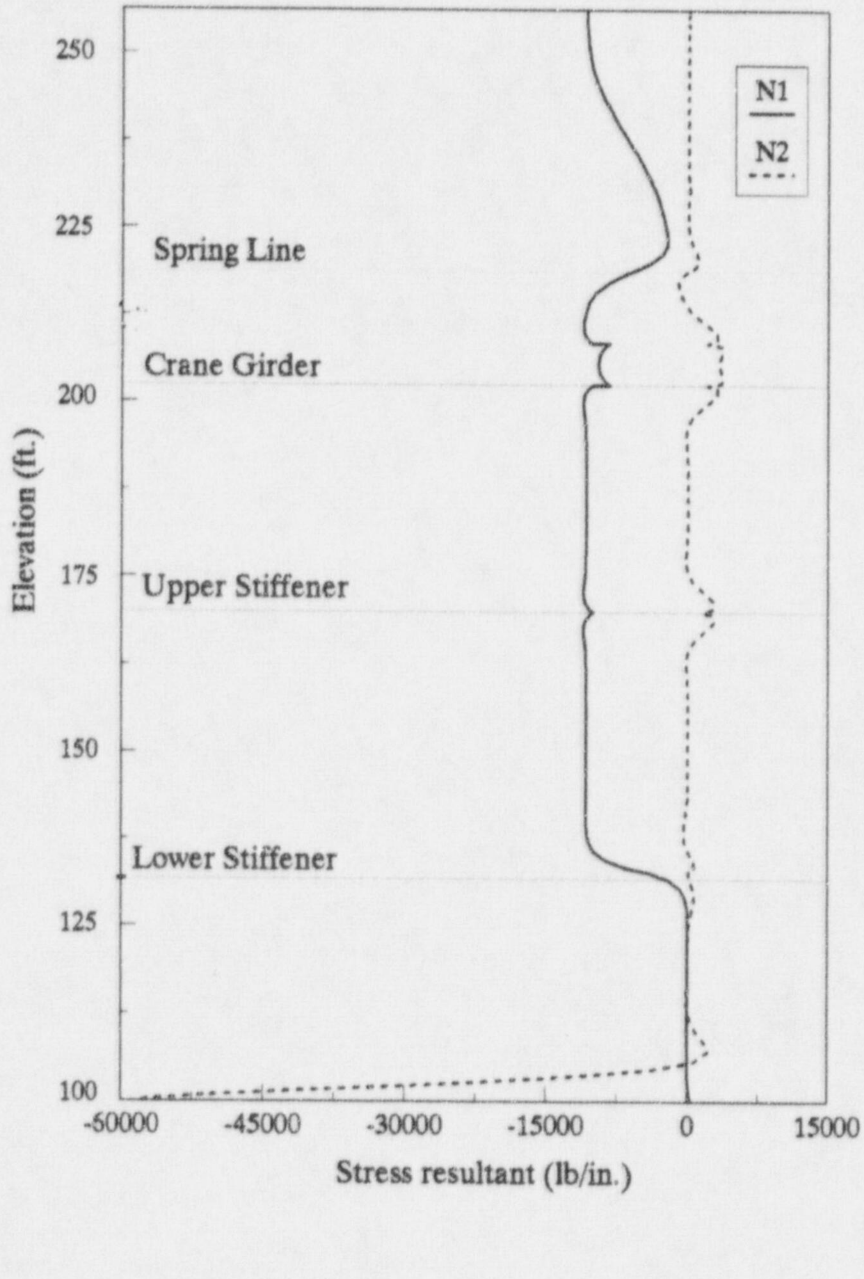

Fig. 2.41 Meridional (N_1) and Circumferential (N_2) Stress Resultants due to Case 2 Temperature Loading (Dry Zone)

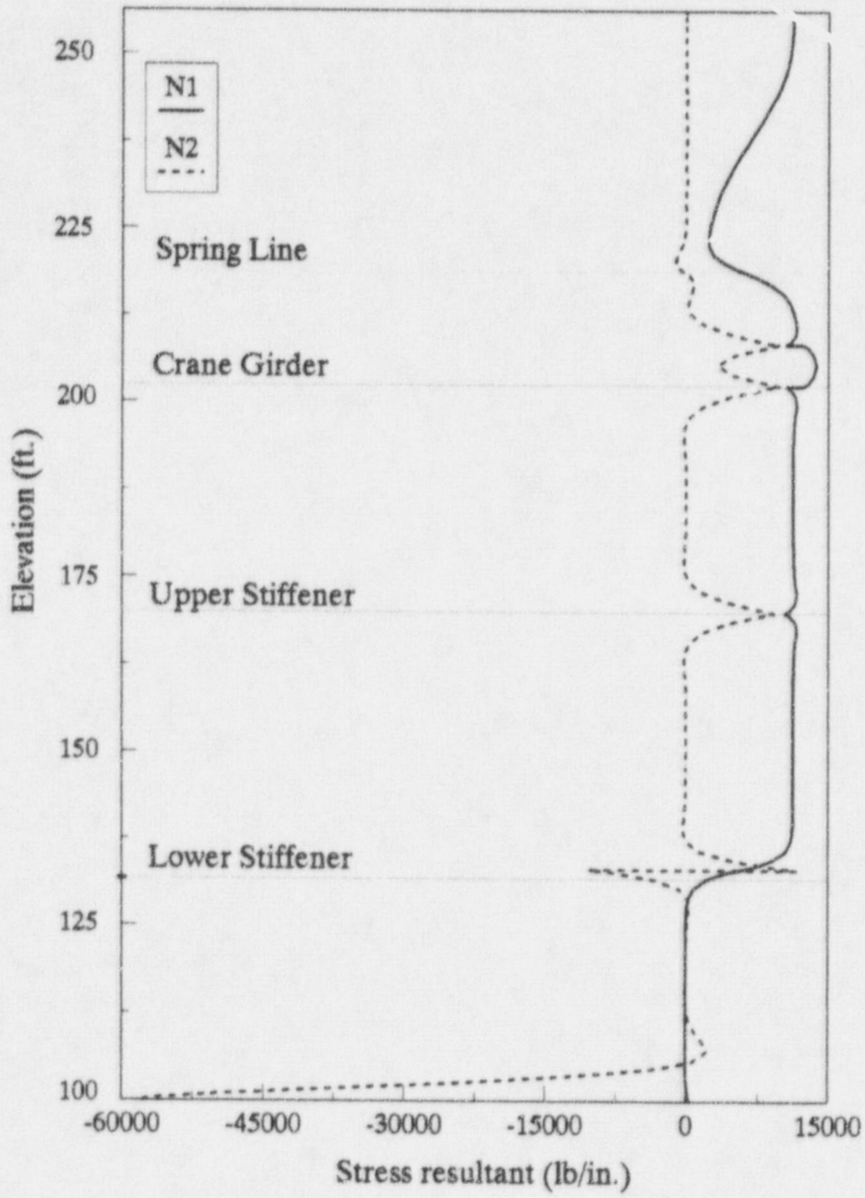

Fig. 2.42 Meridional (N_1) and Circumferential (N_2) Stress Resultants due to Case 2 Temperature Loading (Wet Zone)

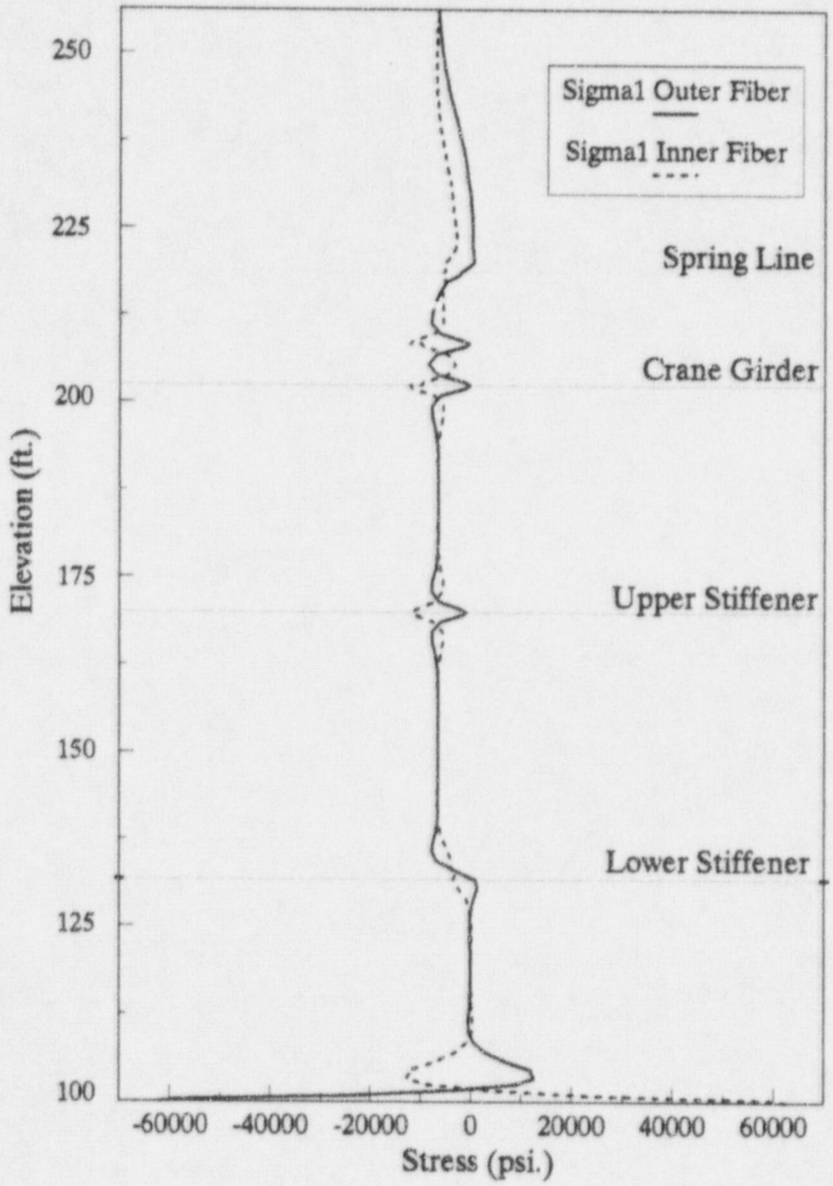

Fig. 2.43 Extreme Fiber Meridional ($Sigma_1$) Stresses due to Case 2 Temperature Loading (Dry Zone)

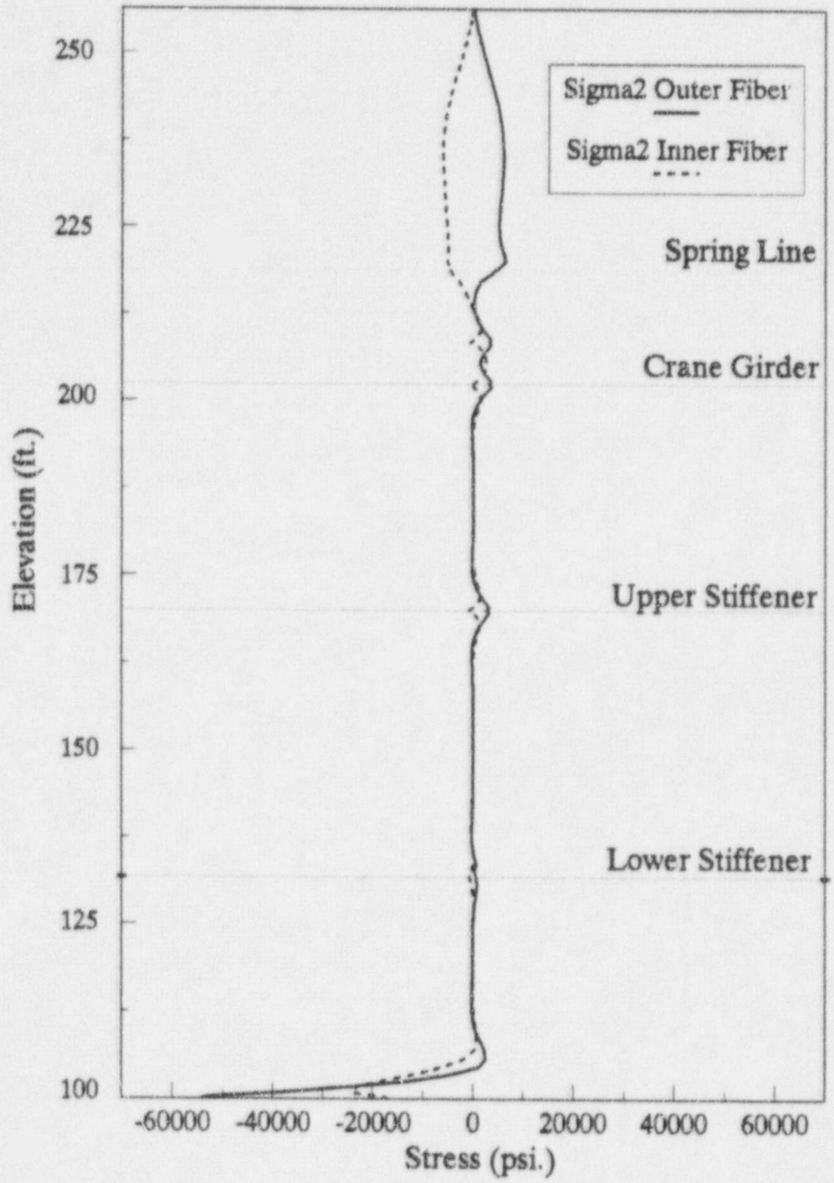

Fig. 2.44 Extreme Fiber Circumferential (Sigma$_2$) Stresses due to Case 2 Temperature Loading (Dry Zone)

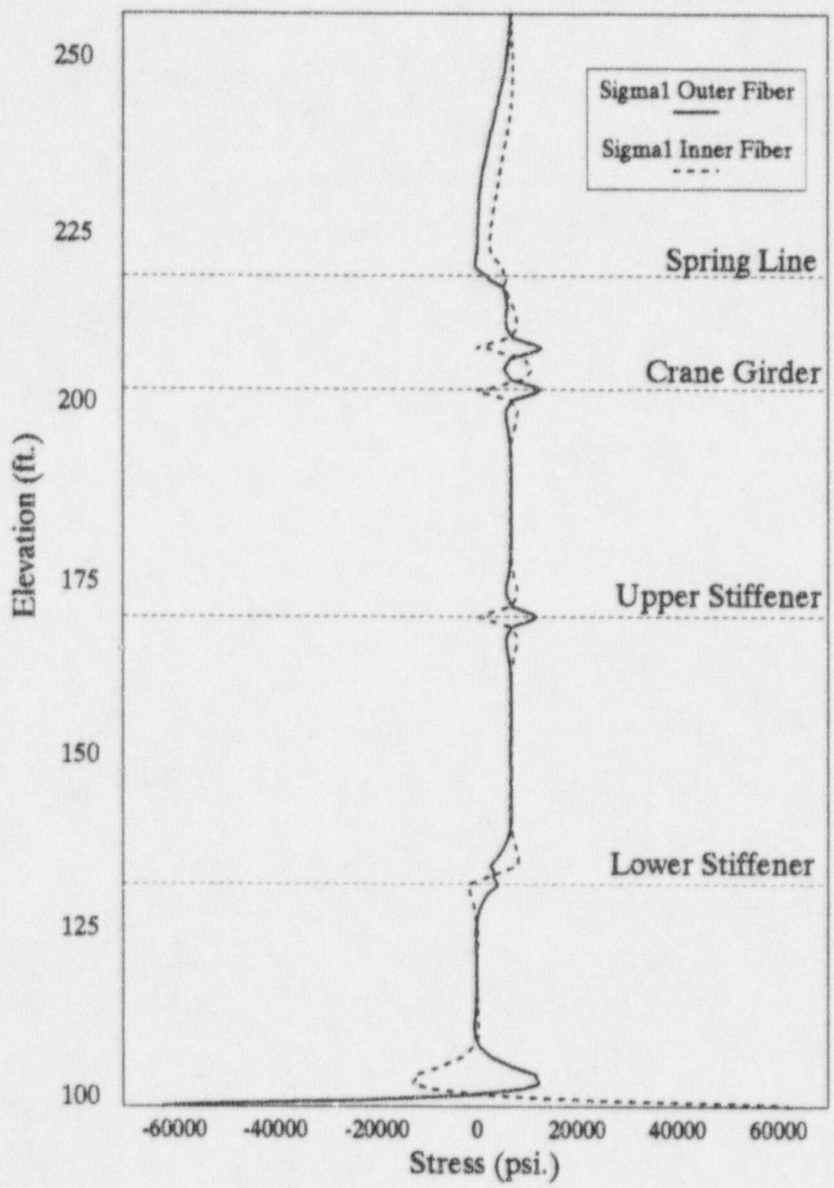

Fig. 2.45 Extreme Fiber Meridional ($Sigma_1$) Stresses due to Case 2 Temperature Loading (Wet Zone)

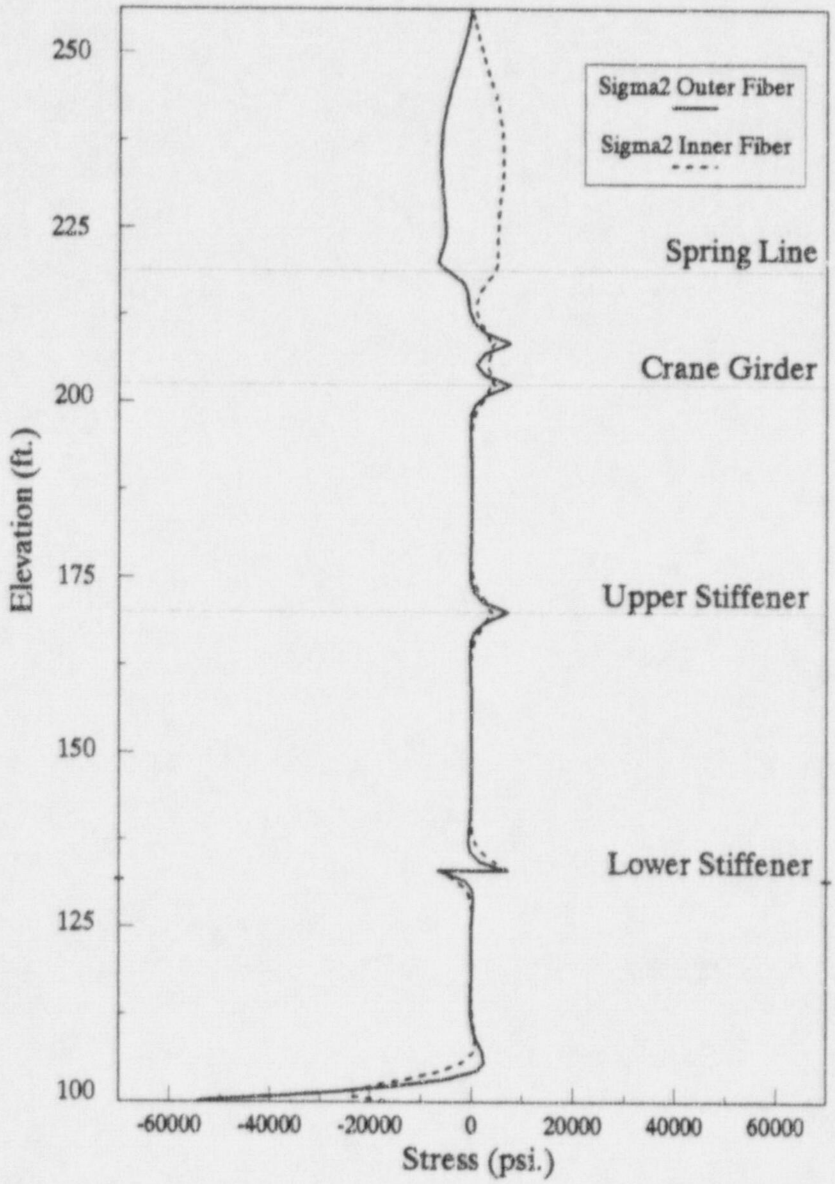

Fig. 2.46 Extreme Fiber Circumferential (Sigma$_2$) Stresses due to Case 2 Temperature Loading (Wet Zone)

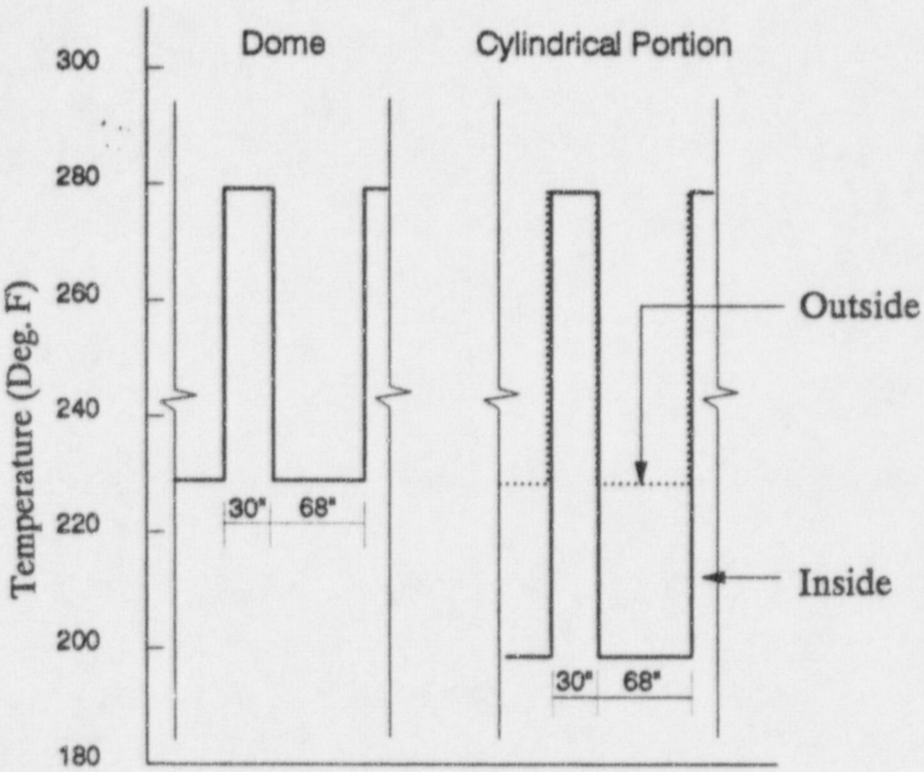

Fig. 2.47 Case 3 Temperature Loading Above Elevation 132'3"

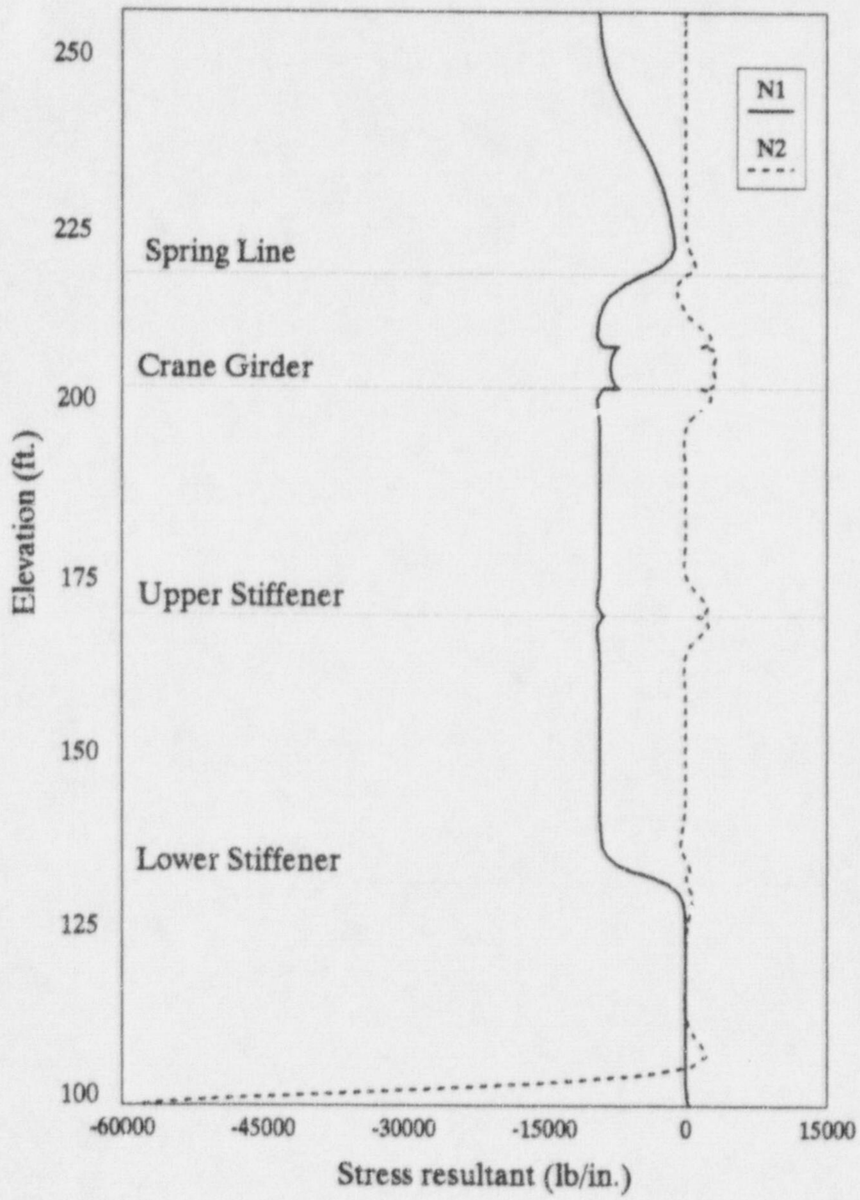

Fig. 2.48 Meridional (N_1) and Circumferential (N_2) Stress Resultants due to Case 3 Temperature Loading (Dry Zone)

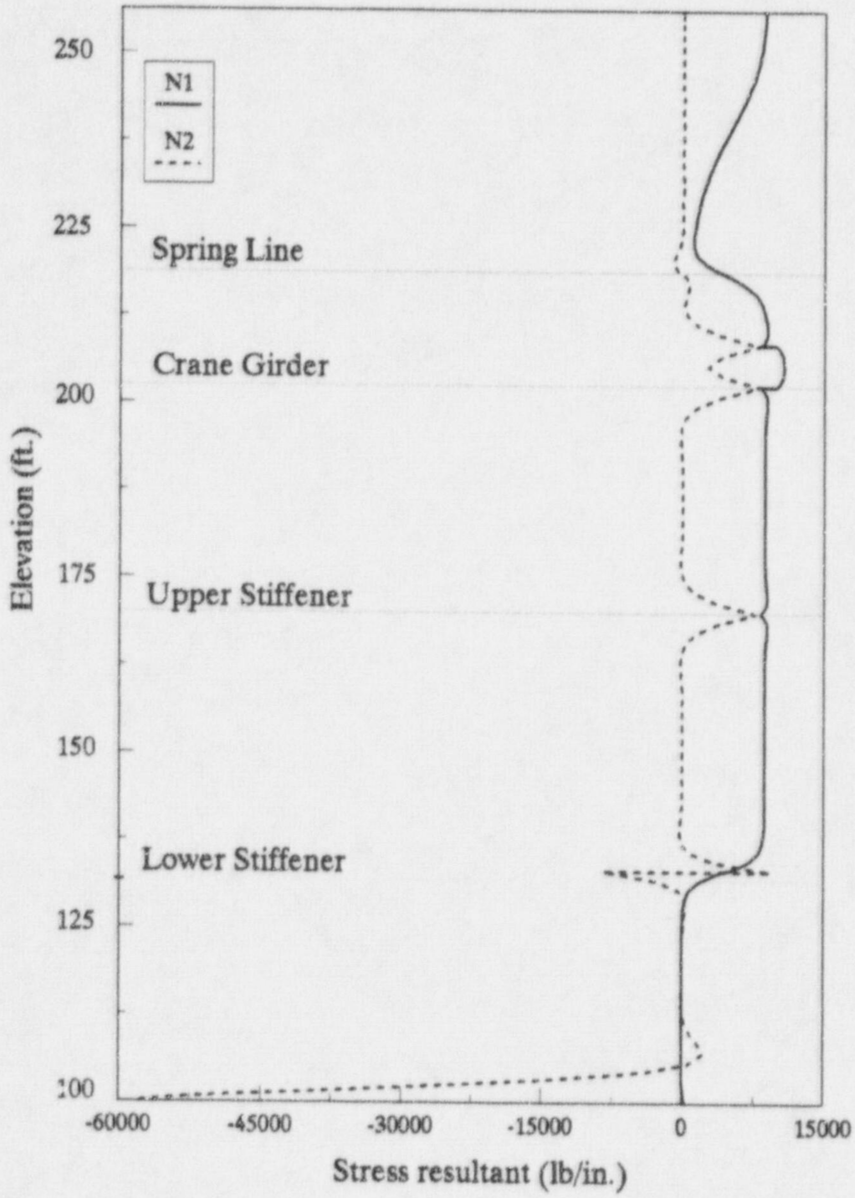

Fig. 2.49 Meridional (N_1) and Circumferential (N_2) Stress Resultants due to Case 3 Temperature Loading (Wet Zone)

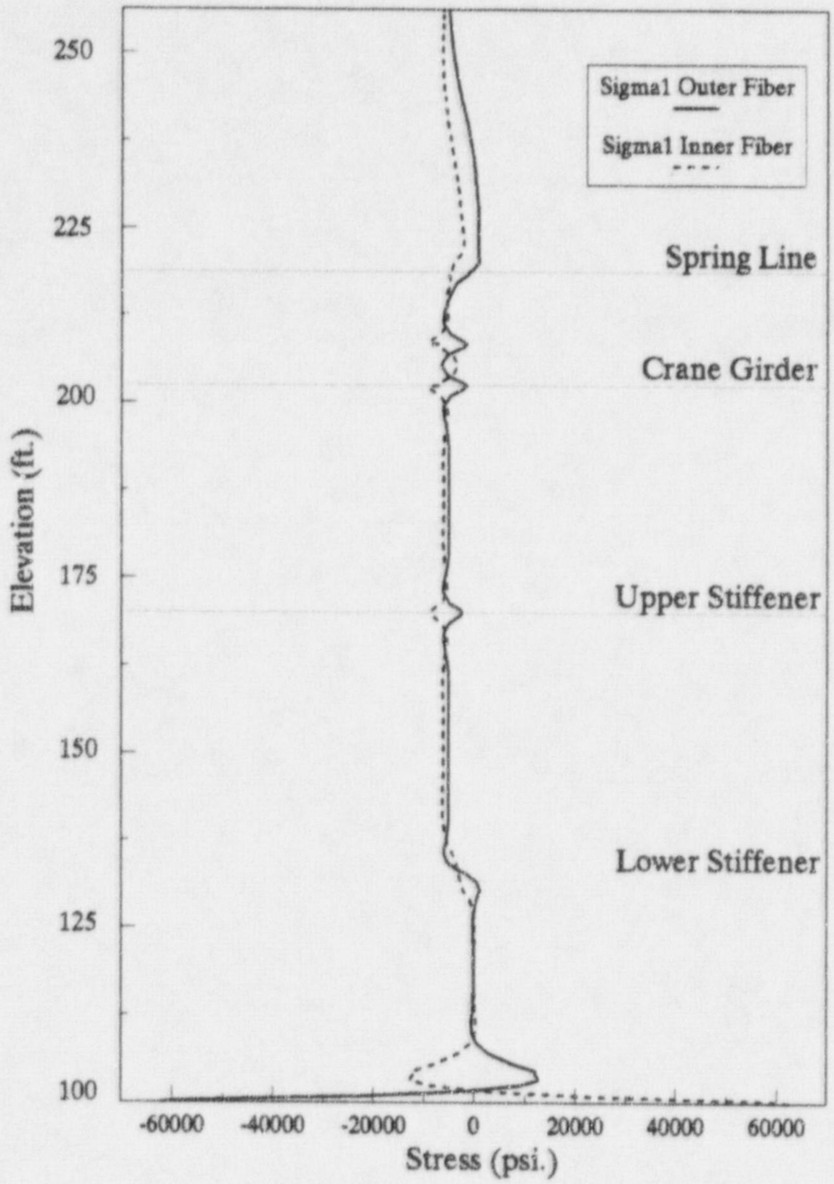

Fig. 2.50 Extreme Fiber Meridional (Sigma$_1$) Stresses due to Case 3 Temperature Loading (Dry Zone)

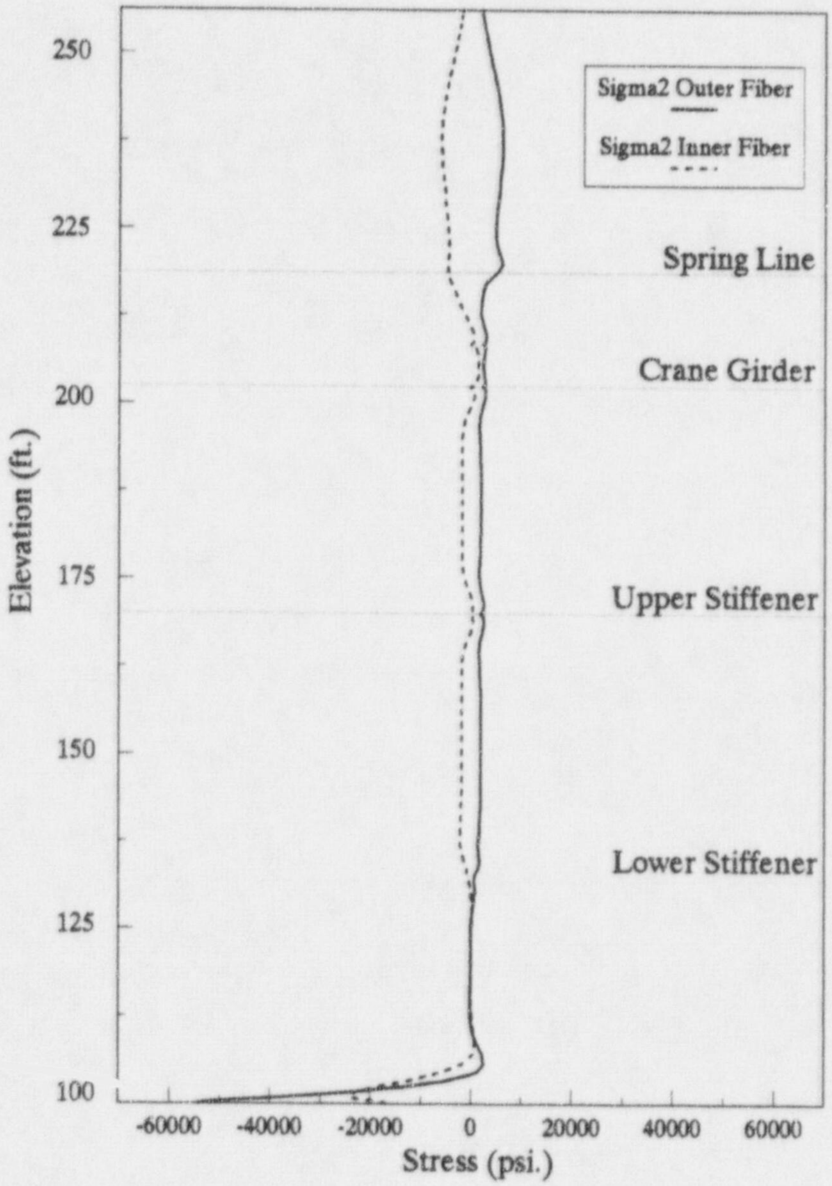

Fig. 2.51 Extreme Fiber Circumferential ($Sigma_2$) Stresses due to Case 3 Temperature Loading (Dry Zone)

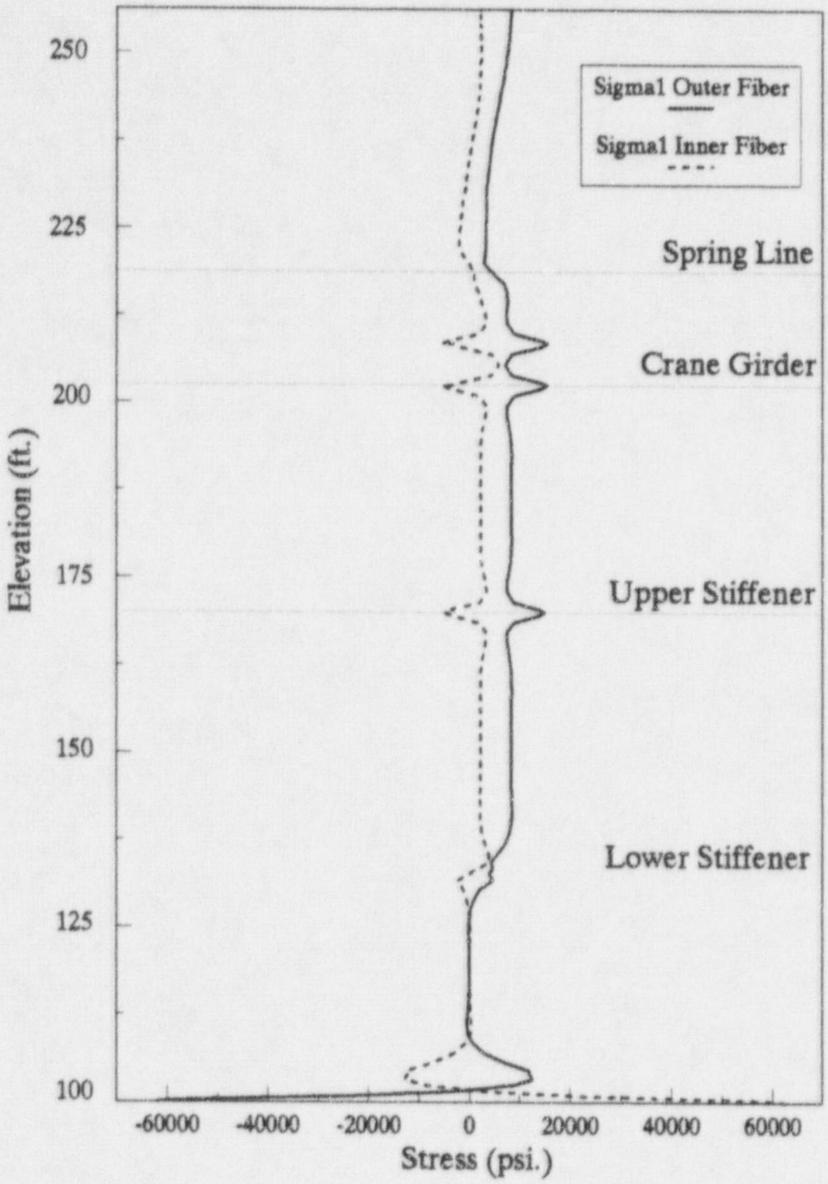

Fig. 2.52 Extreme Fiber Meridional ($Sigma_1$) Stresses due to Case 3 Temperature Loading (Wet Zone)

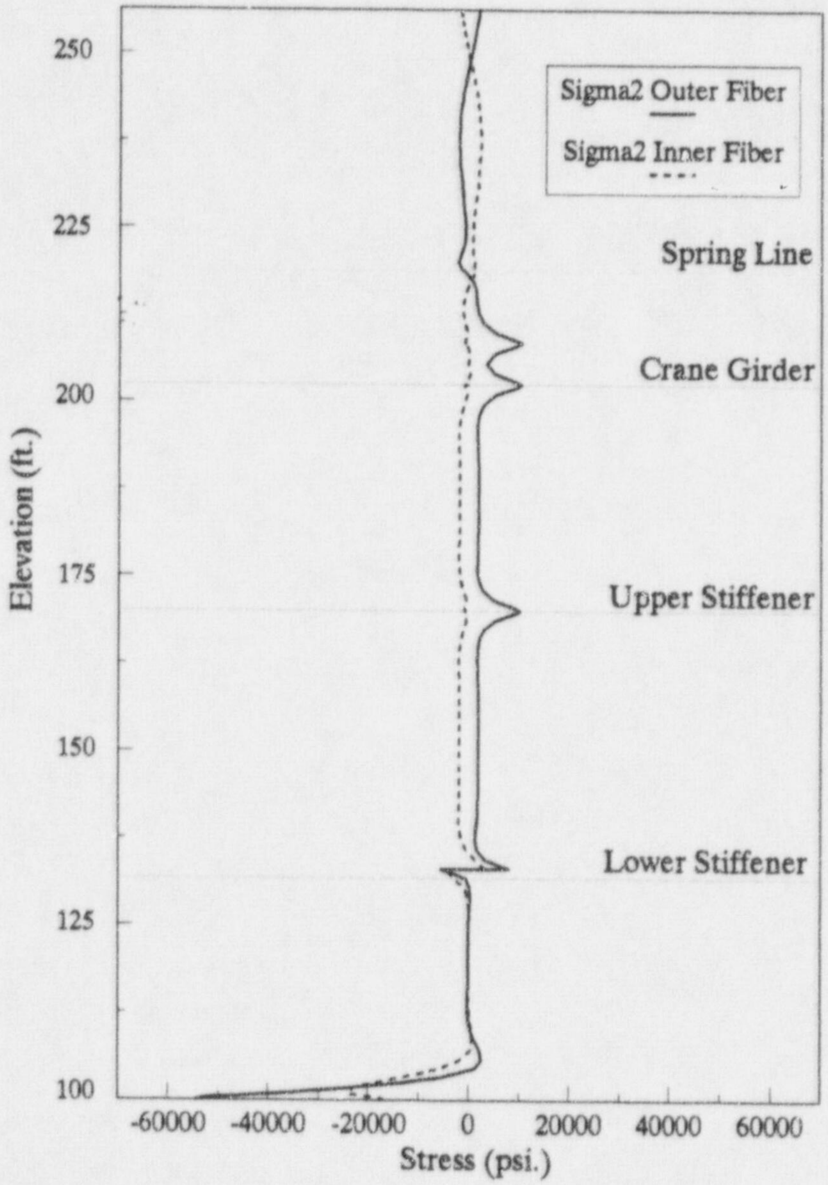

Fig. 2.53 Extreme Fiber Circumferential (Sigma$_2$) Stresses due to Case 3 Temperature Loading (Wet Zone)

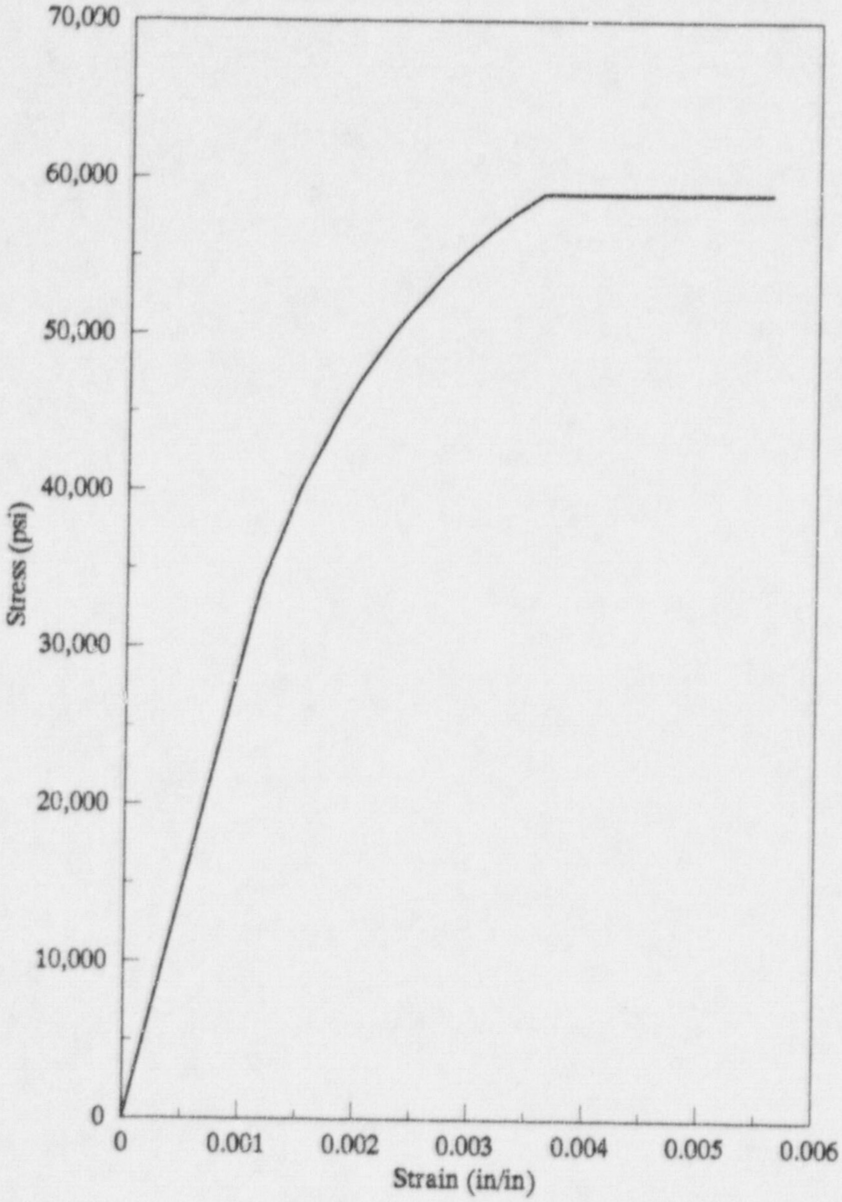

Fig. 3.1 Stress Strain Curve for Temperature of 120°F
(E=29231000 psi σ_y = 59000 psi)

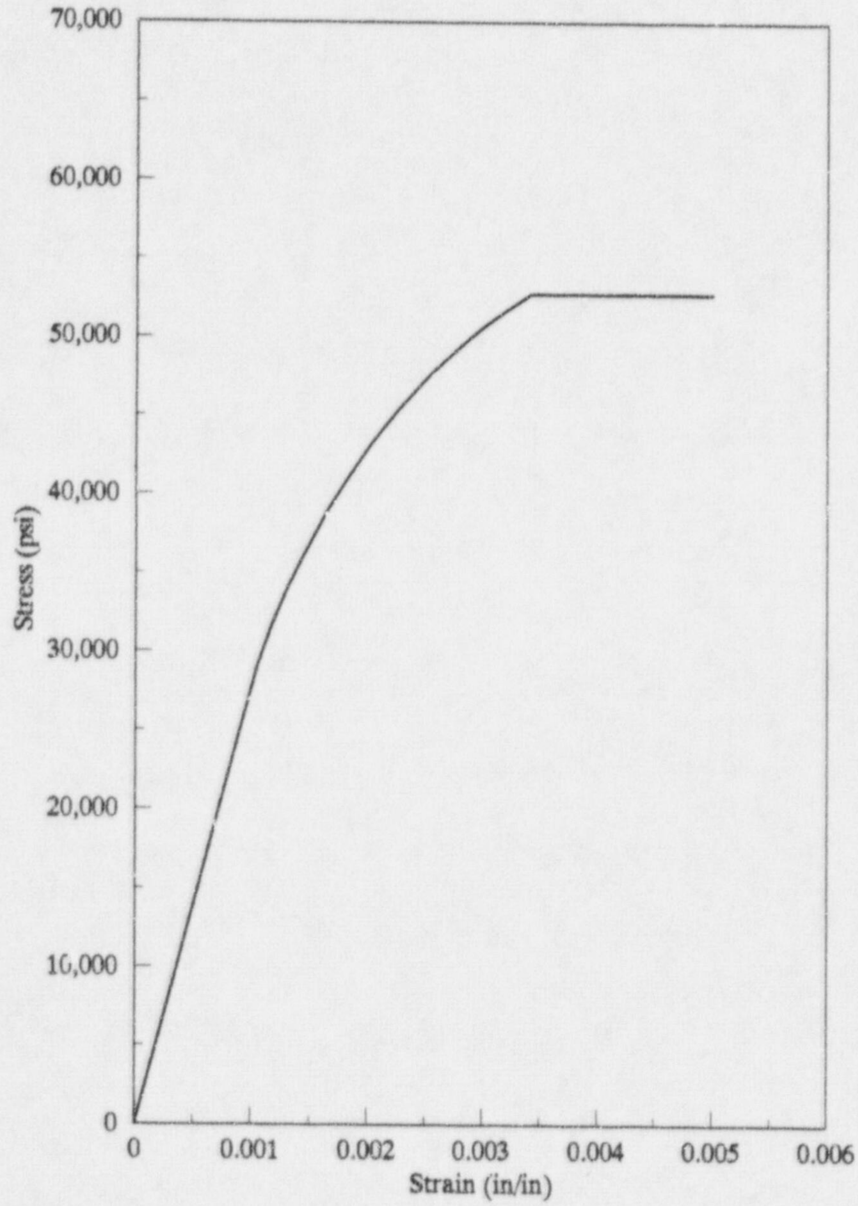

Fig. 3.2 Stress Strain Curve for Temperature of 280°F
(E=27400000 psi σ_y = 52760 psi)

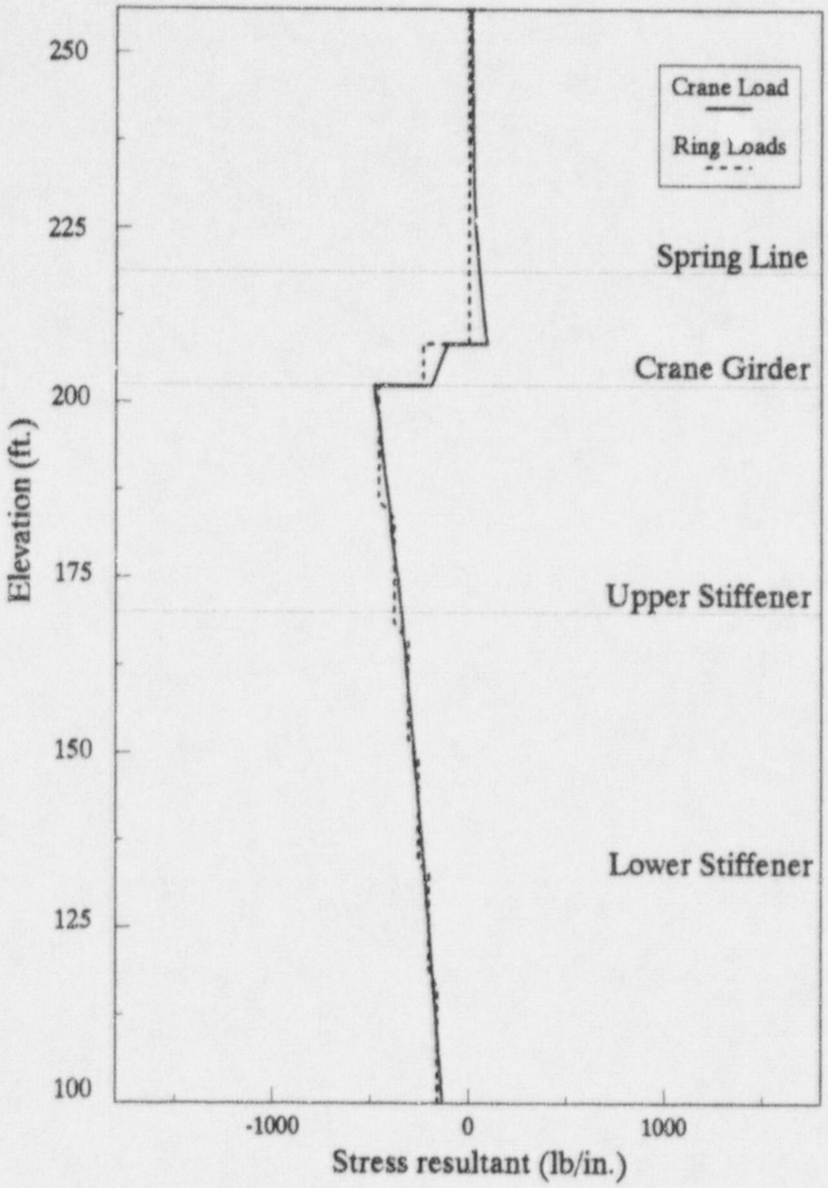

Fig. 3.3 Comparison of Meridional (N_1) Stress Resultants due to Crane Load and Equivalent Ring Loads

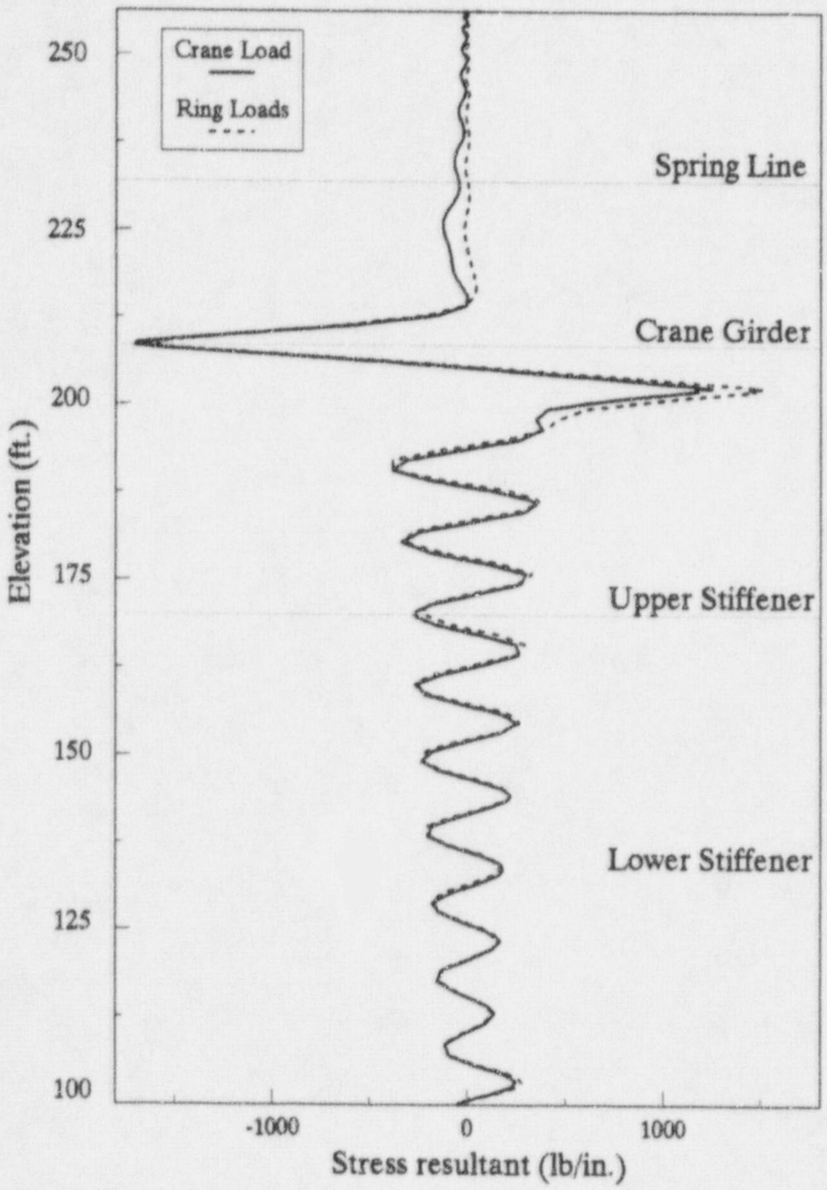

Fig. 3.4 Comparison of Circumferential (N_2) Stress Resultants due to Crane Load and Equivalent Ring Loads

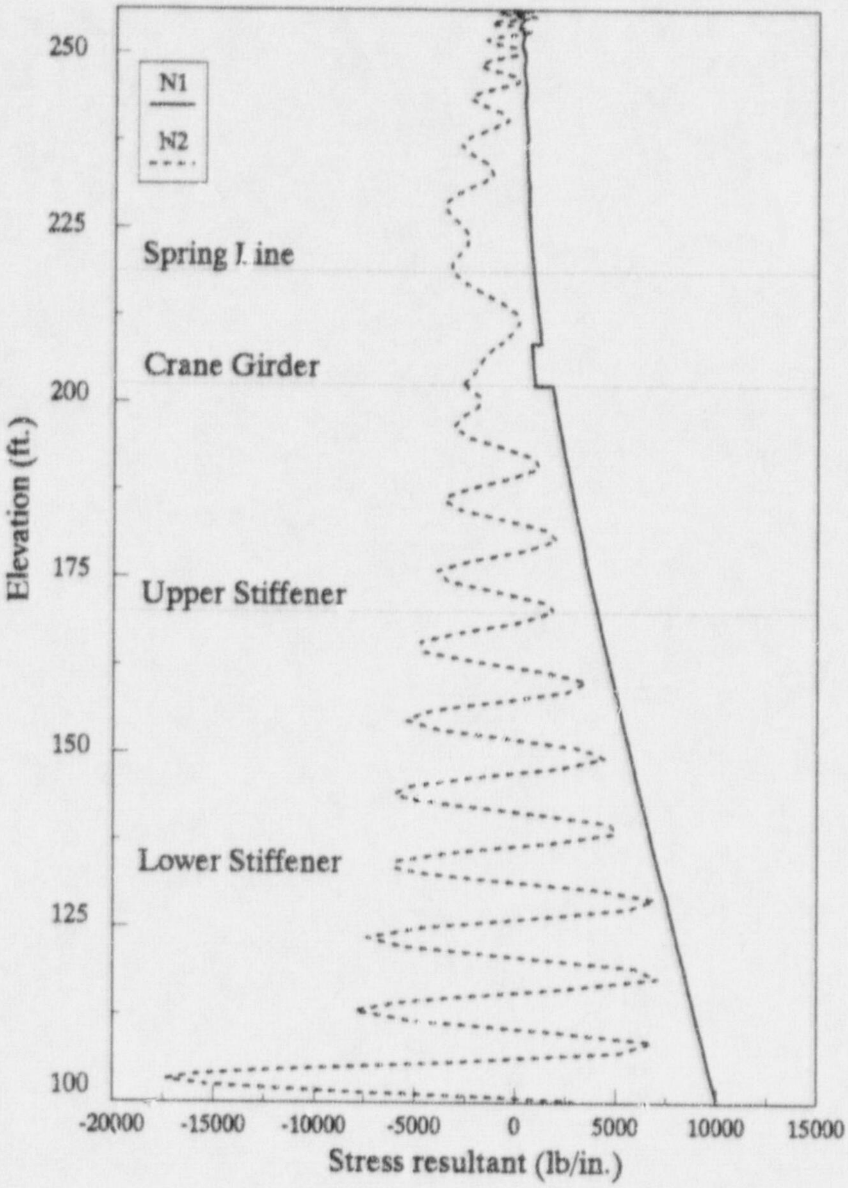

Fig. 3.5 Stress Resultants due to First Mode of Vibration

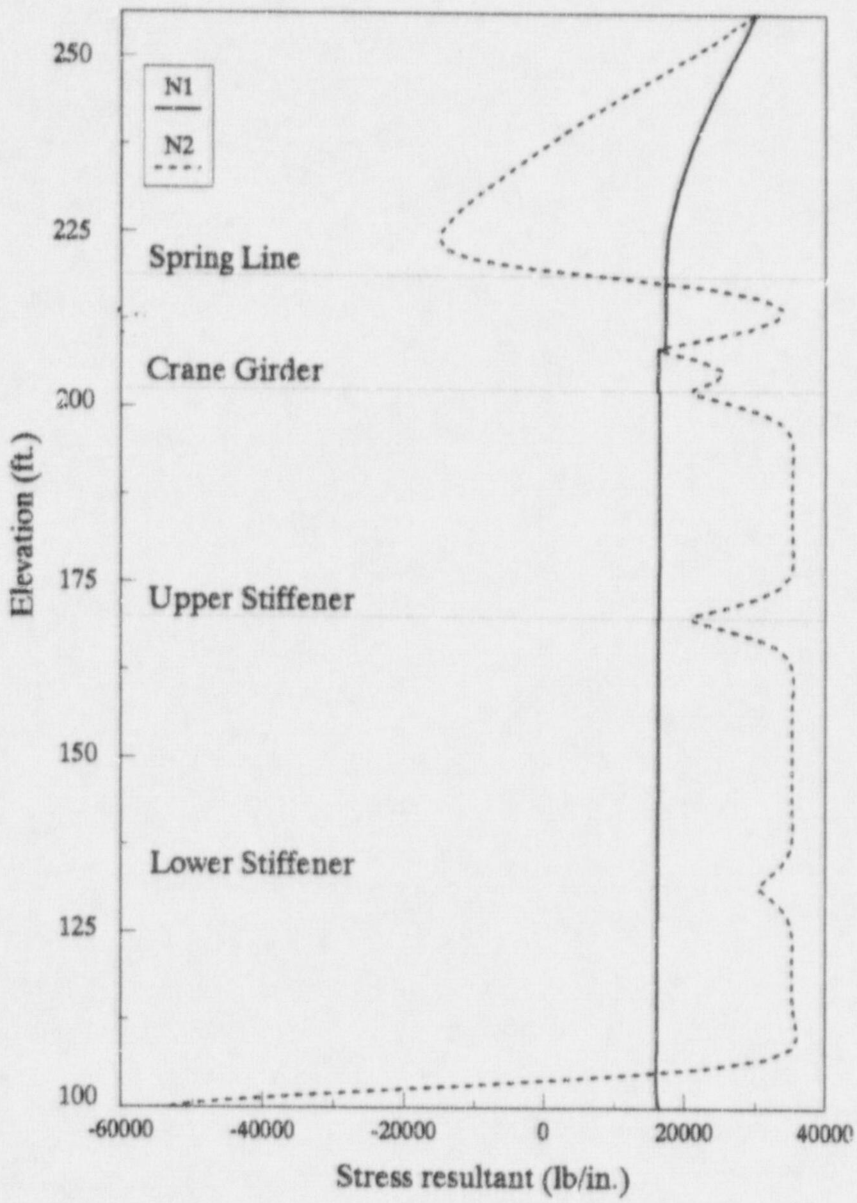

Fig. 3.6 Meridional (N_1) and Circumferential (N_2) Stress Resultants due to DG1 Loading (Elastic Analysis)

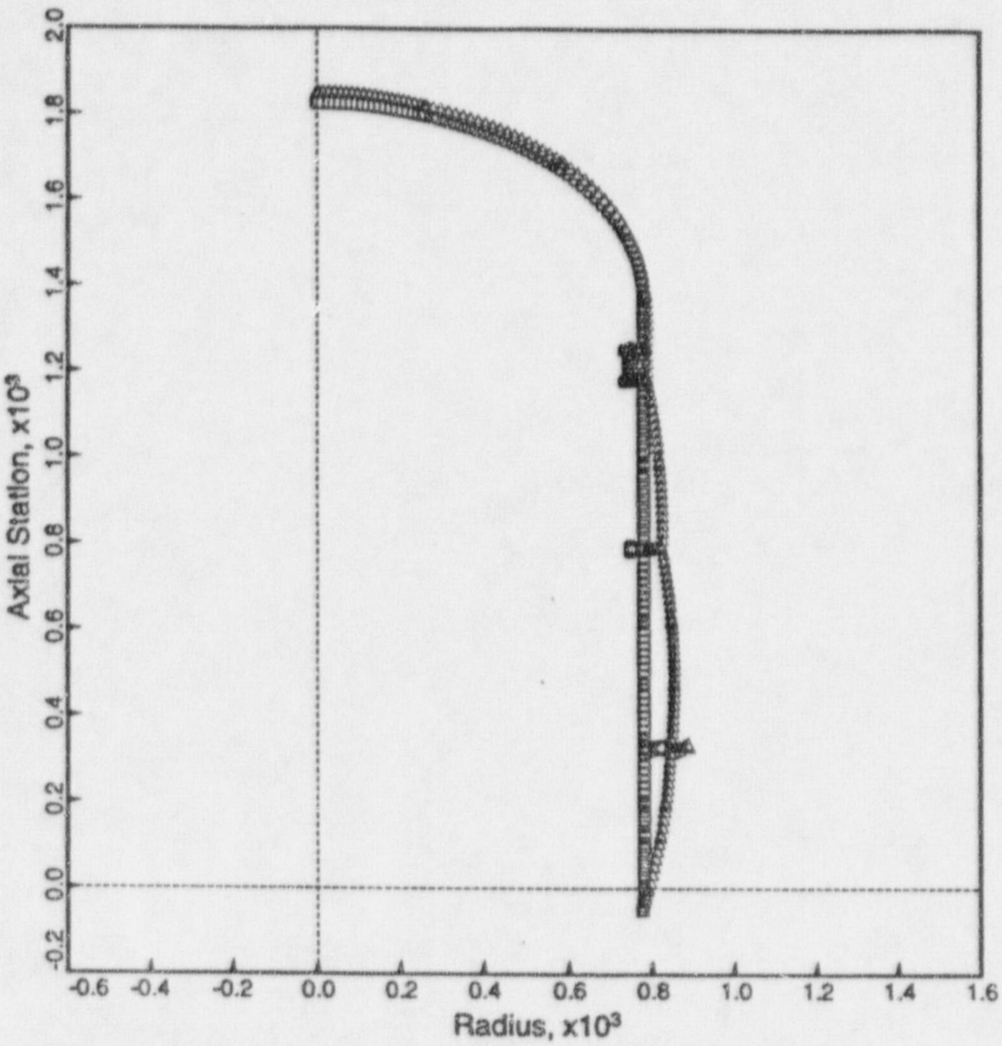

Fig. 3.7 Deformed Shape of the Containment (DBA1 Loading)

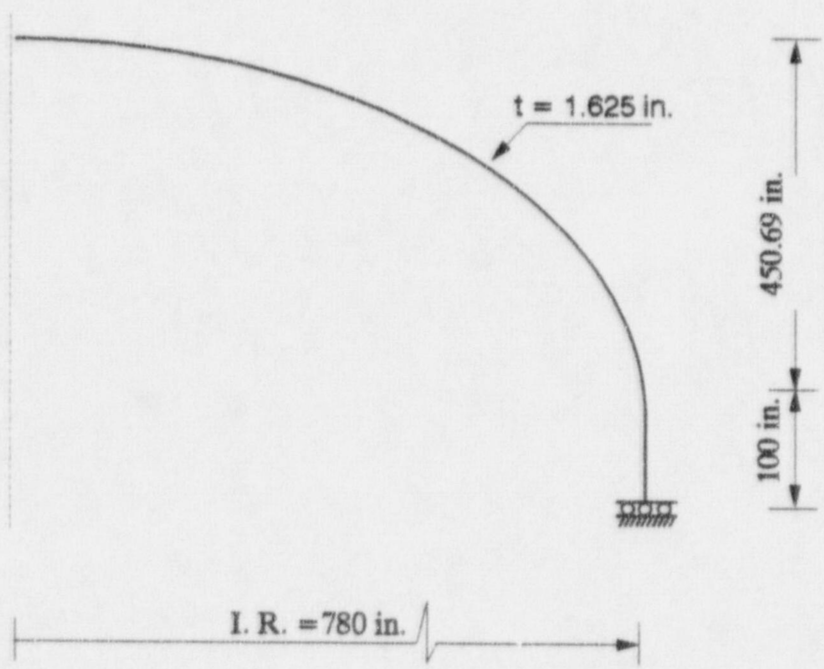

Fig. 3.8 Axisymmetric Model of the Top Ellipsoidal Head

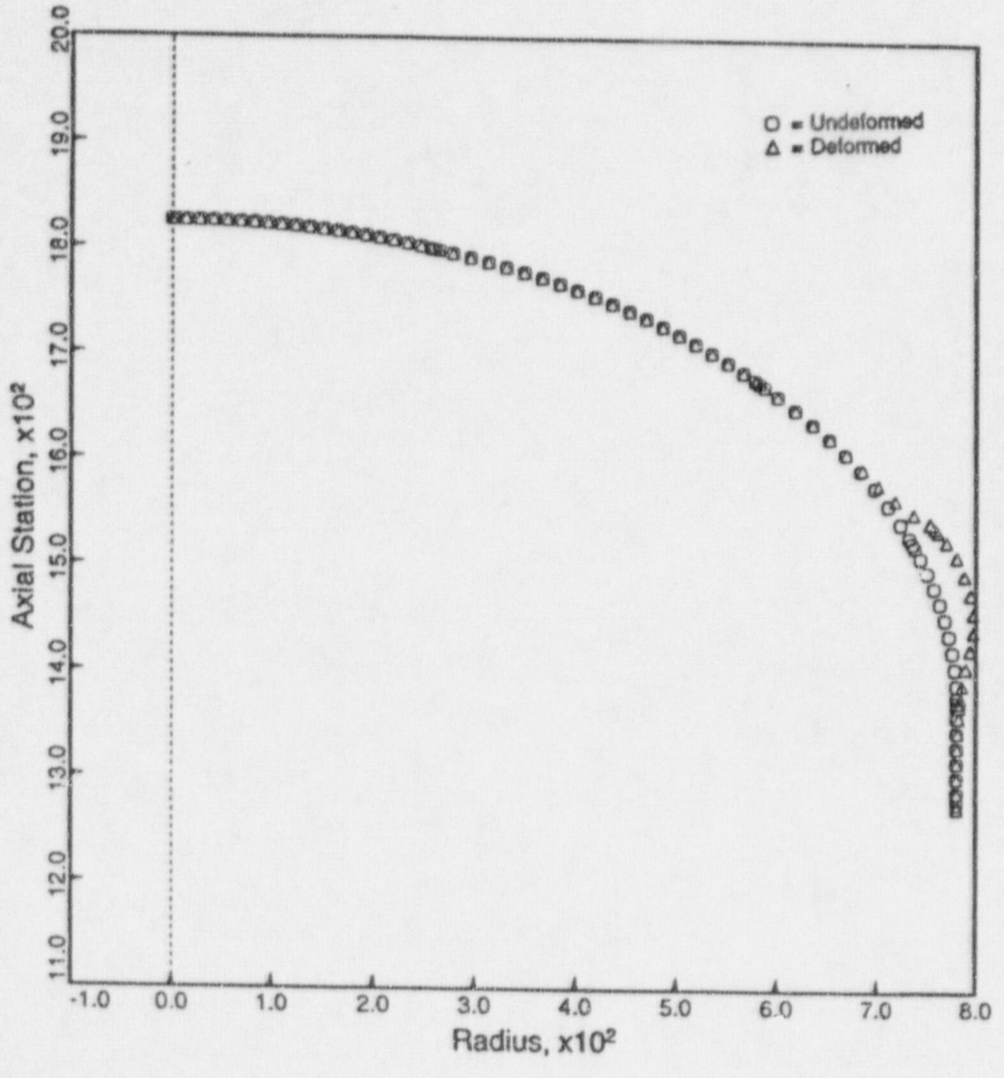

Fig. 3.9 Buckled Shape of the Top Ellipsoidal Head (Elastic Perfectly Plastic Stress Strain Curve)

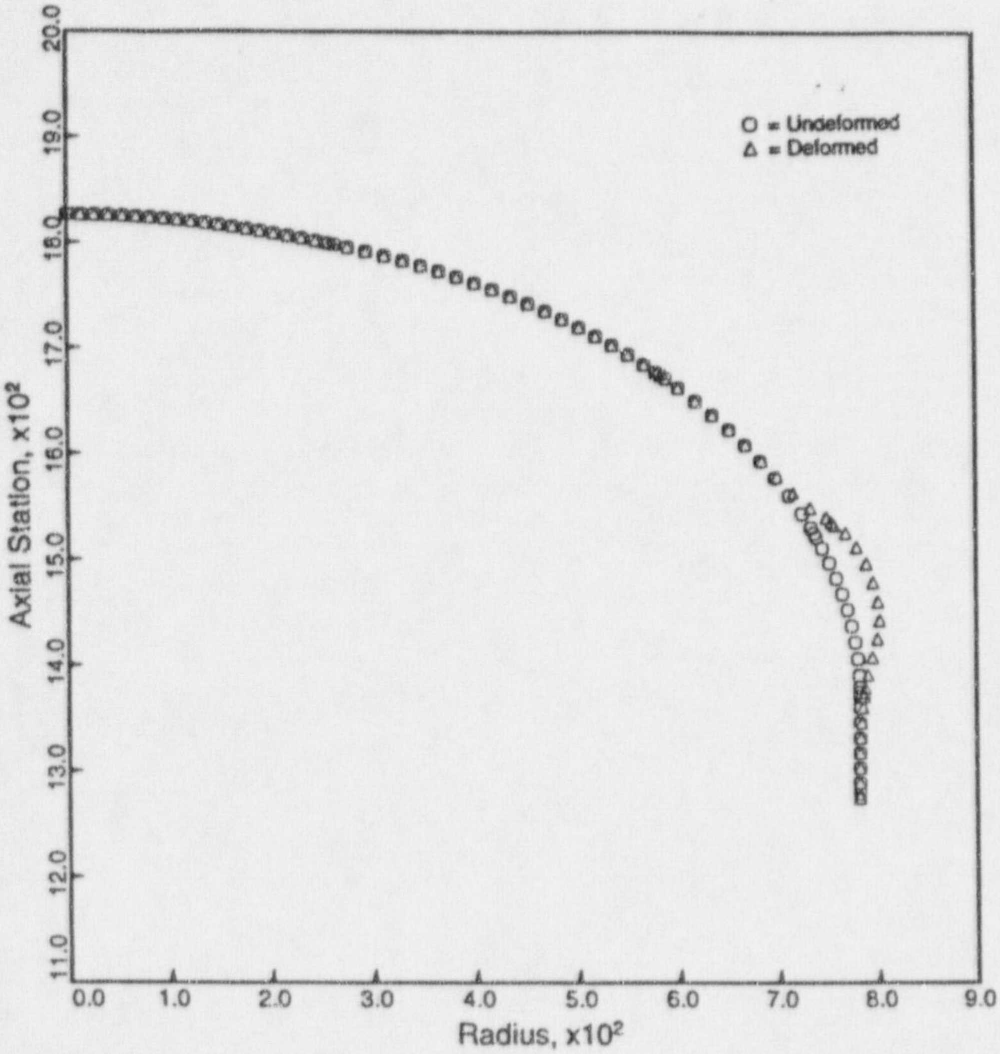

Fig. 3.10 Buckled Shape of the Top Ellipsoidal Head (Using Stress Strain Curve in Fig. 3.2)

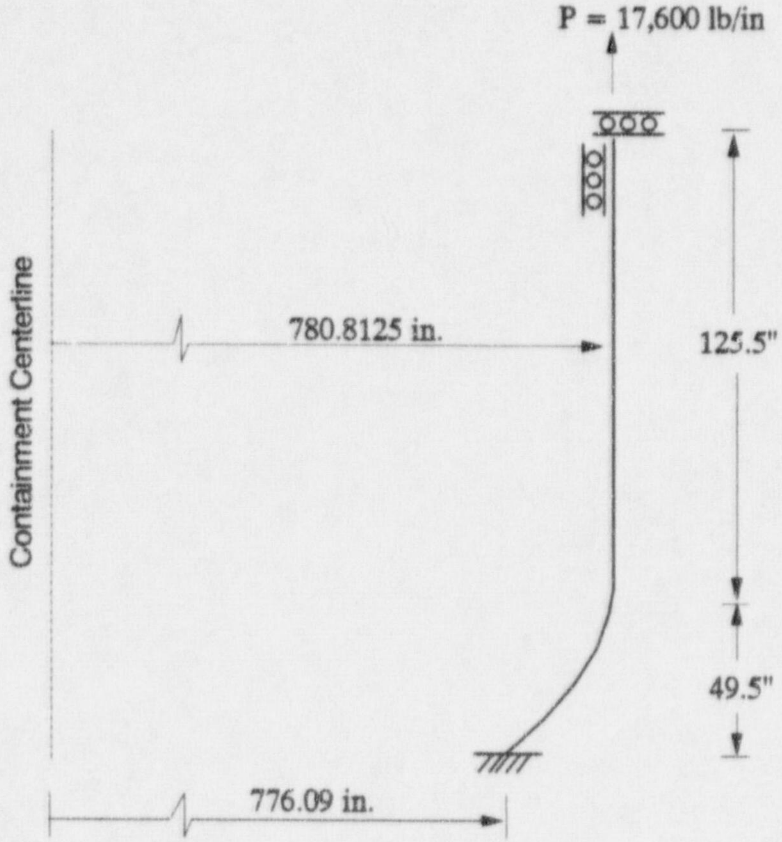

Fig. 3.11 Axisymmetric Model of the Bottom Ellipsoidal Head (Note: Radial Dimension is Distorted)

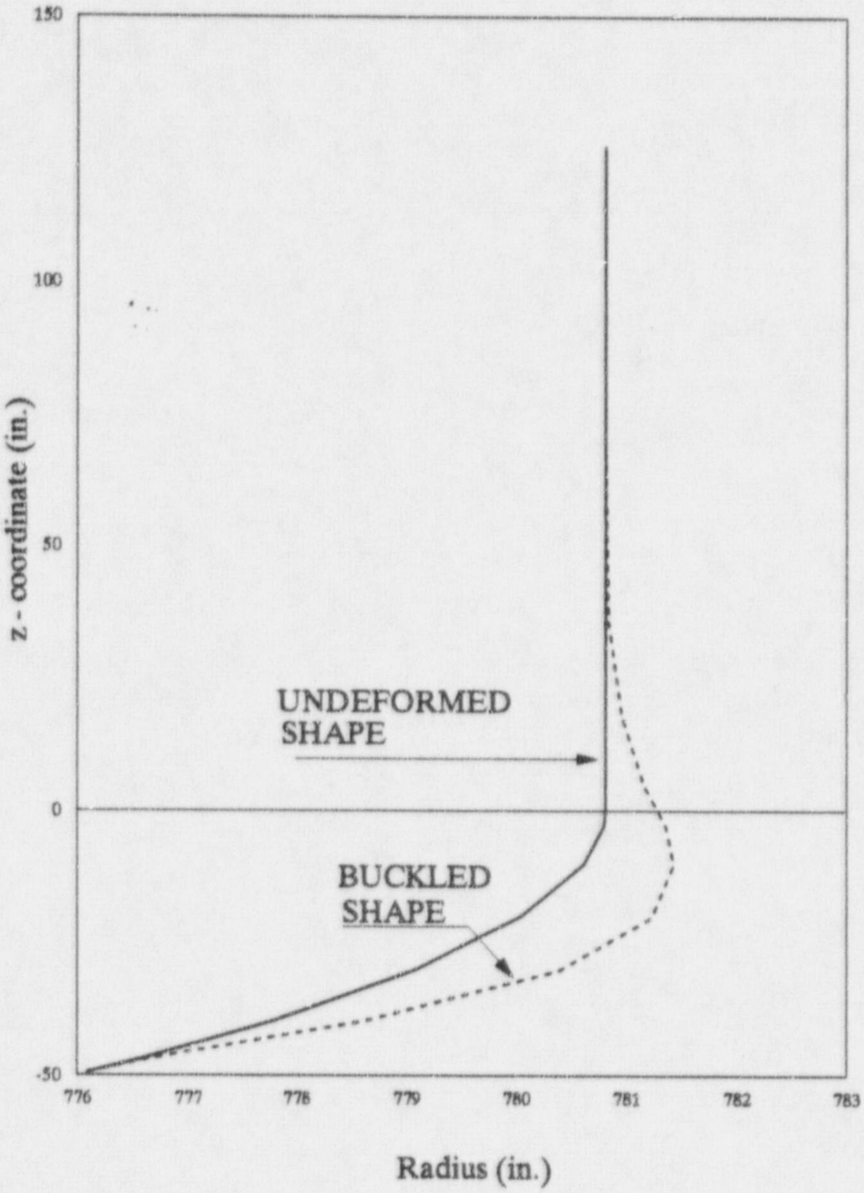

Fig. 3.12 Buckled Shape of the Bottom Ellipsoidal Head (Perfect, Elastic Analysis) (Note: Radial Dimension is Exaggerated)

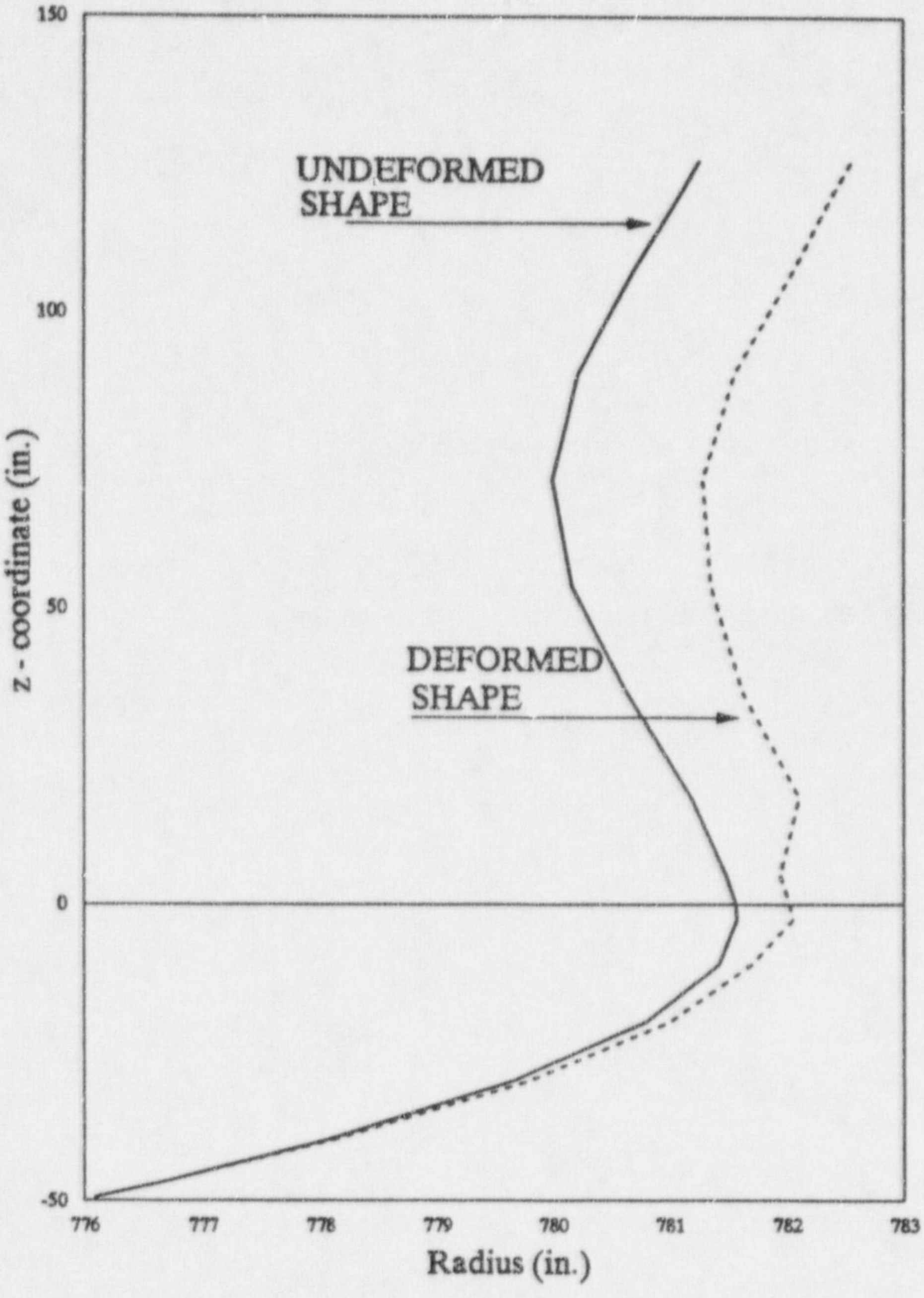

Fig. 3.13 Deformed Shape of the Bottom Ellipsoidal Head (Using Stress Strain Curve in Fig. 3.2) (Note: Radial Dimension is Exaggerated)

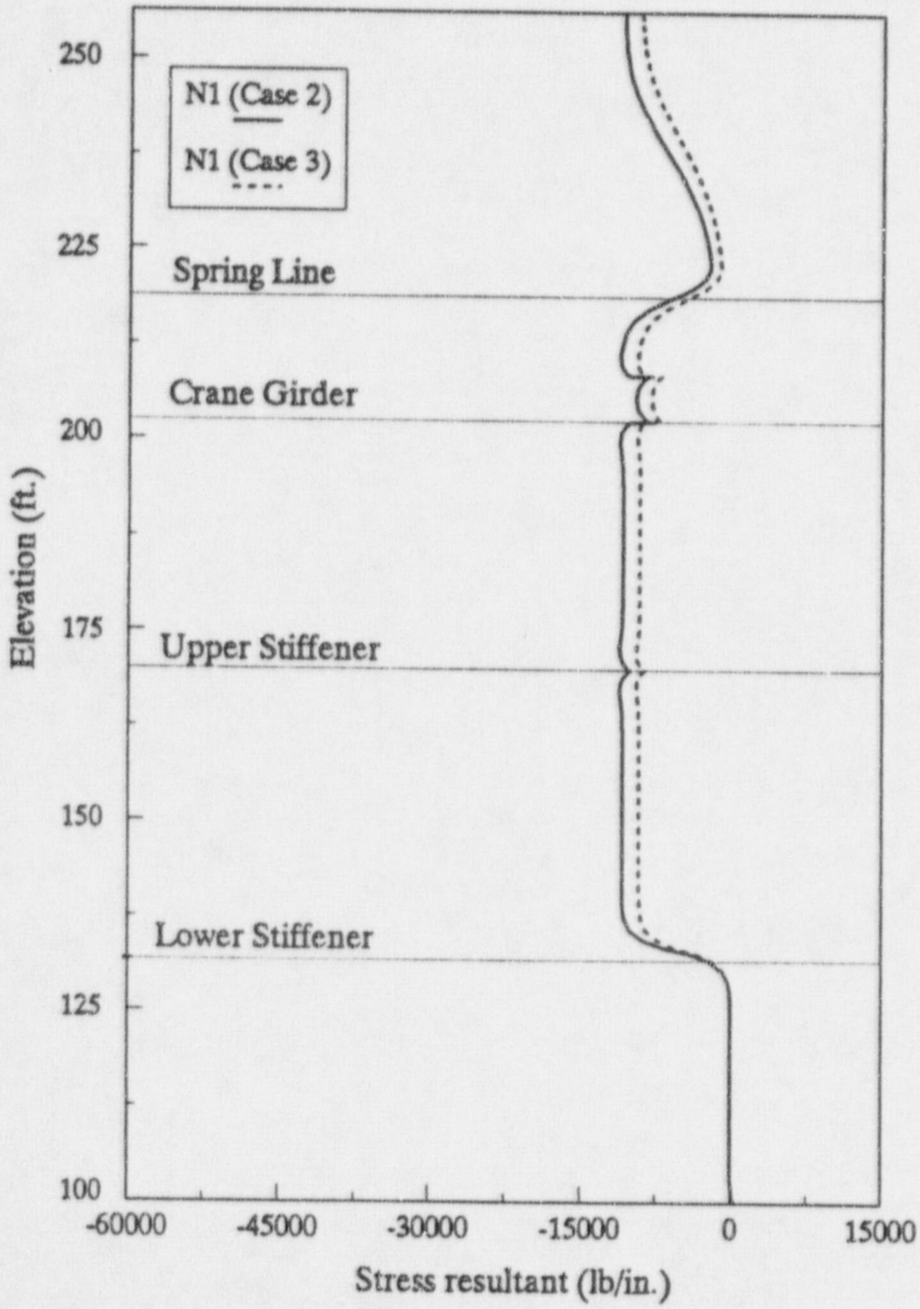

Fig. 3.14 Comparison of Meridional (N_1) Stress Resultants of Case 2 and Case 3 Temperature Loading (Dry Region)

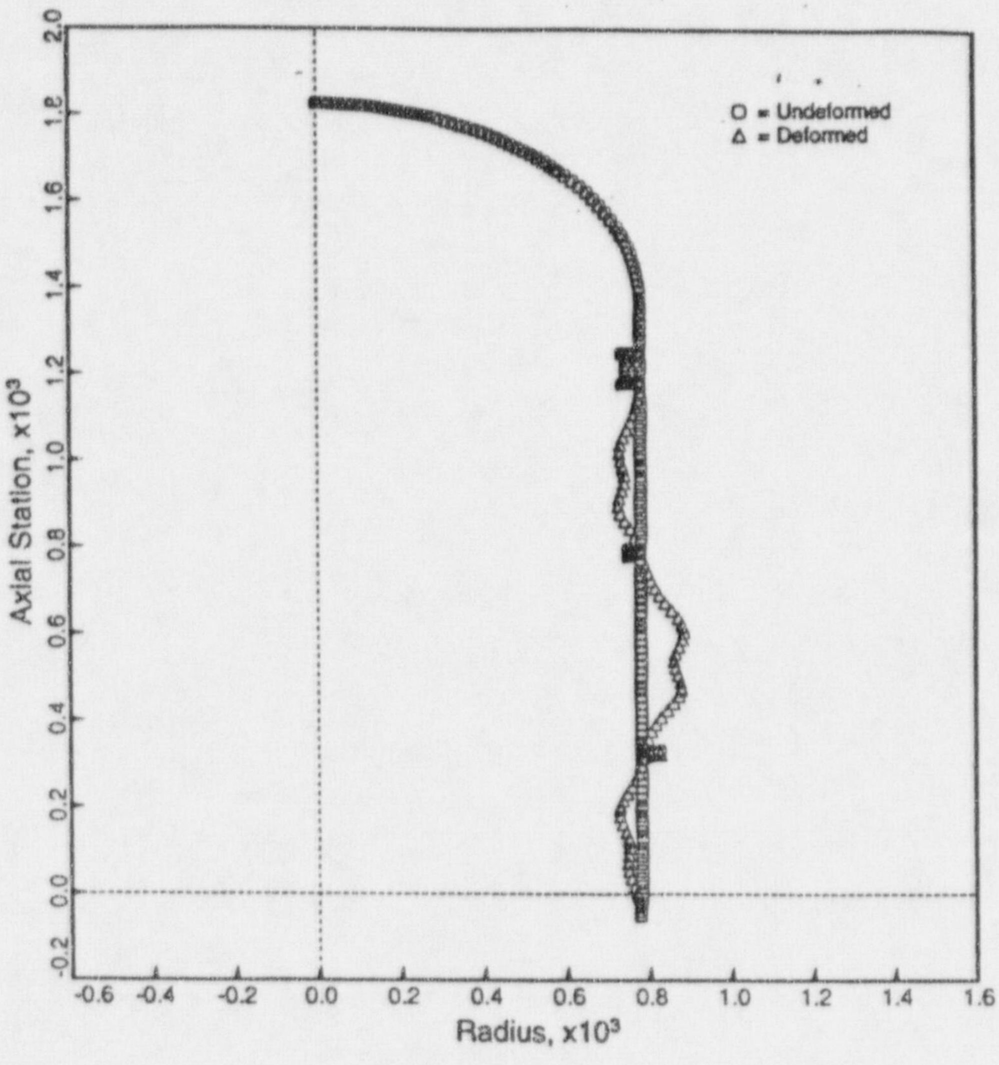

Fig. 3.15 Buckled Shape of the Containment (DBA2 and DG2 Loading)

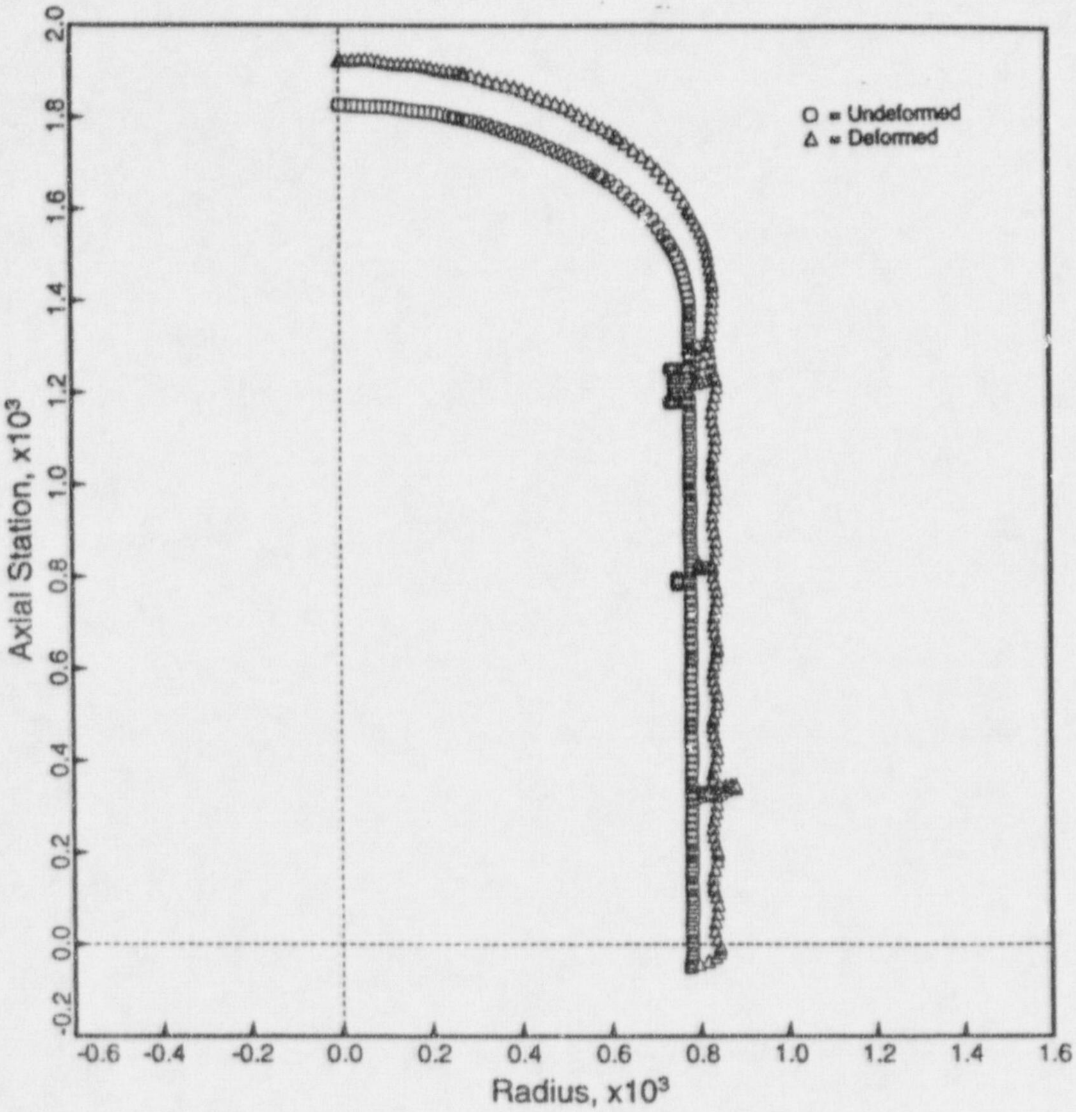

Fig. 3.16 Deformed Shape of the Containment (OC1 Loading)

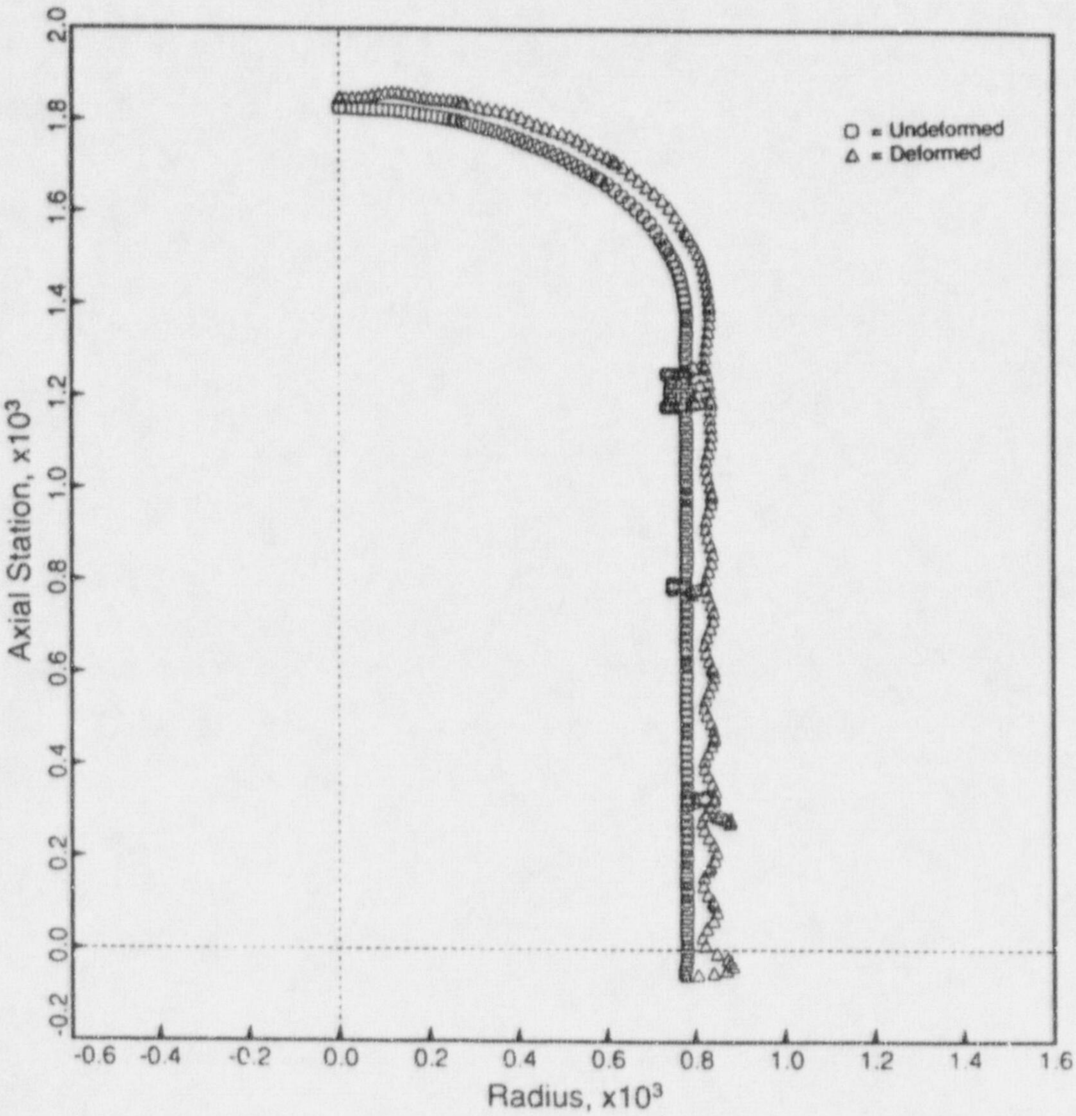

Fig. 3.17 Deformed Shape of the Containment (OC2 Loading)

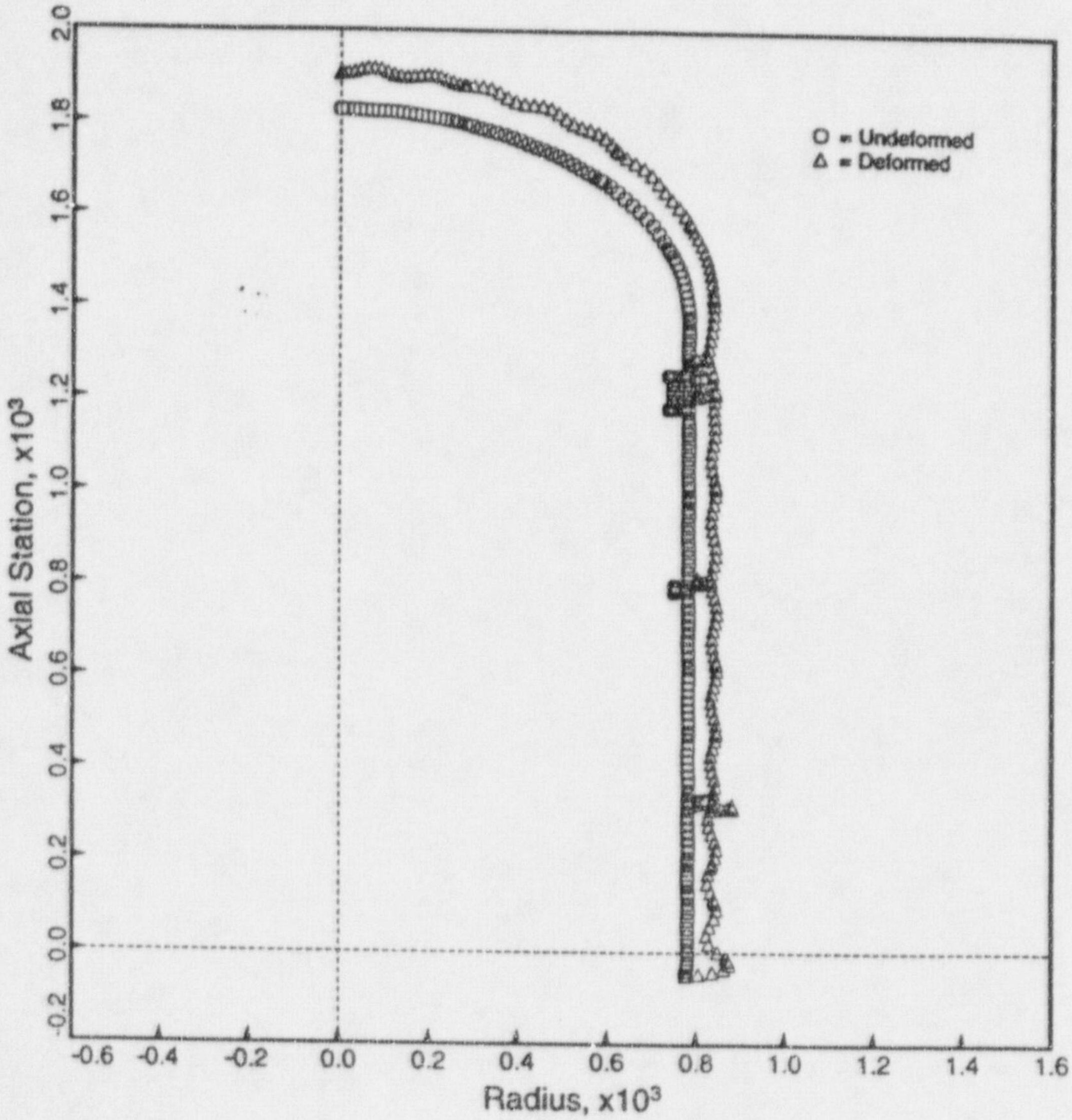

Fig. 3.18 Deformed Shape of the Containment (OC3 Loading)

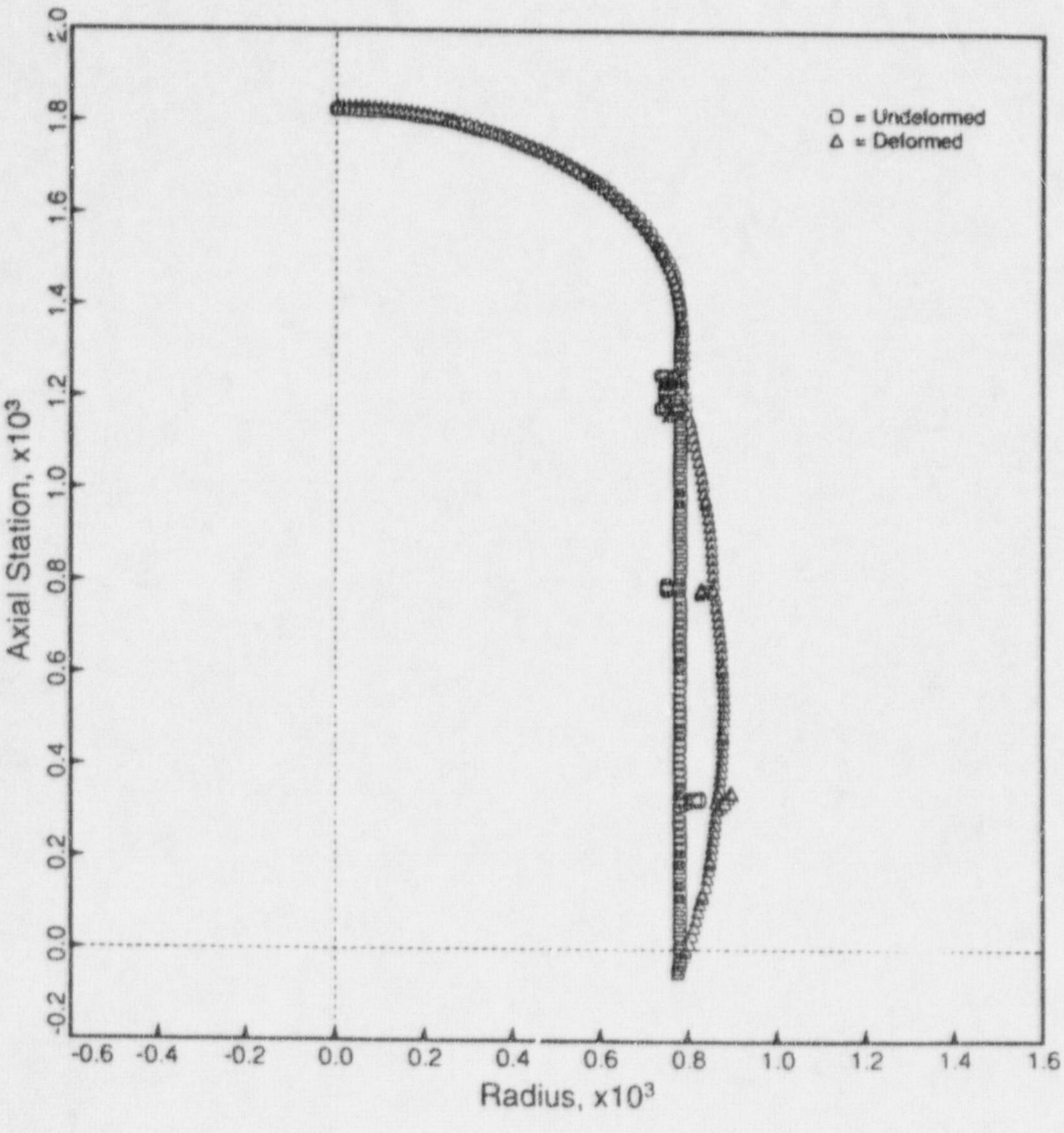

Fig. 3.19 Deformed Shape of the Containment (DBA3 Loading)

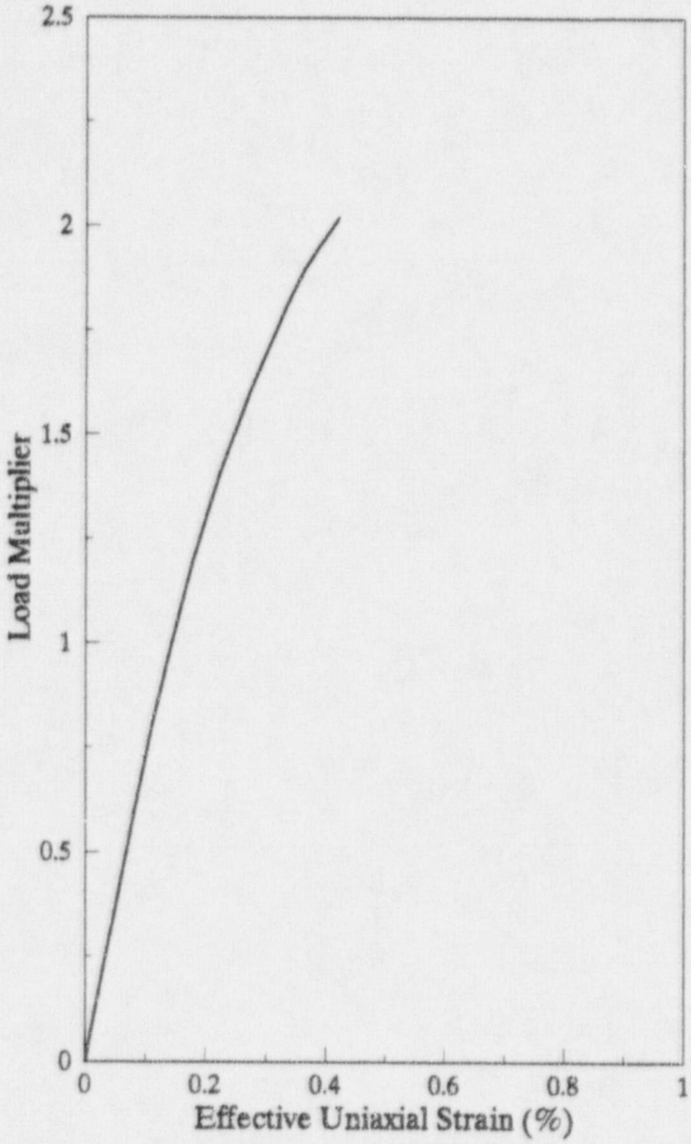

Fig. 3.20 Variation of Effective Uniaxial Strain with Load Multiplier (DBA4 Loading)

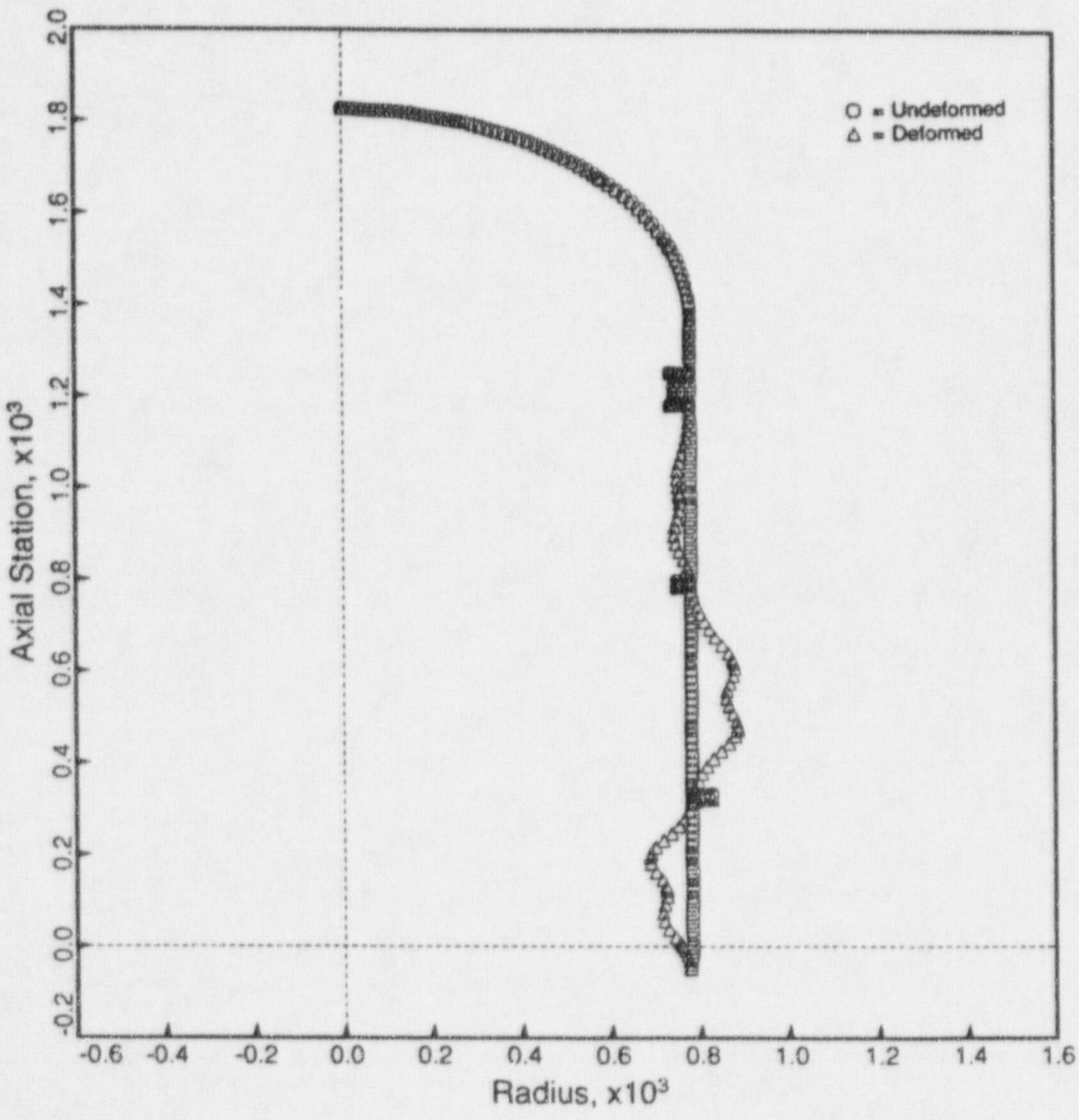

Fig. 3.21 Buckled Shape of the Containment (DBA4 Loading)

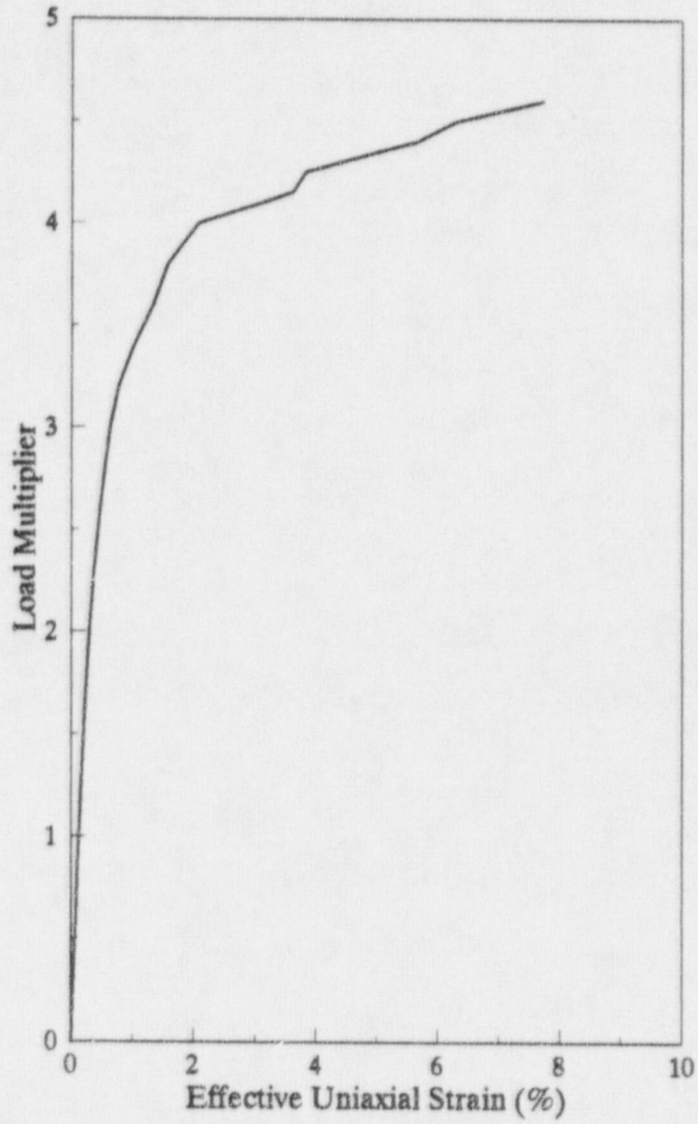

Fig. 4.1 Variation of Effective Uniaxial Strain with Load Multiplier (Seismic Limit Loading)

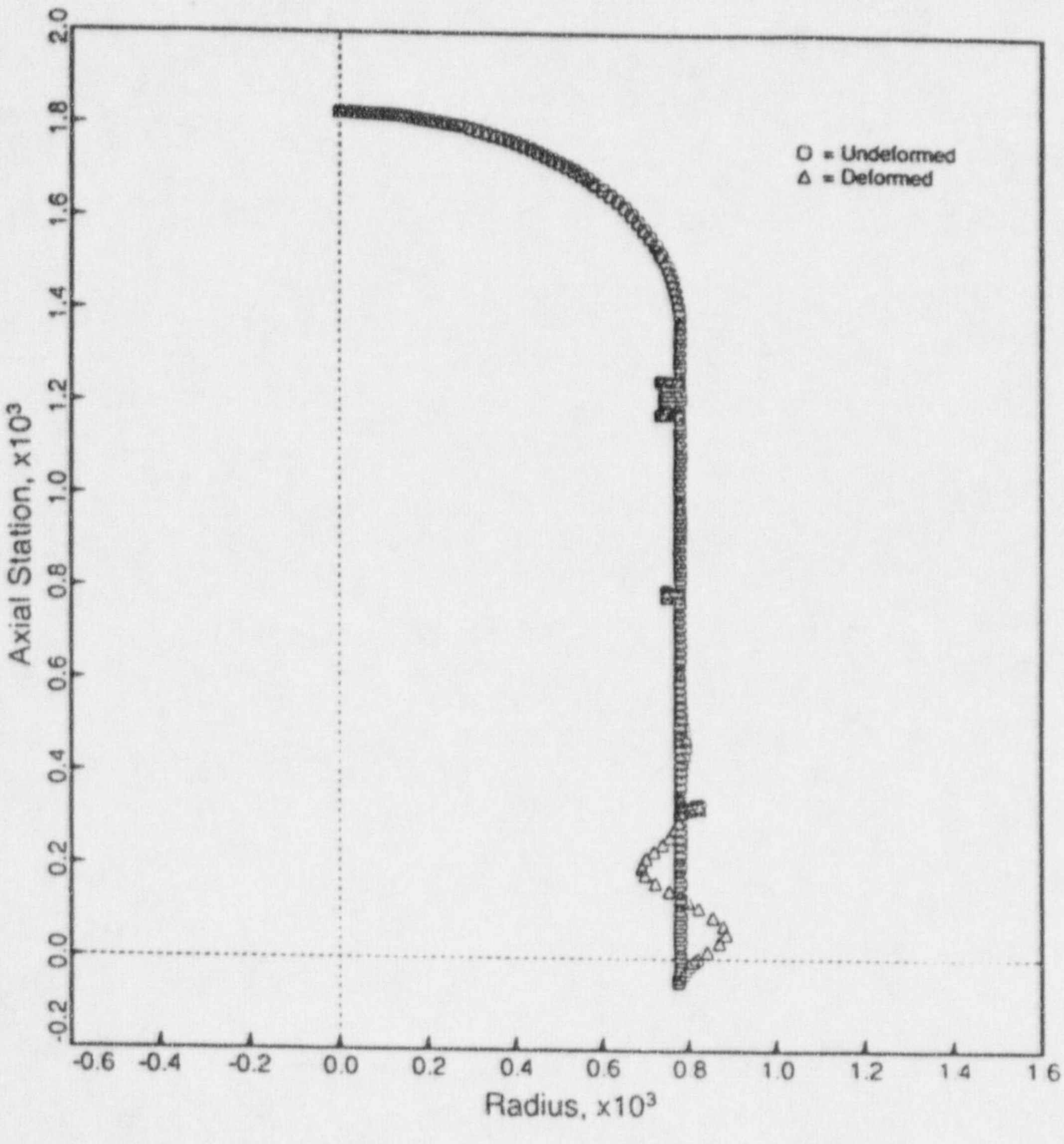

Fig. 4.2 Buckled Shape of the Containment (Seismic Limit Loading)